March 16, 2015,

MEMORANDUM TO: Timothy J. McGinty, Director
Division of Safety Systems
Office of Nuclear Reactor Regulation

FROM: Paul M. Clifford, Senior Technical Advisor ***/RA/***
Division of Safety Systems
Office of Nuclear Reactor Regulation

SUBJECT: TECHNICAL AND REGULATORY BASIS FOR THE REACTIVITY-INITIATED ACCIDENT ACCEPTANCE CRITERIA AND GUIDANCE, REVISION 1

The purpose of this memorandum is to provide an update to the Reactivity-Initiated Accident (RIA) acceptance criteria and guidance in NUREG-0800, "Standard Review Plan (SRP) for the Review of Safety Analysis Reports for Nuclear Power Plants: LWR Edition," SRP Chapter 4.2, "Fuel System Design," Appendix B, "Interim Acceptance Criteria and Guidance for the Reactivity Initiated Accidents." In 2007, the staff published interim acceptance criteria and guidance based upon an assessment of the available empirical data from in-pile RIA test programs. The technical and regulatory basis of the interim criteria is documented in a memorandum dated January 19, 2007. Since 2007, the following information has become available which has prompted the staff to update portions of the interim criteria and guidance:

1. Organization for Economic Cooperation and Development (OECD) Nuclear Energy Agency State-of-the-art Report, "Nuclear Fuel Behaviour under Reactivity-initiated Accident (RIA) Conditions," 2010.

2. Electric Power Research Institute (EPRI) Report 1021036, "Fuel Reliability Program: Proposed RIA Acceptance Criteria," December 2010.

3. Revised RIA transient fission gas release fractions (memo dated 7/26/2011).

4. Pacific Northwest National Laboratory (PNNL) Report 22549, "Pellet-Cladding Mechanical Interaction Failure Threshold for Reactivity Initiated Accidents for Pressurized Water Reactors (PWRs) and Boiling Water Reactors," June 2013.

CONTACT: Paul. M. Clifford NRR/DSS
301-415-4043

5. Japanese Atomic Energy Agency (JAEA) published results from Nuclear Safety Research Reactor (NSRR) Hot Capsule RIA Test VA3, VA4, RH2, BZ3, and LS2 (See Appendix A of PNNL-22549 for details).

6. In September 2014, JAEA published revised fuel enthalpy predictions for 43 previous NSRR test specimens.

The updated technical and regulatory bases for the RIA acceptance criteria and guidance are attached.

CONTACT: Paul. M. Clifford NRR/DSS
301-415-4043

5. Japanese Atomic Energy Agency (JAEA) published results from Nuclear Safety Research Reactor (NSRR) Hot Capsule RIA Test VA3, VA4, RH2, BZ3, and LS2 (See Appendix A of PNNL-22549 for details).

6. In September 2014, JAEA published revised fuel enthalpy predictions for 43 previous NSRR test specimens.

The updated technical and regulatory bases for the RIA acceptance criteria and guidance are attached.

Enclosure:
Technical and Regulatory Basis

CONTACT: Paul. M. Clifford NRR/DSS
301-415-4043

DISTRIBUTION: TMcGinty JDean PClifford CJackson JDonoghue SNPB R/F

Accession: ML14188C423 NRR-106

OFFICE	NRR/DSS/SNPB	NRR/RES
NAME	JDean	RLee
DATE	03/07/2015	03/04/2015

OFFICIAL RECORD COPY

TECHNICAL AND REGULATORY BASIS:
ACCEPTANCE CRITERIA AND GUIDANCE
FOR THE REACTIVITY-INITIATED ACCIDENT

ENCLOSURE

TABLE OF CONTENTS

1.0 INTRODUCTION

The purpose of this report is to document the technical and regulatory bases for the Reactivity-Initiated Accident (RIA) acceptance criteria and guidance. RIAs consist of postulated accidents which involve a sudden and rapid insertion of positive reactivity. These accident scenarios include a Control Rod Ejection (CRE) for Pressurized Water Reactors (PWRs) and a Control Rod Drop Accident (CRDA) for Boiling Water Reactors (BWRs).

As illustrated in Figure 1-1, the uncontrolled movement of a single control rod out of the core results in a positive reactivity insertion which promptly increases local core power. Fuel temperatures rapidly increase prompting fuel pellet thermal expansion. The reactivity excursion is initially mitigated by Doppler feedback and delayed neutron effects followed by reactor trip. Standard Review Plan (SRP) Section 15.4.8 and 15.4.9 provide further detail on the CRE and CRDA respectively.

In 2007, the staff published the interim acceptance criteria and guidance based upon an assessment of the available empirical data from in-pile RIA test programs. The technical and regulatory basis of the interim criteria is documented in a memorandum dated January 19, 2007 (Reference 1). Since 2007, the following information has become available which has prompted the staff to update portions of the interim criteria and guidance:

1. Organization for Economic Cooperation and Development OECD) Nuclear Energy Agency State-of-the-art Report, “Nuclear Fuel Behaviour under RIA Conditions,” 2010 (Reference 2).

2. EPRI Report 1021036, “Fuel Reliability Program: Proposed RIA Acceptance Criteria,” December 2010 (Reference 3).

3. Revised RIA transient fission gas release fractions (Reference 4).

4. Pacific Northwest National Laboratory (PNNL) Report 22549, “Pellet-Cladding Mechanical Interaction Failure Threshold for Reactivity Initiated Accidents for Pressurized Water Reactors and Boiling Water Reactors,” June 2013 (Reference 5).

5. Published results from Nuclear Safety Research Reactor (NSRR) Hot Capsule RIA Test VA3, VA4, RH2, BZ3, and LS2 (See Appendix A Reference 5).

6. In September 2014, JAEA published revised fuel enthalpy predictions for 43 previous NSRR test specimens (Reference 12).

Section 2 documents the updated regulatory basis and Section 3 documents the updated technical basis for the RIA acceptance criteria and guidance.

Figure 1-1: Fuel Response to a Rapid Reactivity Insertion

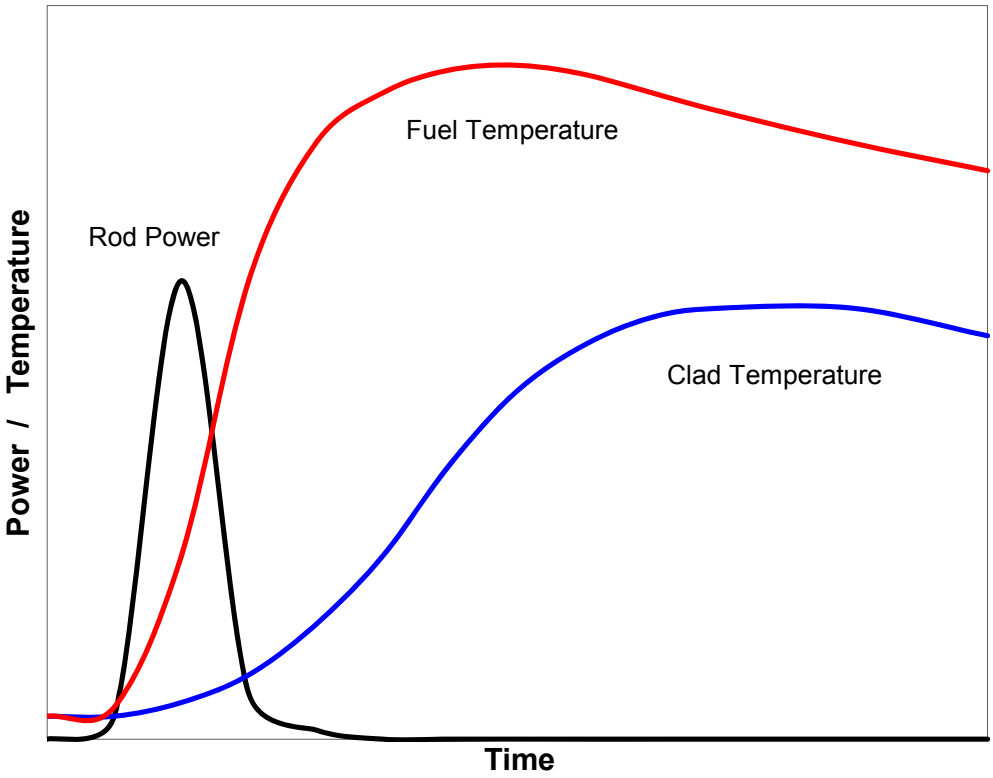

2.0 REGULATORY EVALUATION

10CFR50 Appendix A, General Design Criterion 28 (GDC28) requires the reactivity control system to be designed with appropriate limits on the potential amount and rate of reactivity increase to assure that the effects of postulated reactivity accidents can neither:

a. Result in damage to the reactor coolant pressure boundary greater than limited local yielding, nor

b. Sufficiently impair core cooling capability.

Because the PWR rod ejection and BWR rod drop accidents are classified as Condition IV events, fuel rod failure may occur during these events - provided offsite and control room radiological consequences remain within acceptable limits. Specific guidance on the implementation of GDC28 requirements has been detailed within Regulatory Guide (RG) 1.77 and NUREG-0800 SRP. RG 1.77 identifies acceptable PWR analytical methods and assumptions as well as the following acceptance criteria to address GDC 28.

1. Fuel radial average energy density limited to 280 cal/g at any axial node.Maximum reactor pressure limited to the value that will cause stresses to exceed the Emergency Condition (Service Level C) as defined in the ASME Boiler and Pressure Vessel code.

2. Offsite dose consequences limited to “well within” the guidelines in 10CFR Part 100.

The regulatory basis of the first criterion on fuel enthalpy is to maintain a coolable geometry. As described in Section 3.2 of Reference 1, the current RG 1.77 criterion of 280 cal/g was judged inadequate to ensure a fuel rod bundle array and long-term coolability are maintained.

The regulatory basis of the second criterion on reactor pressure is to maintain the integrity of the reactor pressure boundary. Given the low probability of these postulated accidents, Service Level C is adequate to satisfy this basis. Note that the calculation of the pressure surge must include (1) any RCS pressure increase associated with the core power excursion, (2) any mechanical energy generated from Fuel-Coolant Interaction (FCI) and (3) any contribution to pressure surge from burst rods.

The basis of the third criteria on offsite dose is to protect the health and safety of the public. This criterion, by itself, is adequate and not being altered. The term “well within” equates to 25% of allowable limits. For example, the allowable radiation dose for an individual located on the boundary of the exclusion area for any 2-hour period would be 6.25 rem Total Effective Dose Equivalent (TEDE) (equivalent to 25% of 25 rem TEDE prescribed in 0.CFR50.67(b)(2)(i)).

The total fission product inventory available for release must include (1) steady-state fuel/clad gap fraction and (2) transient-induced gas release from the fuel pellet.

RG 1.77 states that the number of fuel rods experiencing clad failure should be calculated and used to obtain the amount of fission product inventory released to the reactor coolant system. NUREG-0800 SRP Section 4.2 defines RIA fuel clad failure criteria.

1. Radial average fuel enthalpy greater than 170 cal/g for BWRs at zero or low power,

2. Local heat flux exceeding fuel thermal design limits (e.g., Departure from Nucleate Boiling Ratio (DNBR) and Critical Power Ratio (CPR)) for all PWR events and at-power events in BWRs.

SRP Section 4.2.I identifies principle review objectives for fuel designs. Item (3) states that the number of fuel rod failures is not underestimated for postulated accidents. Prior guidance (before 2007) did not identify Pellet Cladding Mechanical Interaction (PCMI) as a fuel cladding failure mechanism. As a result, the number of failed fuel rods may have been underestimated. As described in Reference 1, the PCMI fuel cladding failure threshold (expressed in terms of Δcal/g versus cladding hydrogen content) is more limiting than the 170 cal/g (total enthalpy) for highly corroded fuel rods. Interim PCMI cladding failure criteria for cold BWR conditions and hot PWR conditions were provided in Reference 1.

3.0 TECHNICAL EVALUATION

For many years, the U.S. Nuclear Regulatory Commission (NRC) has been aware of potential problems with the RIA acceptance criteria. In 1980, MacDonald et al. (Reference 6) reviewed earlier test data from the Special Power Excursion Test Reactor (SPERT) and Transient Reactor Test Facility (TREAT) research programs (which form the basis of the initial regulatory limits) and then compared these earlier tests to the then recent Power Burst Facility (PBF) test results. MacDonald concluded that:

1. The NRC expressed the RIA criteria in terms of fuel enthalpy, whereas the SPERT and TREAT data were reported in terms of total energy deposition. Based on this difference, a more appropriate value for the RIA criteria would have been 230 cal/g (radial average fuel enthalpy).

2. LWR fuel rods subjected to the regulatory limit, radial average fuel enthalpy of 280 cal/g, will be severely damaged and post-accident cooling may be impaired.

3. PCMI clad failure may result at a radial average fuel enthalpy of 140 cal/g on irradiated LWR fuel rods as compared to the 170 cal/g failure criteria.

4. Fuel grain-boundary separation and powdering also contribute to a loss of rod geometry during quenching.

5. The mode of fuel rod failure is strongly dependent on previous irradiation history.

Based upon calculated peak fuel enthalpy using best-estimate methods, with the effects of void formation and prompt moderator feedback included, MacDonald et al. concluded that a significant safety concern did not exist.

In 2004, the staff completed a safety assessment of currently operating reactors in response to the latest results from international RIA test programs (e.g. Nuclear Safety Research Reactor (NSRR), CABRI, IGR, and Russian Fast Impulse Graphite Reactor (BIGR). Research Information Letter 0401 (Reference 7) compiled all of the RIA test results and performed limited scaling to account for non-prototypical test conditions. As part of RIL 0401, best-estimate neutronic analyses were performed for a range of LWR conditions and it was found that the control rod worths needed to reach the cladding failure threshold were beyond expected values.

Without cladding failure, coolable geometry is ensured and energetic fuel-to-coolant interaction is avoided. This regulatory position is similar to that of MacDonald 20+ years earlier.

In 2007, the staff issued the following interim RIA acceptance criteria and guidance (SRP 4.2 Appendix B, Revision 3).

Fuel Cladding Failure:

The total number of fuel rods which must be considered in the radiological assessment is equal to the summation of all of the fuel rods failing each of the criteria. Applicants do not need to double count fuel rods which are predicted to fail more than one of the criteria.

- The high cladding temperature failure criteria for zero power conditions is a peak radial average fuel enthalpy greater than 170 cal/g for fuel rods with an internal rod pressure at or below system pressure and 150 cal/g for fuel rods with an internal rod pressure exceeding system pressure. For intermediate and full power conditions, fuel cladding failure is presumed if local heat flux exceeds thermal design limits (e.g. DNBR and CPR).

- The PCMI failure criteria is a change in radial average fuel enthalpy greater than the corrosion-dependent limit depicted in Figure 3.1-3 of Reference 1 (PWR) and Figure 3.1-9 of Reference 1 (BWR).

Coolability Criteria:

Fuel rod thermal-mechanical calculations must be based upon design-specific information accounting for manufacturing tolerances and modeling uncertainties using NRC approved methods including burnup-enhanced effects on pellet power distribution, fuel thermal conductivity, and fuel melting temperature.

1. Peak radial average fuel enthalpy must remain below 230 cal/g.

2. Peak fuel temperature must remain below incipient fuel melting conditions.

3. Mechanical energy generated as a result of (1) non-molten fuel-to-coolant interaction and (2) fuel rod burst must be addressed with respect to reactor pressure boundary, reactor internals, and fuel assembly structural integrity.

4. No loss of coolable geometry due to (1) fuel pellet and cladding fragmentation and dispersal and (2) fuel rod ballooning.

Fission-Product Inventory:

The total fission-product inventory available for release upon cladding failure equals the steady-state gap inventory (from the applicable RG) plus the transient release (calculated with the correlation provided in Section 3.3 of Reference 1).

As described in Section 1, the purpose of this report is to revise, as necessary, the technical and regulatory basis of the RIA acceptance criteria and guidance based upon the latest information. Section 3.1 describes the RIA empirical database including the recent NSRR hot

capsule tests and revised data. Section 3.2 describes changes to the fuel rod cladding failure thresholds. Section 3.3 describes changes to the coolable geometry criteria. Section 3.4 describes changes to the radiological source term.

3.1 RIA Empirical Database

In addition to the recent NSRR hot capsule test results, several of the original reported test results have been revised based on new information. The NEA report provides a detailed summary of the complete RIA empirical database (Appendix A of Reference 2). Note that the NEA report was published prior to the revised NSRR data.

In September 2014, JAEA published revised fuel enthalpy predictions for 43 previous NSRR test specimens (Reference 12). The compiled, up-to-date RIA empirical database is depicted in the following figures:

Figure 3.1-1: Reported Peak and Failed Fuel Enthalpy Versus Burnup

Figure 3.1-2: Reported Peak and Failed Fuel Enthalpy Versus Pulse Width

Figure 3.1-3: Reported Peak and Failed Fuel Enthalpy Versus Oxide Thickness

Figure 3.1-4: Reported Peak and Failed Fuel Enthalpy Versus Oxide/Wall Thickness

Figure 3.1-5: Reported Peak and Failed Fuel Enthalpy Rise Versus Burnup

Figure 3.1-6: Reported Peak and Failed Fuel Enthalpy Rise Versus Cladding Hydrogen

Figure 3.1-7 provides a comparison of the original and revised NSRR data plotted as a function of fuel enthalpy rise versus excess cladding hydrogen content. Note that Reference 12 did not report a revised fuel enthalpy change at failure for test FK9. In conversations with JAEA staff, it was identified that FK9 had a revised failure enthalpy of 349 J/g (83.4 cal/g).

Figure 3.1-1: Reported Peak and Failed Fuel Enthalpy Versus Burnup

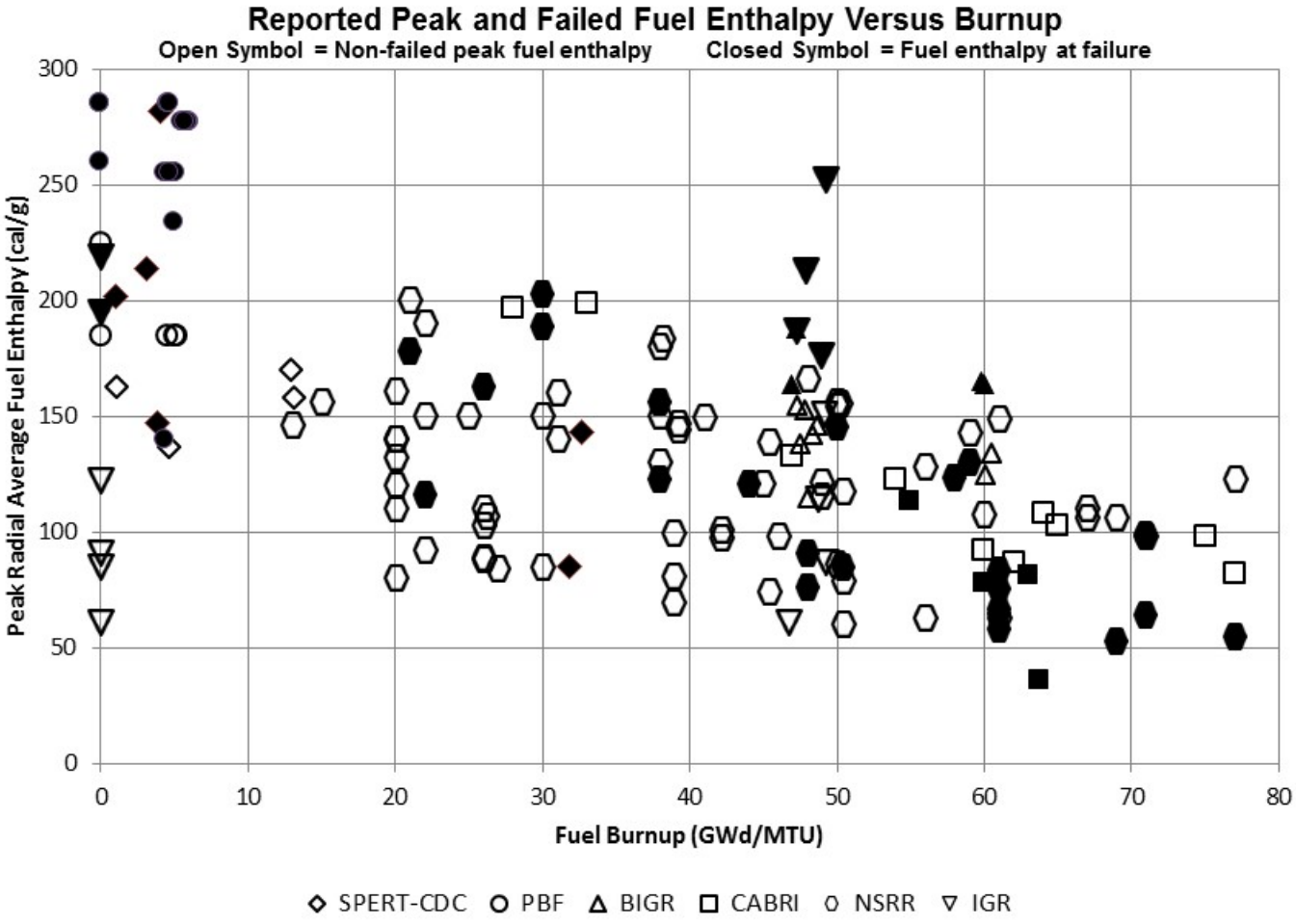

Figure 3.1-2: Reported Peak and Failed Fuel Enthalpy Versus Pulse Width

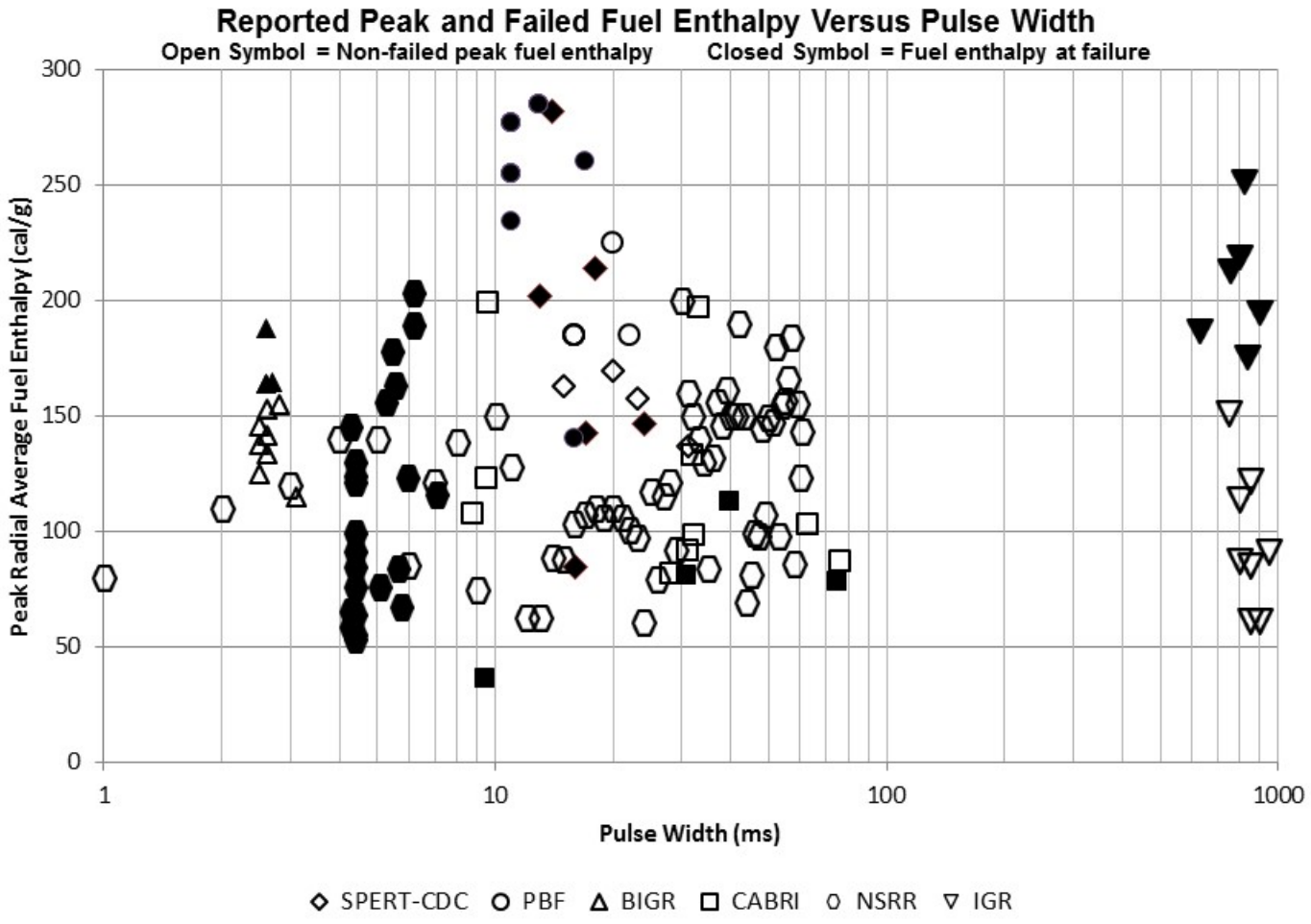

Figure 3.1-3: Reported Peak and Failed Fuel Enthalpy Versus Oxide Thickness

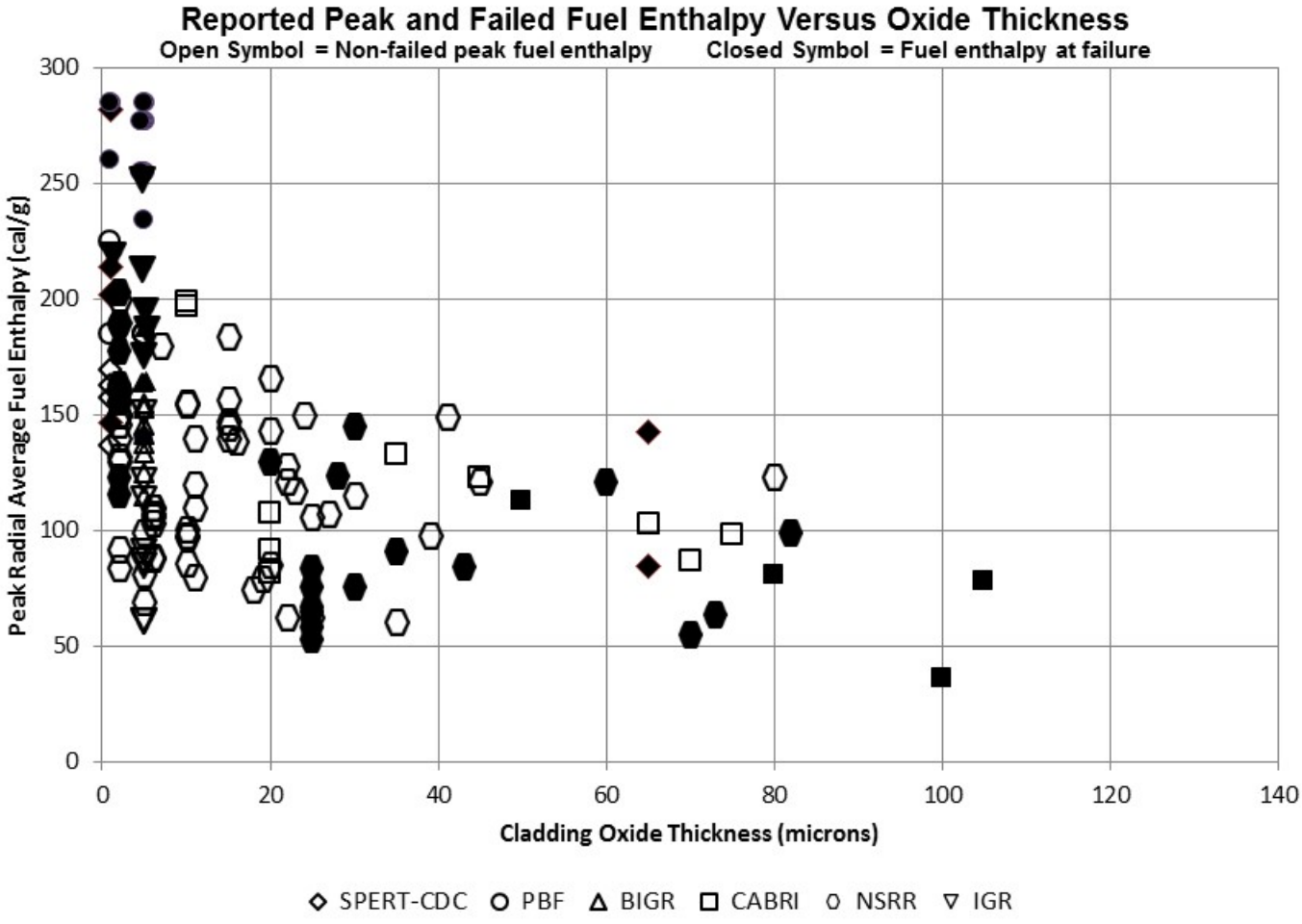

Figure 3.1-4: Reported Peak and Failed Fuel Enthalpy Versus Oxide/Wall Thickness

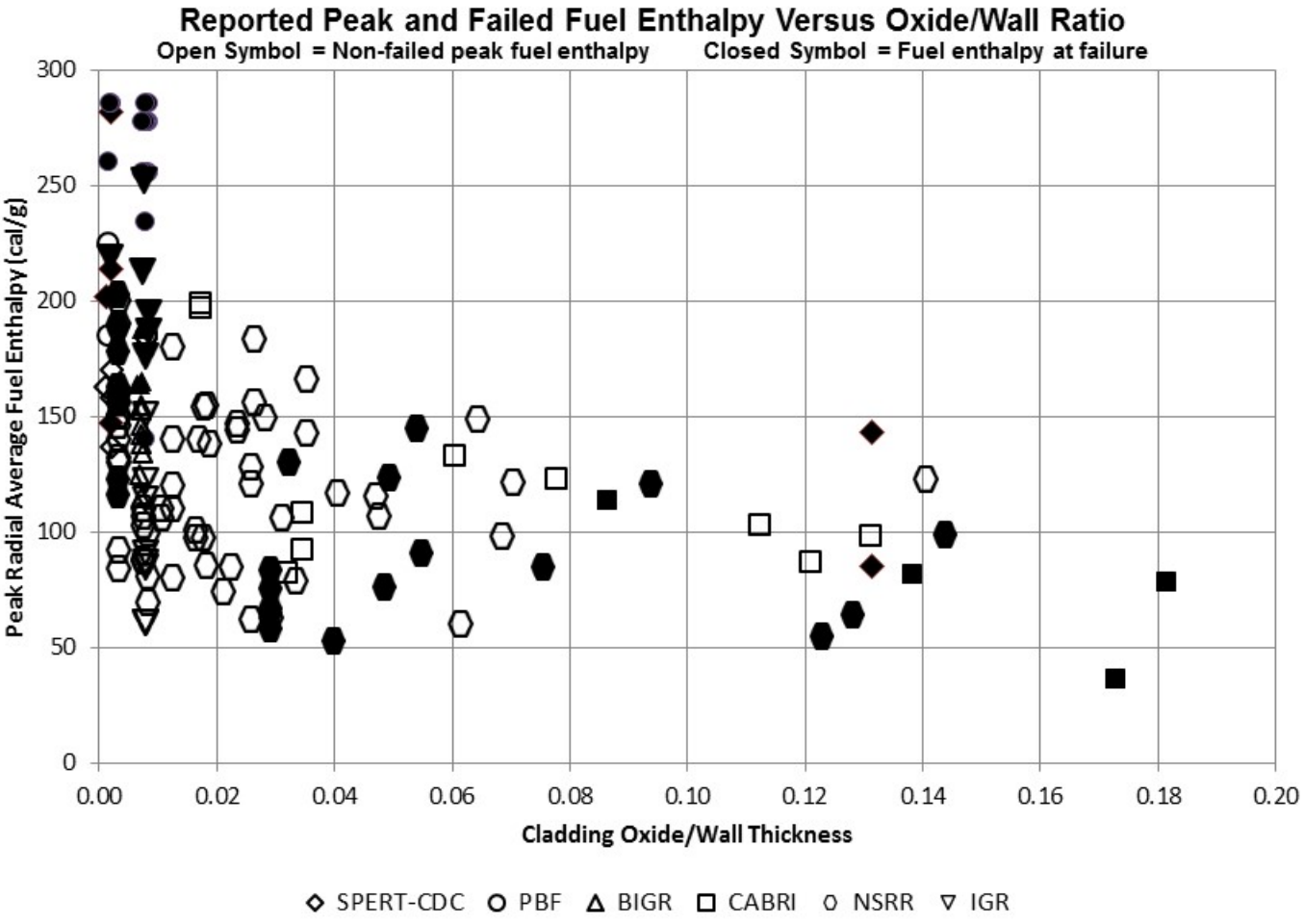

Figure 3.1-5: Reported Peak and Failed Fuel Enthalpy Rise Versus Burnup

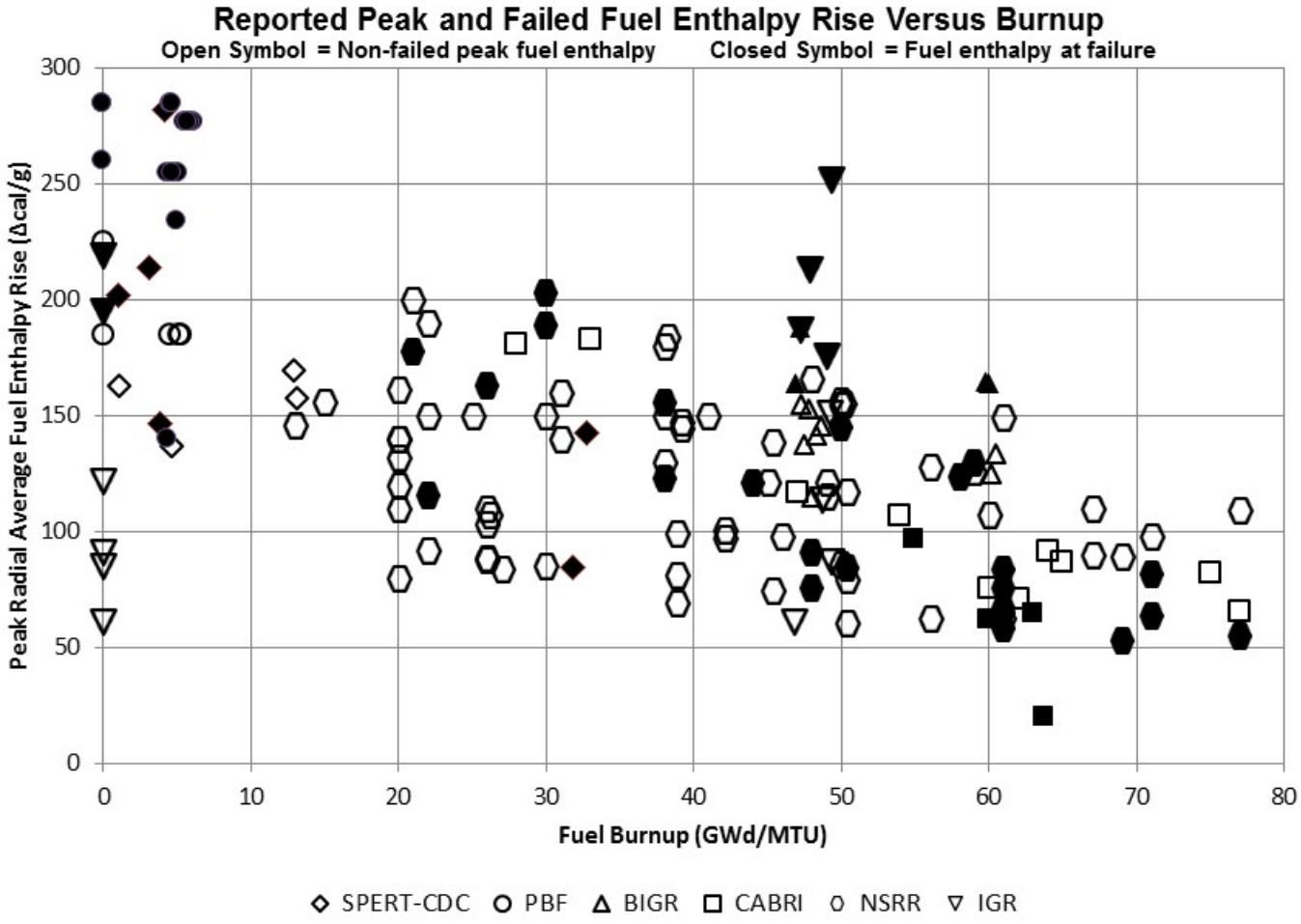

Figure 3.1-6: Reported Peak and Failed Fuel Enthalpy Rise Versus Cladding Hydrogen

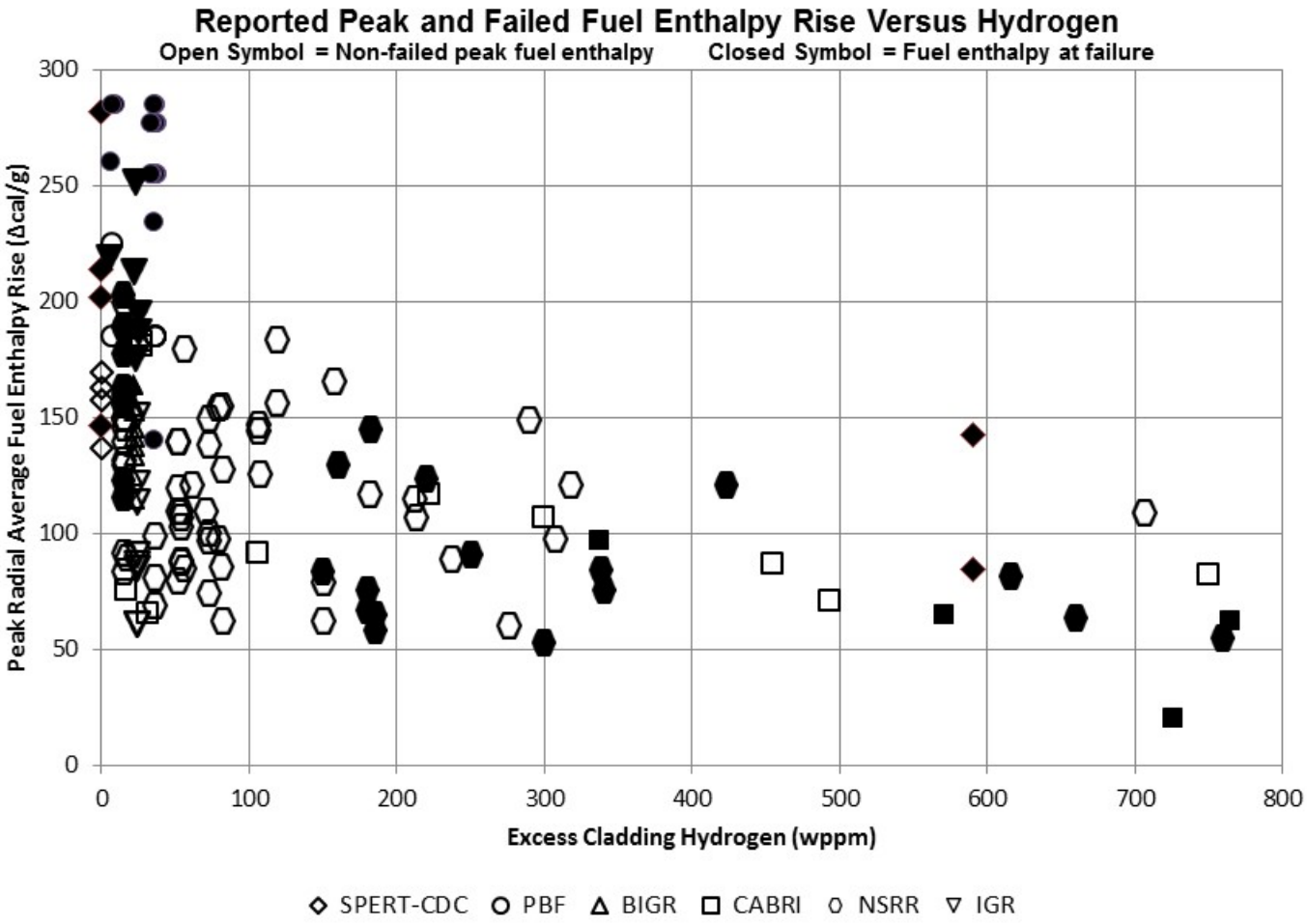

Note: For a majority of the data, cladding hydrogen content calculated using alloy-specific corrosion and hydrogen uptake models based on measured oxide thickness and reported fuel burnup. An average value was utilized for instances where a range of oxide thickness was reported. Several recent NSRR and CABRI tests reported cladding hydrogen content. Similar to oxide thickness, an average value was utilized where a range was presented.

Figure 3.1-7: Revised NSRR RIA Empirical Database

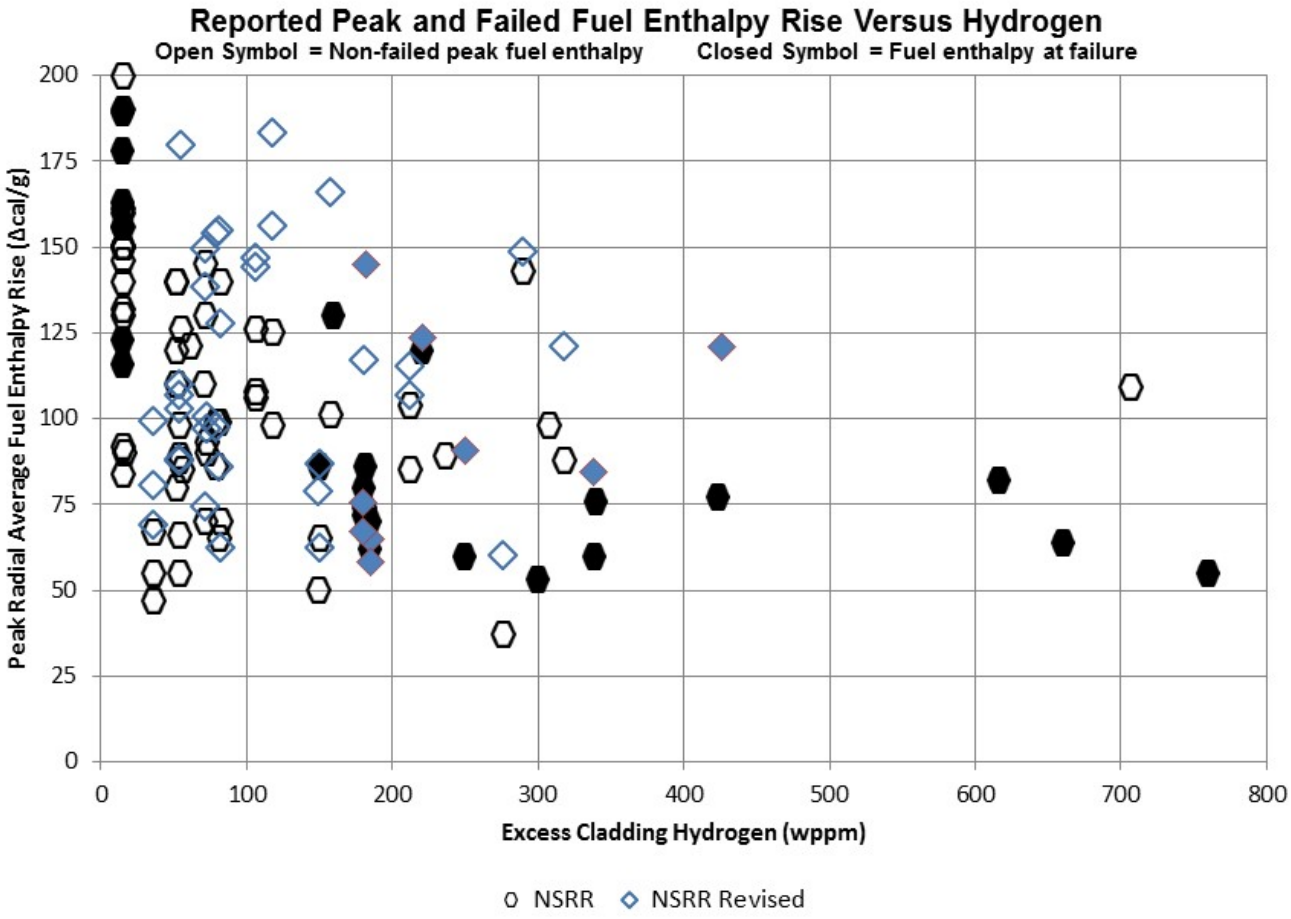

3.2 Fuel Cladding Failure Thresholds

To ensure that regulatory criteria associated with offsite and onsite radiological consequences are satisfied, the number of fuel rod failures must not be underestimated. Fuel cladding failure mechanisms associated with RIAs include:

1. Brittle Failure: High-temperature post-Departure from Nucleate Boiling (DNB) (film-boiling) oxygen-induced embrittlement and fragmentation.

2. Ductile Failure: High-temperature cladding creep (rod ballooning and burst).

3. PCMI: Hydrogen-enhanced PCMI cladding failure.

4. Fuel Melt: Molten fuel-induced swelling PCMI cladding failure.

MacDonald et al. concluded that the mode of fuel rod failure is strongly dependent on previous irradiation history. Irradiation history would include power history, burnup, and in-service cladding corrosion (oxidation). Other important factors contributing to fuel rod failure include (1) the initial conditions of the fuel rod (e.g. initial fuel enthalpy, fuel-to-clad gap, rod internal pressure), (2) the initial conditions of the reactor coolant (e.g. temperature, pressure, mass flow), and (3) fuel design. Of course, the governing influence on the fuel rod's response to the postulated transient is the amount and rate of reactivity insertion. The influence of each of these factors differs for each failure mechanism.

PCMI cladding failure is predicted to occur relatively early in the event prior to any significant increase in cladding temperature. Whereas, failure mechanisms #1 and #2 involve high cladding temperature phenomena (e.g. reduced yield strength, oxygen diffusion into base metal) and will experience failure later in the event progression.

3.2.1 High-Temperature Cladding Failure Technical Basis

To address the above high-temperature failure mechanisms (#1 and #2), the interim RIA acceptance criteria and guidance (SRP 4.2 Appendix B) define the following cladding failure thresholds:

- The high cladding temperature failure criteria for zero power conditions is a peak radial average fuel enthalpy greater than 170 cal/g for fuel rods with an internal rod pressure at or below system pressure and 150 cal/g for fuel rods with an internal rod pressure exceeding system pressure. For intermediate and full power conditions, fuel cladding failure is presumed if local heat flux exceeds thermal design limits (e.g. DNBR and CPR).

The impact of new information (items #1 through #6, Section 1) on the interim high-temperature cladding failure thresholds are described below.

1. OECD Nuclear Energy Agency State-of-the-art Report, "Nuclear Fuel Behaviour under RIA Conditions," 2010 (Reference 2).
    - Section 6.2.5.2 of the NEA report details high-temperature cladding failure mechanisms and the empirical database. No new data is presented, however, the NEA report offers some important perspectives which are discussed below.

2. Electric Power Research Institute (EPRI) Report 1021036, "Fuel Reliability Program: Proposed RIA Acceptance Criteria," December 2010 (Reference 3).

    - Section 3.2 of the EPRI report provides background on high-temperature cladding failure and the following industry position:

        - At maximum radial average fuel enthalpy levels below 150 cal/g, the cladding temperatures will remain well below the conditions to produce failure by oxidation-induced embrittlement.
        - Cladding failure by ballooning and burst in high burnup fuel rods are unlikely below a maximum fuel enthalpy of 170 cal/g.
        - Based on these observations, it can be concluded that cladding failure of UO2 fuel below fuel enthalpy levels of 150 cal/g is only possible by pellet-cladding mechanical interaction.

3. Revised RIA transient fission gas release fractions (Reference 4).

    - No new information related to high-temperature cladding failure.

4. PNNL Report 22549, "Pellet-Cladding Mechanical Interaction Failure Threshold for Reactivity Initiated Accidents for Pressurized Water Reactors and Boiling Water Reactors," June 2013 (Reference 5).

    - No new information related to high-temperature cladding failure.

5. JAEA published results from NSRR Hot Capsule RIA Test VA3, VA4, RH2, BZ3, and LS2 (See Appendix A Reference 5).

    - No new information related to high-temperature cladding failure.

6. JAEA published revised fuel enthalpy predictions for 43 previous NSRR test specimens (Reference 12).

JAEA data relied upon to develop the empirically-based cladding failure criteria. Hence, the revised data will have a direct impact.
Section 6.2.5.2 of the NEA report documents the following observation:

> "The peak fuel enthalpy to failure clearly drops with increasing fill pressure for the un-irradiated NSRR rods, but the irradiated rods seem to fail at about 650-700 $J(gUO_2)^{-1}$, irrespective of the initial gas pressure. Since the irradiated rods had burn-ups of 47-60 $MWd(kgU)^{-1}$, it is likely that transient fission gas release under the film-boiling phase made up the dominant part of the pressure loading in the low pressure rods, and that the initial fill gas pressure was relatively unimportant for the high burn-up rods."

The high temperature ballooning failure database used in the development of the SRP interim criteria (Figure 3.1-2 of Reference 1) was reproduced as Figure 3.2.1-1 of this report. Note that this figure is similar to the data discussed in the NEA report (See Figure 49 of Reference 2) and the EPRI report (See Figure 3-4 of Reference 3). These figures show peak fuel enthalpy from

various BIGR and Impulse Graphite Reactor (IGR) tests on irradiated fuel rod segments and NSRR tests on pressurized, unirradiated fuel rod segments. Figure 3.2.1-2 combines this high temperature ballooning failure database with the entire RIA database and illustrates peak fuel enthalpy as a function of fuel burnup. Figure 3.2.1-3 provides the same information but as a function of rod fill pressure. Test results from high burnup and heavily corroded fuel rods which failed due to PCMI have been removed. All CABRI test results were removed due to non-prototypical cladding temperatures experienced in the Sodium loop (relative to water). In addition, test results from failed Japanese Material Test Reactor (JMTR) rodlets were also removed. As described in Section A.5.4 of Reference 2, these JMTR rodlets and their results are not representative of LWR fuel.

Before we discuss these figures and the development of a failure threshold, it is important to highlight that the data is presented as peak fuel enthalpy. Unlike the PCMI failure plots, the fuel enthalpy at the time of cladding failure (i.e., failure enthalpy) is not reported. Hence, cladding failure may have occurred at a lower enthalpy than the reported peak fuel enthalpy. Under these circumstances, more data sets for each variable are necessary to establish the boundary between failure and non-failure.

Examination of Figure 3.2.1-2 does not reveal a significant burnup effect on failure threshold. Based on data from fresh and irradiated fuel, the boundary between failure and non-failure remain constant at approximately 160 cal/g. A closer look at the data is necessary to confirm NEA's observation regarding the impact of burnup. Table 3.2.1-1 provides a comparison of select IGR/BIGR data sets. A comparison of RT-8, RT-9, and RT-10 suggests that transient fission gas release in these high burnup rods dominated the initial fill pressure. This observation is consistent with the NEA report. Since the fuel enthalpy at failure is unknown, the effect of any difference in transient fission gas release between RT-8 (60 GWd/MTU) and RT-10 (47 GWd/MTU) is difficult to quantify. A similar comparison of non-failed specimens RT-6 and RT-12 confirms the minimal impact of initial pressure on failure threshold.

The tight grouping of narrow pulse BIGR and wide pulse IGR test results in Figures 3.2.1-2, as well as the comparison of RT-6 and H1T in Table 3.2.1-1, suggests that pulse width effects are minimal on failure threshold.

In contrast, Figure 3.2.1-3 illustrates a clear trend of decreasing failure threshold with increasing cladding differential pressure. The pressurized, unirradiated NSRR test results suggest a linear relationship between failure enthalpy and cladding differential pressure dropping from 190 cal/g at 0 MPa with a slope of 20 cal/g/MPa. As shown in Figure 3.2.1-3, the IGR and BIGR test results on irradiated fuel support this y-intersect and slope. Incorporating a cladding differential pressure dependent failure threshold is consistent with NEA observations and the slope of this relationship is consistent with an earlier EPRI presentation (See Figure 3.1-2 of Reference 1). Based upon expected fuel rod conditions, including fission gas release, rod power history, and restricted axial gas flow, the EPRI report concludes that failure by ballooning and burst in high burnup, overpressure fuel rods is unlikely. The EPRI report also states that low to intermediate burnup fuel rods have internal gas pressure below system pressure and therefore the driving forces are insufficient to produce ballooning deformations. As a result of these observations, the industry proposed a peak radial average fuel enthalpy failure threshold of 170 cal/g. While these observations have some merit, fuel rod designs and operating conditions continue to evolve and it is prudent to define failure thresholds based on limiting conditions.

In Section 3.2.1 of Reference 3, EPRI concludes the following:

> "A comparison of cladding temperature from RIA-simulation tests with the failure boundary from Figure 3-1 indicates that cladding failure by oxidation-induced embrittlement following an RIA event is unlikely at fuel enthalpy levels below 170 cal/gm."

As described above, the EPRI report documents an industry position with respect to the cladding failure thresholds for (1) oxidation-induced embrittlement and (2) ballooning and burst. Based upon experimental data including measured cladding surface temperatures from NSRR experiments with post-DNB operation, the EPRI report concludes the following limiting high temperature failure threshold:

> "At maximum radial average fuel enthalpy levels below 150 cal/g, the cladding temperatures will remain well below the conditions to produce failure by oxidation-induced embrittlement."

It is likely this position was based on the historical practice of truncating PCMI failure for low corrosion rods at 150 Δcal/g. Within the main body of their report, EPRI concludes that fuel failure from either oxidation-induced embrittlement or ballooning and burst is unlikely below 170 cal/g peak fuel enthalpy.

An examination of the empirical database depicted in Figure 3.2.1-3 reveals only 1 failed rod below data point the red dotted line. BIGR test RT-9 consisted of a 60 GWd/MTU fuel rod segment clad in E110 alloy and failed at a reported peak enthalpy of 165 cal/g. As described in the NEA report, it is likely that RT-9 experienced transient Fission Gas Release (FGR) during the power pulse which increased rod internal pressure.

Both differential pressure and elevated temperature are necessary to achieve cladding failure due to balloon rupture. Hence, at some point, the relationship between differential pressure and cladding failure (negative slope of 20 cal/g per MPa) is no longer valid since cladding temperature remains low enough to preclude balloon rupture. Figure 29 of the NEA report provides measured cladding surface temperatures under RIA simulation tests in NSRR. Examination of this figure reveals that cladding temperatures remain below 800 °F during tests where peak radial average fuel enthalpy was less than 80 cal/g. Figure 6 of Reference 12 provides measured cladding surface temperature based on JAEA's revised fuel enthalpies for the NSRR test program. Consideration of the revised data increases the 800 °F threshold to above 100 cal/g peak radial average fuel enthalpy. Note that only the irradiated test results were considered since high rod internal pressure (above system pressure) may only occur in high exposure fuel rods.

NUREG-0630 provides cladding rupture models based upon mechanical testing of zirconium alloy tubes. Examination of NUREG-0630 reveals that cladding rupture at 800 °F is unlikely at end-of-life (EOL) rod internal pressure design limits (proprietary limits established to avoid cladding liftoff). Note that the $\alpha \rightarrow \alpha+\beta$ phase transition temperature (approximately 1340 °F, depends on alloy composition) is well above 800 °F. Based on this information, the staff has set a lower threshold for cladding failure of 100 cal/g.

Based upon a review of the entire empirical database and an analytical requirement to consider transient FGR, the staff recommends maintaining the upper high temperature failure threshold of 170 cal/g. This failure threshold considers both oxidation-induced embrittlement and balloon

and burst failure modes. Combining this upper threshold with the cladding differential pressure relationship yields a composite high temperature cladding failure threshold. The red line on Figure 3.2.1-4 depicts this composite failure threshold which is represented by the following equation:

High-Temperature Cladding Failure Threshold:

Cladding differential pressure $\leq$ 1.0 Mpa,
Peak radial average fuel enthalpy = 170 cal/g

Cladding differential pressure > 1.0 Mpa, < 4.5 MPa
Peak radial average fuel enthalpy = 170 – ((ΔP – 1.0)*20) cal/g

Cladding differential pressure $\geq$ 4.5 Mpa,
Peak radial average fuel enthalpy = 100 cal/g

Following a brief discussion on high-temperature oxidation tests, the NEA report concludes,

> "… since it cannot be ruled out that the film-boiling phase in some scenarios for RIA in light water reactors may have longer duration, and that embrittlement-induced clad failure thus is possible at lower cladding temperatures and at lower fuel enthalpies than the typical pulse reactor threshold value of 1 050 $J(gUO_2)^{-1}$, acceptance criteria usually postulate that fuel rod failure should be assumed when film-boiling is predicted to occur under the reactivity-initiated accident."

For many reactor designs, technical specification limits on allowable rod insertion will preclude a prompt critical power excursion for at-power RIAs. Unlike narrow pulse prompt excursions, the broad power pulse experienced in these scenarios allows for cladding temperatures to rise and transfer heat to the coolant. As the rate and amount of reactivity insertion decreases, these scenarios begin to behave more like traditional overpower events (e.g., excess load, bank Control Element Assembly withdrawal, rod withdrawal error). Since the empirical database used above to define the high cladding temperature failure does not encompass all power operating conditions (e.g., coolant conditions, DNB/CPR thermal margin), the staff maintains that for at-power conditions (> 5% rated thermal power) any fuel rod predicted to exceed thermal design limits (DNB and CPR) must be assumed to fail and must be accounted for in dose calculations.

Regulatory Guide 1.77 established the presumption of cladding failure at the onset of DNB. However, RG 1.77 also included the following provision:

> "Other DNB or clad failure correlations may be used if they are adequately justified by analytical methods and supported by sufficient experimental data."

Alternative cladding failure criteria will be addressed on a case-by-case basis.

3.2.1.1 Applicability

As described below in Table 3.2.1-2, the RIA database encompasses a wide array of fuel rod designs, cladding alloys, and experimental conditions (e.g. pulse width, temperature, etc.). Fuel

specimens were fabricated from BWR, PWR, and VVER commercial rods and research reactor fuel rods and included several commercial-grade cladding alloys: Zr-2, Zr-4, low tin Zr-4, ZIRLO, M5, E110, NDA, and MDA. BWR Zr-2 fuel rods samples include both liner (e.g., natural or low alloy Zr-2 bonded to cladding ID) and non-liner configurations. Based upon this comprehensive database, it is judged that the proposed non-PCMI, high cladding temperature fuel cladding failure criteria conservatively predict cladding failure (i.e., balloon/burst, post-DNB oxidation/embrittlement) at zero power conditions for both BWRs and PWRs.

Thermal-hydraulic conditions in the test capsules for the empirical database depicted in Figures 3.2.1-1 through 3.2.1-4 (e.g., stagnant water at 1 ATM and room temperature) more closely resemble BWR cold start-up conditions than PWR Hot Zero Power (HZP) conditions. However, due to the rapid temperature excursion experienced by the cladding, the initial cladding temperature (and associated mechanical properties) is not as important as in the prompt PCMI-type failure mode. Given the relatively large coolant volumes, mass flow rate, and fluid conditions of PWR coolant systems, application of the empirically-derived cladding failure threshold to PWR HZP conditions is conservative.

Section 6.2.5.2 of the NEA report also describes the potential impact of annular fuel pellets on reported test results. Based upon observations of clad ballooning and burst in rods with annular pellets whereas comparable rods with solid pellet survived, the NEA report postulates that “the central hole provides a channel for axial gas and a high gas pressure can therefore be maintained in regions where clad ballooning occurs.” This improved gas communication, relative to a high burnup, closed gap solid pellet rods, makes fuel rods with annular pellets more susceptible to clad ballooning. The NEA report also notes that annular pellets may affect PCMI since a portion of the fuel thermal expansion will be accommodated by the central hole.

Figure 3.2.1-3 shows that the annular and non-annular test results support the same relationship between failure threshold and cladding differential pressure. Application of the high temperature failure threshold (empirically derived based on both solid and annular pellet tests) to solid pellet designs is conservative. Further, modern PWR integral fuel burnable absorbers (IFBA) fuel rod designs often include axial zones with annular fuel pellets. So, any attempt to divide the limited database into solid and annular subsets may not prove useful. In addition, modern BWR fuel assembly designs include part-length fuel rods. As a result, the distance between the rod plenum region and peak fuel enthalpy may be reduced; allowing for improved axial gas communication even at high burnup conditions.

In summary, the range of applicability is limited to the following conditions:

- All PWR and BWR UO2 fuel rod designs with zirconium-based cladding, including barrier designs and fuel rods with both annular and solid pellets.
- BWR cold startup conditions up through PWR hot zero conditions.

3.2.1.2 Analytical Considerations

In addition to the above observations, Section A.4 of the NEA report provides further discussion on transient FGR and its impact on gas pressure loading. The observed failure enthalpy for the irradiated rods, 650-700 $J(gUO_2)^{-1}$ or 155-167 cal/g, is similar to the interim failure thresholds (i.e., 150-170 cal/g). However, the interim guidance does not explicitly account for transient FGR. Instead, the interim guidance provides two failure thresholds based on pre-transient rod

internal pressure. Ignoring the potential contribution of transient FGR may lead to a non-conservative application relative to the empirical database.

In contrast, Section 3.2.2 of the EPRI report concludes that the NSRR test results demonstrate that transient fission gas release will not enhance cladding ballooning and burst. Based upon expected fuel rod conditions, including fission gas release, rod power history, and restricted axial gas flow, the EPRI report concludes that failure by ballooning and burst in high burnup, overpressure fuel rods is unlikely. The EPRI report also states that low to intermediate burnup fuel rods have internal gas pressure below system pressure and therefore the driving forces are insufficient to produce ballooning deformations. While these observations have some merit, fuel rod designs and operating conditions continue to evolve and it is prudent to define failure thresholds based on limiting conditions. For example, IFBA fuel designs may promote higher rod internal pressure at a given burnup due to (1) higher fission gas release for an equivalent rod power and burnup level (e.g., Gadolinium, Erbium) and (2) potential helium generation (e.g., boron coating).

After reviewing the material presented in the NEA and EPRI reports, the staff has decided to amend the interim criteria to require the addition of transient FGR when implementing the pressure-dependent failure threshold. Hence, the initial rod internal pressure must be increased by the amount of transient fission gas release. An acceptable means of determining the amount of transient FGR is described in Section 3.5 of this report.

An approved analytical method must be used to calculate the quantity of fission gas (i.e., moles) as a function of fission density (e.g., fissions/cm^3) to convert transient FGR to a quantity of gas released.

Due to the large variation fuel enthalpy increase along the axial length of a fuel rod, the applicant may elect to (1) calculate transient fission gas release for several axial regions and (2) combine each axial contribution, along with the pre-transient gas inventory, within the calculation of total rod internal pressure. If non-equal volumes are used this needs to be accounted for in the calculation of release fractions and total gas inventory (i.e., moles) released. The number of axial regions is up to the analyst with the guidance that the fuel enthalpy within a given axial region not be underestimated. The peak radial average enthalpy change in each axial region should be used to calculate the transient fission gas release component of the gap fraction within each axial region. DG-1199 (soon be published as a revision to RG 1.183) provides further guidance.

For the application of the new cladding failure threshold, an approved fuel rod thermal-mechanical performance code must be used to predict the initial, pre-transient rod internal conditions (e.g., void volume, FGR, rod internal pressure) and final, transient rod internal pressure accounting for the above transient FGR.

Pre- and post-transient rod internal pressures are expected to vary widely (1) across the population of fuel rods in the core and (2) among different fuel rod designs within a core (e.g., standard UO2, IFBA, part-length). The applicant may elect to subdivide fuel rod populations based on peak fuel enthalpy and rod internal pressure in order to demonstrate compliance. CZP and HZP calculations should encompass both (1) BOC conditions and (2) re-start following recent full power operation. Intermediate power levels up to HFP conditions should be evaluated to confirm power-dependent core operating limits (e.g., control rod insertion limits, rod

power peaking limits, axial and azimuthal power distribution limits).

For the purpose of calculating peak fuel enthalpy for CZP, zero fuel enthalpy is defined at 20 °C (68 °F). In summary, the following analytical considerations accompany the cladding failure thresholds:

- Cladding differential pressure should include contribution from transient (fracture-induced) FGR. An approved fuel rod thermal-mechanical performance code must be used to predict the initial, pre-transient rod internal conditions (e.g., moles of fission gas, void volume, FGR, rod internal pressure) and final, transient rod internal pressure. The amount of transient FGR may be calculated using the BU-dependent correlation described in Section 3.5 of this report.

- Due to the large variation fuel enthalpy increase along the axial length of a fuel rod, the applicant may elect to (1) calculate transient fission gas release for several axial regions and (2) combine each axial contribution, along with the pre-transient gas inventory, within the calculation of total rod internal pressure.

- CZP and HZP calculations should encompass both (1) BOC conditions and (2) re-start following recent full power operation.

- Intermediate power levels up to HFP conditions should be evaluated to confirm power-dependent core operating limits (e.g., control rod insertion limits, rod power peaking limits, axial and azimuthal power distribution limits).

- For the purpose of calculating peak fuel enthalpy for CZP, zero fuel enthalpy is defined at 20 °C (68 °F).

3.2.1.3 Revised Criteria and Guidance

Based upon the above discussion, the following revision to the RIA acceptance criteria and guidance is proposed:

1) For zero power conditions, the high temperature cladding failure threshold is expressed in the following relationship, as shown in Figure 3.2.1-5.

   - Cladding differential pressure $\leq$ 1.0 MPa,
     Peak radial average fuel enthalpy = 170 cal/g

   - Cladding differential pressure > 1.0 MPa, < 4.5 Mpa
     Peak radial average fuel enthalpy = 170 – ((ΔP – 1.0)*20) cal/g

   - Cladding differential pressure $\geq$ 4.5 MPa,
     Peak radial average fuel enthalpy = 100 cal/g

2) Predicted cladding differential pressure must consider the impact of transient FGR on internal gas pressure. An acceptable means of determining the amount of transient FGR is described in Section 3.5 of this report.

3) For intermediate and full power conditions, fuel cladding failure is presumed if local heat flux exceeds thermal design limits (e.g. DNBR and CPR).

Table 3.2.1-1: Data Set Results

Test Rod	Burnup (GWd/MTU)	Fill Pressure (Mpa)	Pulse Width (ms)	Failure (F/NF)	Peak Fuel Enthalpy (cal/g)
RT-8	60	2.0	2.6	F	164
RT-9	60	0.1	2.7	F	165
RT-10	47	2.0	2.6	F	164
- - - -Failure Boundary - - - -					
RT-6	48	2.1	2.6	NF	153
RT-12	48	0.2	2.8	NF	155
H1T	49	1.7	750	NF	151

Table 3.2.1-2: RIA Empirical Database

Parameter	Minimum	Maximum
Cladding O.D. (mm)	7.92	14.5
Wall Thickness (μm)	495	915
Oxide Thickness (μm)	0	110
Oxide/Wall Ratio	0.001	0.19
Cladding Hydrogen (wppm)	0	800
Fuel Rod Burnup (GWd/MTU)	0	79
Pulse Width (msec)	2.5	950
Deposited Energy (cal/g)	51	695
Peak Fuel Enthalpy (cal/g)	37	350
Fuel Enthalpy Rise (cal/g)	14	335

Figure 3.2.1-1: High Burnup Ballooning Failures

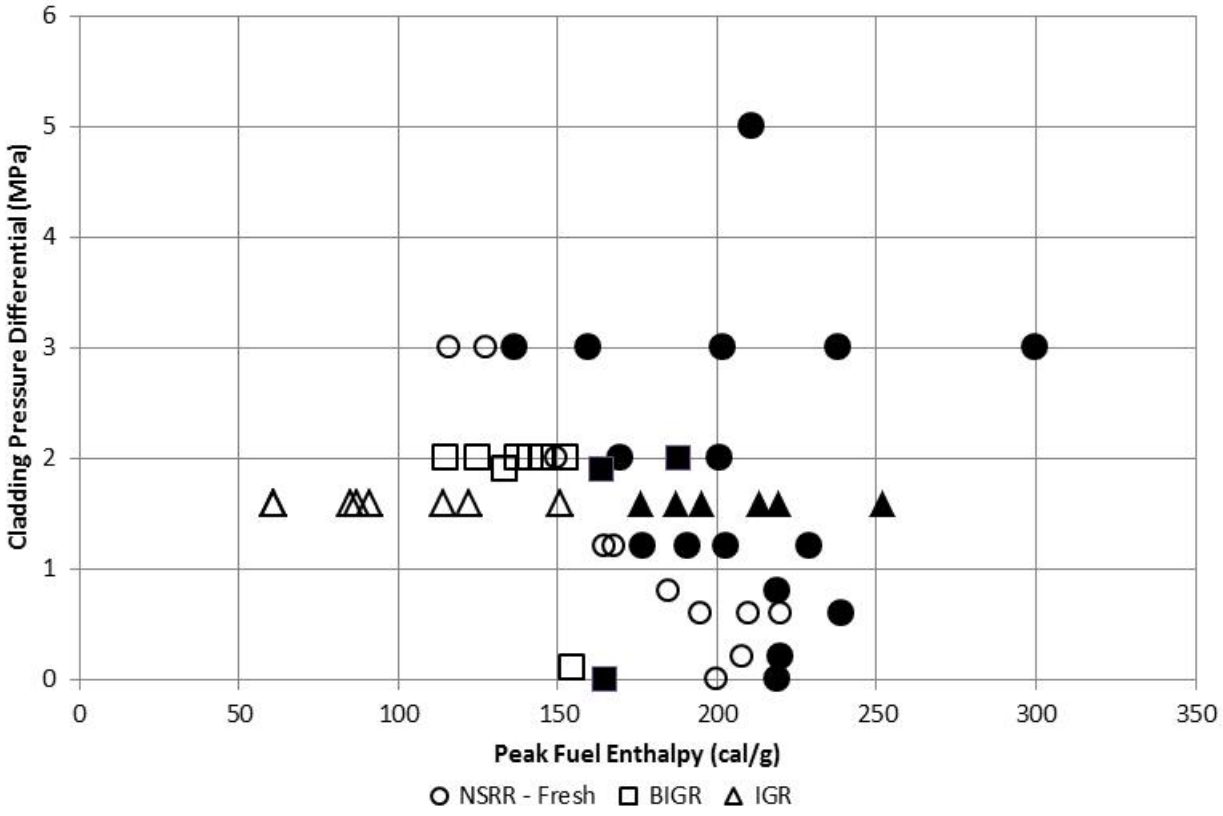

Figure 3.2.1-2: Non-PCMI Empirical Database – Peak Fuel Enthalpy Versus Burnup

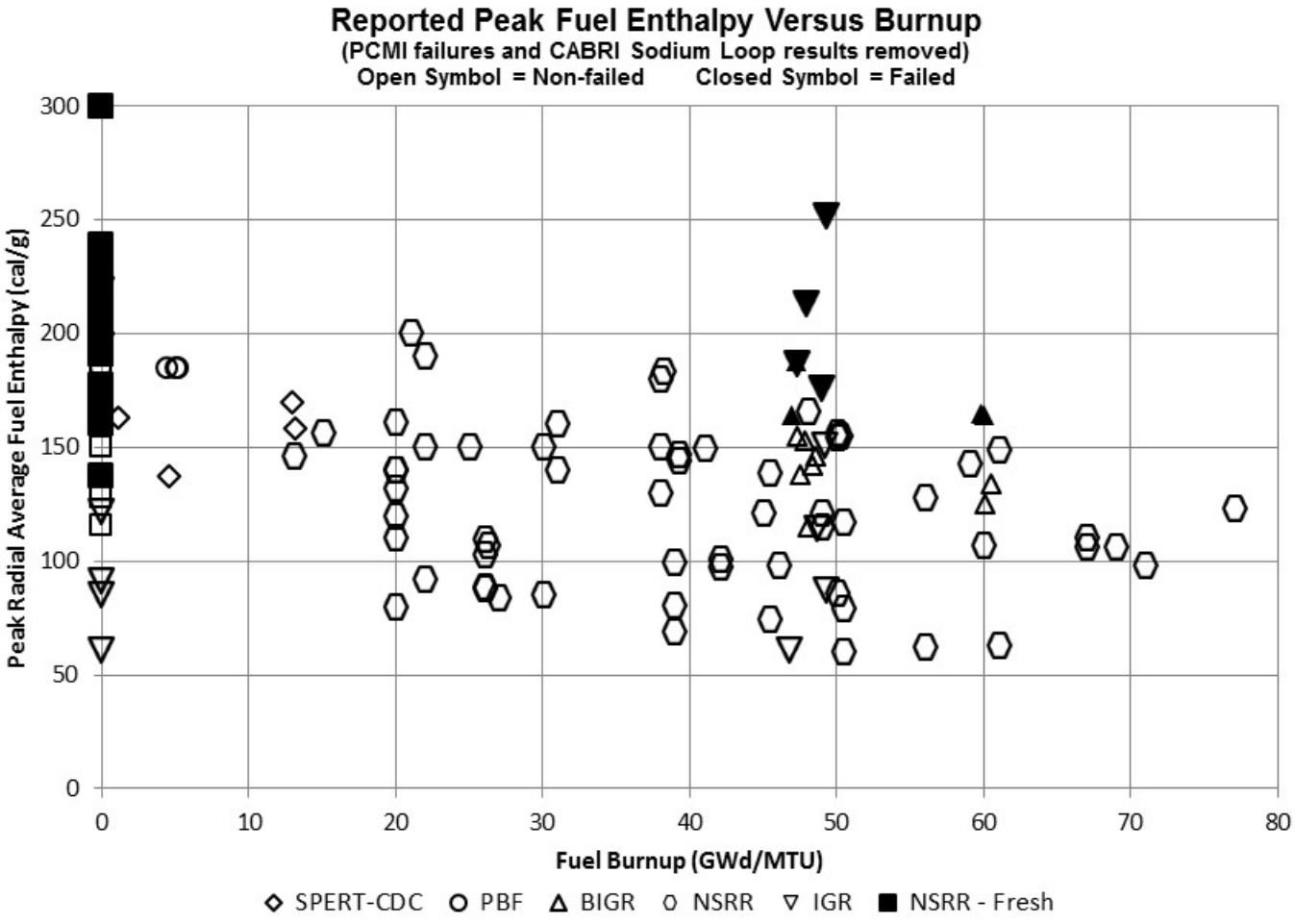

Figure 3.2.1-3: Non-PCMI Empirical Database – Peak Fuel Enthalpy Versus ΔPressure

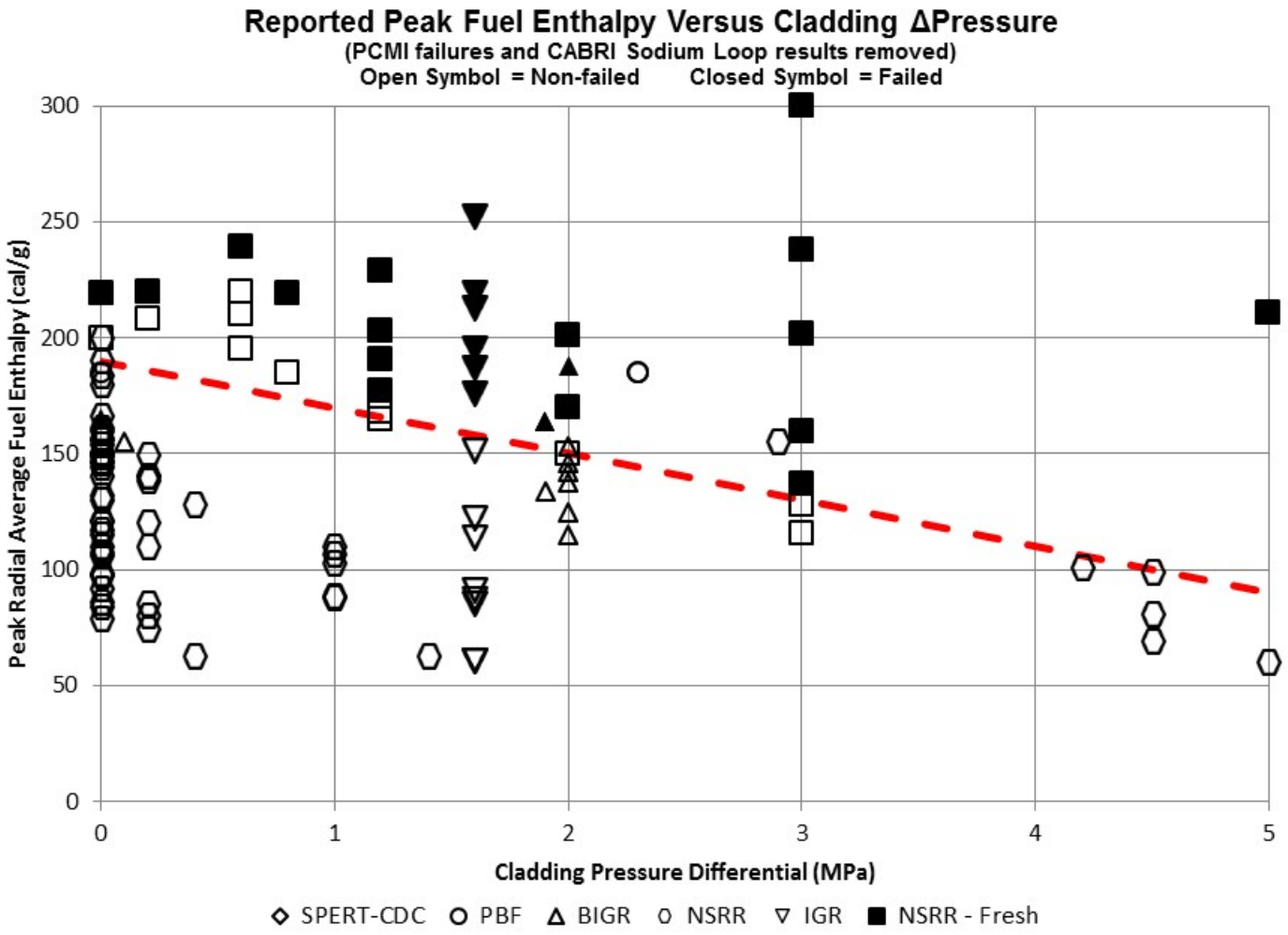

Figure 3.2.1-4: Proposed High Temperature Cladding Failure Threshold

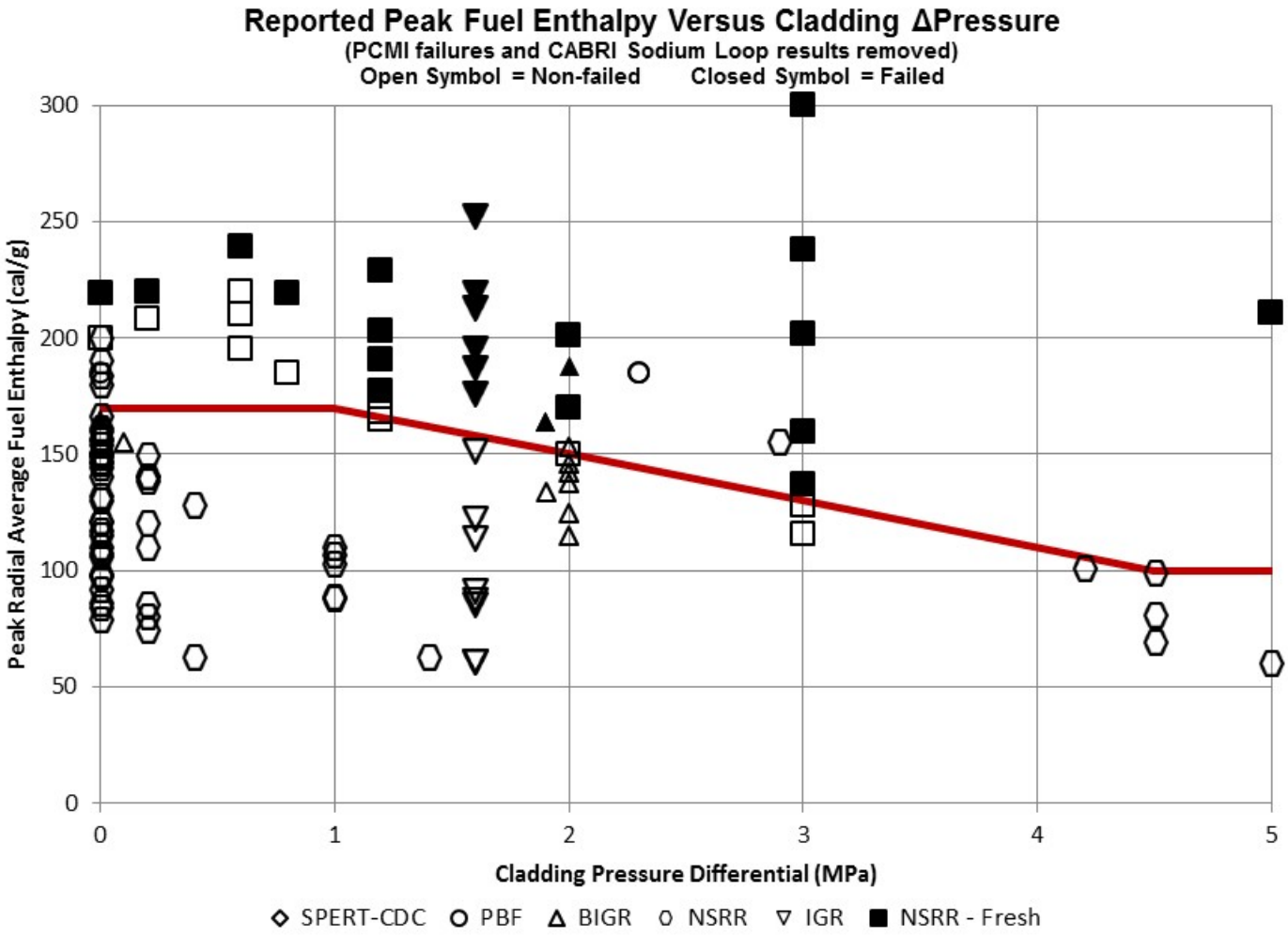

Figure 3.2.1-5

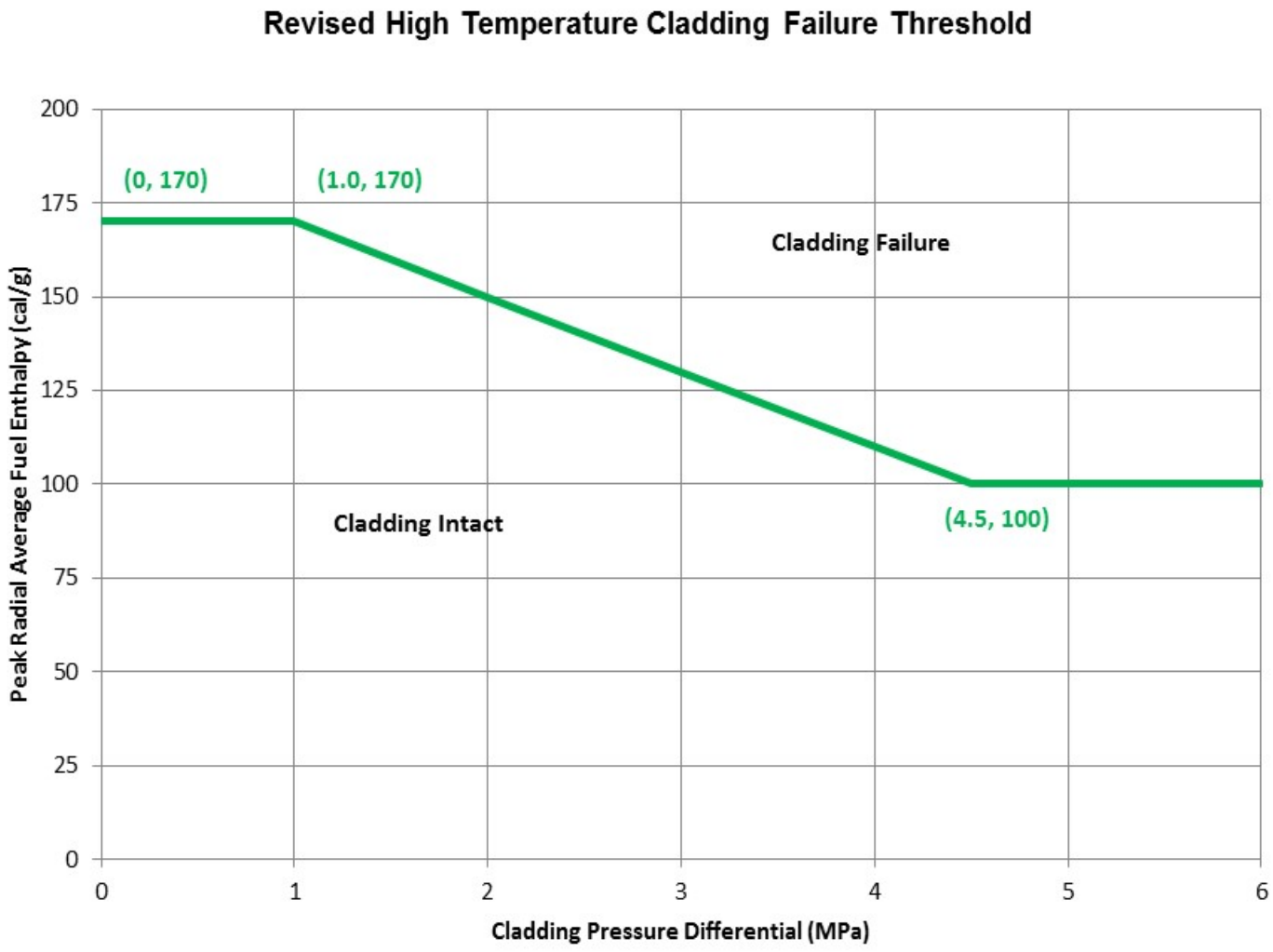
Revised High Temperature Cladding Failure Threshold
(0, 170)
(1.0, 170)
Cladding Failure
Cladding Intact
(4.5, 100)
Peak Radial Average Fuel Enthalpy (cal/g)
Cladding Pressure Differential (MPa)
200
175
150
125
100
75
50
25
0
0
1
2
3
4
5
6

3.2.2 Hydrogen-Enhanced PCMI Cladding Failure Technical Basis

To address hydrogen-enhanced PCMI cladding failure, the interim RIA acceptance criteria and guidance (SRP 4.2 Appendix B) define the following cladding failure thresholds:

- The PCMI failure threshold is a change in radial average fuel enthalpy greater than the corrosion-dependent limit depicted in Figure 3.1-3 of Reference 1 (PWR) and Figure 3.1-9 of Reference 1 (BWR).

The impact of new information (items #1 through #6, Section 1) on the interim PCMI cladding failure thresholds are described below.

1. OECD Nuclear Energy Agency State-of-the-art Report, "Nuclear Fuel Behaviour under RIA Conditions," 2010 (Reference 2).

    - The influence of temperature, hydride distribution, and hydride orientation on hydrogen-enhanced PCMI cladding failure thresholds is described.

2. EPRI Report 1021036, "Fuel Reliability Program: Proposed RIA Acceptance Criteria," December 2010 (Reference 3).

    - Proposed PCMI cladding failure thresholds are provided for PWR (SRA) and BWR (RXA) cladding alloys. Failure thresholds expressed as a function of radial average fuel enthalpy increase versus cladding hydrogen.

    - Based on critical strain energy density (CSED) cladding failure function derived from separate-effects mechanical testing and FALCON predicted strain energy density (SED) under RIA conditions.

3. Revised RIA transient fission gas release fractions (Reference 4).

    - No new information related to PCMI cladding failure.

4. PNNL Report 22549, "Pellet-Cladding Mechanical Interaction Failure Threshold for Reactivity Initiated Accidents for Pressurized Water Reactors and Boiling Water Reactors," June 2013 (Reference 5).

    - Proposed PCMI cladding failure thresholds are provided for cold RXA, hot RXA, cold SRA, and hot SRA cladding alloys. Failure thresholds expressed as a function of radial average fuel enthalpy increase versus cladding excess hydrogen.

    - Based on empirical database of failed rods under RIA test conditions.

5. Published results from NSRR Hot Capsule RIA Test VA3, VA4, RH2, BZ3, and LS2 (See Appendix A Reference 5).

    - The test results from the NSRR Hot Capsule program provide valuable insight on the effect of cladding temperature on failure enthalpy. This information was utilized to scale the earlier NSRR RIA test results performed at room temperature to PWR hot

conditions.

6. JAEA published revised fuel enthalpy predictions for 43 previous NSRR test specimens (Reference 12).

    - JAEA data relied upon to develop the empirically-based cladding failure criteria. Hence, the revised data will have a direct impact.

Both PNNL and EPRI recommend changes to the interim PCMI cladding failure thresholds presented in SRP 4.2 Appendix B. Figure 3.2.2-1 provides a comparison of PNNL's and EPRI's proposed PCMI failure threshold against the SRP interim failure threshold for SRA zirconium cladding at PWR hot operating conditions. Figure 3.2.2-2 provides PNNL's proposed PCMI failure threshold for RXA zirconium cladding at PWR hot operating conditions. Note that the EPRI and SRP interim failure thresholds are based on SRA cladding and therefore may not be directly applicable to RXA cladding. Figures 3.2.2-3 and 3.2.2-4 provide similar comparison plots for BWR cold startup conditions.

PNNL's and EPRI's proposed PCMI cladding failure thresholds were derived before the publication of revised NSRR data. Section 3.2.2.1 describes the impact of the revised NSRR data.

3.2.2.1 Impact of Revised NSRR Data

An examination of the EPRI, NEA, and PNNL reports reveal differences in the empirical databases. While most of the differences are small and within the uncertainty in the data, the predicted cladding hydrogen content for NSRR test TK7 is potentially significant since this failed rod is at an important junction with respect to hydrogen content and failure enthalpy. The various hydrogen levels for TK7 are summarized below.

Hydrogen reported in PNNL report	= 360 wppm
Hydrogen reported in EPRI report	= 223 wppm
Hydrogen reported in open literature[1]	= 140 wppm

With a reported 30 microns of oxide, the PNNL hydrogen model predicts a hydrogen level of 212 wppm for TK7. For the purpose of this report, an average hydrogen content of 182 wppm (over the range: 140 – 223 wppm) will be assumed for TK7. The revised TK7 hydrogen level has no impact on RXA failure thresholds.

Of major concern is the impact of revised fuel enthalpy values for 43 prior NSRR test specimens. Figure 3.1-7 provides a comparison of the original and revised NSRR data plotted as a function of fuel enthalpy rise versus excess cladding hydrogen content. Examination of this figure reveals significant changes. Since the various proposed failure thresholds were based on direct fits to the data (or scaled data), the revised NSRR data will have a first order impact. Figure 3.2.2-5 illustrates the impact of the revised NSRR data on the SRA cladding failure

1 Hideo Sasajime, Japan Atomic Energy Agency, "Summary of the Pulse Irradiation Experiments, TK and FK," Fuel Safety Research Meeting, May 2010.

threshold at PWR operating conditions. The solid green line shows a fit to the revised failure data following the same methods employed in the PNNL report. Examination of this figure reveals an increasing trend in reported failure enthalpy relative to the original data. This translates to a relaxation in the cladding failure threshold.

Figure 3.2.2-6 illustrates the impact of the revised NSRR data on the SRA cladding failure threshold at BWR cold startup conditions. The solid green line shows a fit to the revised failure data following the same methods employed in the PNNL report. Examination of this figure reveals an increasing trend in reported failure enthalpy relative to the original data. This translates to a relaxation in the cladding failure threshold.

Figure 3.2.2-7 illustrates the impact of the revised NSRR data on the RXA cladding failure threshold at PWR operating conditions. The solid green line shows a fit to the revised failure data following the same methods employed in the PNNL report. Examination of this figure reveals a decreasing trend in reported failure enthalpy relative to the original data. This translates to a more restrictive cladding failure threshold.

Figure 3.2.2-8 illustrates the impact of the revised NSRR data on the RXA cladding failure threshold at BWR cold startup conditions. The solid green line shows a fit to the revised failure data following the same methods employed in the PNNL report. Examination of this figure reveals a decreasing trend in reported failure enthalpy relative to the original data. This translates to a more restrictive cladding failure threshold.

3.2.2.2 EPRI CSED(TE) versus CSED (UE)

As described in Section 2.3.2 of Reference 3, EPRI's CSED is developed from material property tests as a function of material conditions, including temperature, fast fluence, outer surface corrosion, hydrogen concentration, and hydride morphology. The database of mechanical property tests on irradiated cladding material used to develop the CSED relations contains a variety of cladding designs, irradiation conditions, corrosion (oxide thickness and hydrogen concentration), testing conditions (e.g., temperature, stress state, strain rate), and anticipated cladding damage mechanisms (e.g., hydride lenses, hydride rim, spalled oxide, cracks).
The overall goal of this section is to define the threshold for cladding failure. Specifically, the point at which a through wall crack (i.e., breach) in the cladding may allow the release of fission gas. The goal is not to define gross cladding failure as that is addressed in separate criteria related to coolable geometry. For the purpose of defining the threshold of cladding failure, measured uniform elongation is a more appropriate and repeatable characterization of the fuel rod cladding's resistance to PCMI.

The PCMI cladding failure thresholds proposed in the EPRI report are based on total elongation data (i.e., CSED(TE)). However, in response to staff concerns, the EPRI report also includes CSEDs based on uniform elongation data. Figure 3.2.2-9 shows EPRI's Zircaloy-4 (SRA) CSED(TE) and CSED(UE) as a function of cladding hydrogen content. As expected, limiting the failure data to uniform elongation results in a significant reduction in CSED. As shown in Figure 3.2.2-9, differences between CSED (TE) and CSED(UE) are strongly influenced by temperature. Cladding hydrogen content and hydride distribution and orientation are also likely to influence this relationship.

Using their FALCON fuel rod thermal-mechanical model, EPRI scaled several of the cold NSRR

test results (i.e., measured failure enthalpy) to PWR hot operating temperatures based upon CSED(UE), CSED(TE), and a lower bound CSED(TE). Figure 4-13 of Reference 3 shows the predicted increase in failure enthalpy. Figure 4-14 of Reference 3, reproduces herein as Figure 3.2.2-10, plots the scaled failure data along with the proposed Zircaloy-4 (SRA) HZP failure threshold. Figure 3.2.2-11 adds a fit of the CSED(UE) scaled data. Note that this fit is almost indistinguishable compared to that of the lower bound CSED(TE). Examination of these figures reveals a significant reduction in the temperature scaling factor between the CSED functions.

3.2.2.3 Discussion of Key Parameters

The potential impact of key fuel design parameters, irradiation and conditioning, experimental conditions, and operating conditions on the development of PCMI cladding failure thresholds is discussed below.

Fuel Burnup:

During irradiation, each fuel rod undergoes several evolutions which alter its behavior under RIA conditions. These include, but are not limited to, the following:

- Irradiation-induced fuel swelling and cladding creep reduce the size of the as-fabricated pellet-to-cladding gap. The rate and timing of gap closure depends on fuel design and power history. Once gap closure is complete and hard contact predicted, the fuel rod is more susceptible to PCMI failure under RIA conditions.

- Self-shielding promotes a higher exposure, plutonium rich region toward the pellet periphery. As a result, the pellet radial power distribution is skewed toward the pellet periphery during RIA power pulses.

- Key core physics parameters change with core depletion.

    - Control rod worth changes with exposure.
    - Reactor kinetics change with exposure. For example, the fraction of delayed neutrons, β, decreases with fuel exposure. This change in β influences the dynamic behavior of the reactor under transients.
    - The fuel temperature reactivity coefficient, Doppler, decreases (becomes more negative) with fuel exposure.

- Cladding corrosion increases with time-at-temperature.

- Fuel thermal conductivity and solidus temperature decrease as a function of exposure.

Sections 3.5 and 3.8 of the PNNL report describe the potential effects of fuel burnup and initial gap size on PCMI susceptibility. Based on an examination of the RIA empirical database, PNNL concludes that only a weak burnup dependence is observed. FRAPCON-3.4 and FRAPTRAN-1.4 calculations were used to explore the dependency on initial gap size and timing of gap closure. An analytical approach was necessary since all of the PCMI failed rods in the empirical database were beyond 33 GWd/MTU and likely exhibited gap closure and hard contact (prior to the RIA test). PNNL's calculations were based on Zircaloy-4 cladding which is conservative with respect to time-dependent PCMI susceptibility relative to modern alloys. Based upon the predicted timing of gap closure for two different PWR fuel rod designs, PNNL

concludes that initial as-fabricated gap has little or no effect on the PCMI failure threshold and that low burnup fuel rods with an existing gap will likely fail by ballooning and rupture.

The EPRI and NEA reports support the position that low burnup, low corrosion fuel rods will likely fail by high temperature modes before PCMI.

In conclusion, the timing of pellet-to-cladding gap closure, which is strongly dependent on fuel rod design and power history, is such that low burnup fuel rods with an existing gap will likely fail by high-temperature modes before PCMI. Nevertheless, application of an empirically-based PCMI failure threshold based on medium to high burnup rods (with closed gaps and hard contact) is conservative over the entire range of burnup; especially for low to medium burnup ranges where an existing gap may accommodate a portion of the pellet thermal expansion.

Pulse Width:

Table 3.2.2-1 lists the minimum and maximum pulse widths from the various RIA test facilities along with predicted pulse widths for commercial PWRs and BWRs. Examination of this table reveals that many of the NSRR and CABRI tests experienced shorter pulse widths than would be expected during postulated accidents.

Section 3.7 of the PNNL report (Reference 5) investigated pulse width effects on the proposed PCMI cladding failure thresholds. This investigation concludes that no obvious bias with pulse width between 4.4 and 76 ms exists in the NSRR and CABRI failure data set. Further investigation using the FRAPTRAN transient fuel rod performance code revealed that predicted cladding temperature will increase with pulse widths greater than 20 ms and the higher cladding temperatures should increase the failure threshold. For example, the predicted failure enthalpy for a standard 17x17 PWR rod with Zry-4 Cold Work Stress Relief Annealed (CWSRA) cladding at 40 GWd/MTU was 100 cal/g with a 5 ms pulse width. The predicted failure enthalpy increased to 145 cal/g with a 30 ms pulse width. Recognizing analytical limitations and experimental observations of brittle failure in the hydride rim at the outer diameter, the PNNL report concludes that either the ductility (fracture toughness) of the hydride rim is not sensitive to temperature, or the rim temperature does not increase sufficiently before the crack initiates in a 75 ms pulse to increase the ductility (fracture toughness) of the hydride rim. Based on the above studies, the PNNL report concludes that the PCMI cladding failure empirical correlation should be used with no adjustment for pulse width.

While both reports recognize the importance of pulse width on the overall fuel performance, neither the EPRI nor NEA reports attempt to scale the empirical data to account for differences between the pulse reactor and commercial reactor characteristic pulse width.

Based on the above discussion, the staff decided not to scale the data for the potential impact of pulse width.

Hydrogen Content and Hydride Distribution and Orientation:

Hydrogen is absorbed into the cladding during normal operation mainly as a result of water-side zirconium oxidation ($Zr + 2\ H_20 \rightarrow ZrO2 + 4\ H$). The solubility of hydrogen in zirconium alloys is expressed in the following equation:

$H_{sol} = 1.2 \times 10^5 \exp(-8550/1.985887T)$(Reference 8)
Where, H_{sol} is hydrogen solubility in wppm and T is temperature in Kelvin.

At PWR hot operating conditions, hydrogen solubility ranges 50 wppm (535 °F) to 150 wppm (700 °F). At BWR cold startup conditions, hydrogen solubility is less than 1.0 wppm (70 °F). Any hydrogen above solubility precipitates as zirconium hydrides. In this report, the term "excess hydrogen" refers to the amount of hydrogen above solubility (i.e., precipitated hydrogen).

As discussed in the PNNL, EPRI, and NEA reports, hydrogen content and hydride distribution and orientation have a first-order impact on the PCMI resistance of fuel rod cladding. The amount of hydrogen absorbed during normal operation depends on many factors, including the corrosion resistance of the zirconium alloy, time at elevated temperature, and hydrogen pickup fraction of the zirconium alloy (which may be also dependent on fluence). The orientation of the hydrides is affected by the thermal and mechanical treatment of cladding tubes during manufacturing, and by the stress state prevailing under hydride precipitation (Reference 2).

Figure 3.2.2-12 shows the distribution and orientation of hydrides in high burnup fuel rod cladding segments. Figure (a) illustrates the characteristic distribution and random orientation (including radial) of hydrides in a high burnup Zircaloy-2 and M5 RXA cladding. Figure (b) illustrates the characteristic distribution with a pronounced "rim" and circumferential orientation of the hydrides in a high burnup Zircaloy-4 and ZIRLO SRA cladding. In Section 6.2.6.3 of Reference 2, NEA concludes the following with respect to the effect of hydride distribution and orientation:

- For the same average hydrogen content, materials with uniformly distributed hydrides are more ductile than those having local concentrations of hydrides in certain regions.

- Ductility decreases rapidly with increasing thickness of the hydride rim at the clad outer surface. This embrittlement seems to saturate beyond a rim thickness of 100 μm and it is not clear whether the effects of oxide thickness are additive.

- In BWR Zircaloy-2 cladding with an inner liner of zirconium (e.g., barrier cladding), local concentrations of hydrides were observed not only on the clad outer surface, but within the liner zirconium. It seems that the liner material, due to its lower solubility for hydrogen, is more sensitive to hydrogen-induced embrittlement than the Zircaloy-2 base material.

- The orientation of zirconium hydrides platelets strongly influences embrittlement.

- The more deleterious radial hydrides are more common in RXA materials; however, may appear in any material as a result of applied tensile stress or residual stress (e.g., rod internal pressure). Radial hydrides may also form as a result of power cycling or overpower transients; where existing circumferential hydrides may dissolve by the temperature excursion, and then re-precipitate as radial hydrides, if the tensile hoop stress is large enough.

As described above, the EPRI CSED is based on separate effects mechanical testing of irradiated cladding specimens. Figure 3.2.2-13 compares the predicted CSED(TE) for Zircaloy-

4 (SRA) and Zircaloy-2 (RXA) test results. Examination of this figure confirms that the RXA material is more susceptible to hydrogen-induced embrittlement under a variety of loading conditions.

Research into hydride reorientation during pre-storage drying-transfer operations and early stage storage provides further evidence of the detrimental role of radial hydrides on cladding ductility. In this research, drying conditions (i.e., temperature and loading) were varied to study their influence on hydride reorientation. Mechanical testing was subsequently performed on these test specimens to quantify the impact of varying degrees of hydride reorientation on the mechanical properties of these high burnup fuel cladding segments. Examination of the test results documented in References 9 and 11 show a decrease in cladding ductility with increasing proportion of radial hydrides. While the ring compression tests performed in these studies are not prototypical of the loading expected during an RIA, the results provide further evidence of the increased sensitivity of cladding to hydrogen-induced embrittlement with the introduction of radial hydrides versus the sensitivity of the same material with the same amount of circumferential hydrides.

While the above separate effects mechanical testing demonstrates the increased sensitivity of cladding containing radial hydrides to hydrogen-induced embrittlement, the true effect of radial hydrides on hydrogen-enhanced PCMI under RIA loading conditions may be best observed by studying a subset of the RIA empirical database. Figure 3.2.2-14 shows a plot of fuel enthalpy versus excess hydrogen content for the cold NSRR pulse reactor RIA tests. The data is divided between SRA and RXA cladding material. Examination of this figure confirms that the RXA material is more susceptible to hydrogen-induced embrittlement under RIA loading conditions.

The interim RIA criteria and guidance (Reference 1) provides PCMI cladding failure thresholds for PWR hot conditions and BWR cold conditions. However, since a vast majority of the PWR fuel rods (including all of the failed rods) were SRA and all of the BWR fuel rods were RXA, the applicability of the interim criteria is limited to SRA cladding at PWR hot conditions and RXA cladding at BWR cold conditions. This limitation also applies to the PCMI failure thresholds proposed in the EPRI report. Hence, no PCMI failure curves are directly applicable to RXA cladding at PWR hot conditions (e.g., M5 alloy) or SRA cladding at BWR cold conditions (e.g., AREVA Atrium design).

Recognizing this first-order effect that zirconium hydride distribution and orientation have on mechanical properties, the PNNL report segregated the RIA empirical database into CWSRA and RXA cladding types and developed unique PCMI cladding failure thresholds as a function of cladding excess hydrogen for each type of cladding microstructure.

Based upon the above discussion, the staff decided to segregate the data and derive separate PCMI cladding failure thresholds (fuel enthalpy rise versus excess cladding hydrogen) for SRA and RXA cladding material.

Cladding Temperature:

Differing opinions on the magnitude of scaling for the cold NSRR test results to PWR HZP operating conditions was an important contributor to a staff decision to await the NSRR hot capsule tests before finalizing the RIA criteria and guidance. Temperature effects the cladding yield strength, ductility, and hydrogen solubility (which also effects ductility).

In Section 6.2.6.2 of Reference 2, NEA concludes the following with respect to the effect of cladding temperature:

- The ductile-to-brittle temperature for irradiated cladding increases with increasing hydrogen.

- The ductile-to-brittle temperature for a given hydrogen content increases with increasing strain rate.

- Experimental results demonstrate that the time necessary for hydride dissolution exceeds the timing of PCMI loading during the early stage of an RIA.

Section 3.3 of the PNNL report (Reference 5) investigated cladding temperature effects on the proposed PCMI cladding failure thresholds. Based upon comparisons of similar hot and cold RIA test results, PNNL concluded that an adjustment of 18-20 cal/g on cold NSRR failure enthalpy is appropriate to account for HZP operating conditions. Furthermore, based on results from NSRR RIA tests FK10 and FK12, PNNL concluded that the ductile to brittle transition temperature for irradiated Zry-2 cladding is beyond 85°C. Hence, the proposed scaling of the BWR data and resulting PCMI failure threshold is not supported by the available data.

As described above, EPRI's FALCON fuel rod thermal-mechanical model was employed to scale several of the cold NSRR test results (i.e., measured failure enthalpy) to PWR hot operating temperatures based upon CSED (UE), CSED (TE), and a lower bound CSED (TE). Figure 3.2.2.11 shows the scaled data along with the proposed Zircaloy-4 (SRA) HZP failure threshold and a fit to the CSED(UE) scaled data. Figure 3.2.2-15 shows the magnitude of scaling (Δcal/g) based on EPRI's CSED (TE) and CSED(UE) and PNNL's proposed scaling. Note that since PNNL's failure curves are expressed in terms of excess hydrogen, the effective scaling factor would also include the worth of the increase in hydrogen solubility at the higher temperature. Examination of this figure reveals that the PNNL scaling factor lies between the two EPRI scaling factors.

Based upon the above discussion, the staff decided to apply the PNNL scaling factor to adjust test results from BWR cold startup conditions to PWR hot operating conditions. Since the NSRR test conditions are prototypical of BWR cold startup conditions, no adjustment is being applied.

Mixed Oxide Fuel

Based upon the reported failure enthalpies between standard UO2 and Mixed Oxide (MOX) fuel rods, PNNL concludes that there is no conclusive evidence of an inherent MOX effect. In Section 5 of Reference 3, EPRI concludes that gaseous swelling-enhanced PCMI is an important contributor to the mechanical behavior of MOX fuel rods under RIA conditions, especially at operating temperatures. The NEA report notes that MOX effects have been observed and this issue needs further investigation. The staff agrees that MOX effects require further investigation.

Based on the above discussion, the staff decided to limit the applicability of the PCMI failure threshold to UO2 fuel rods.

3.2.2.4 Applicability of PCMI Failure Thresholds

PWR technical specification Power Dependent Insertion Limits (PDILs) restrict control bank insertion (as well as alignment and overlap) which limits the worth of any individual control rod. Core neutronics calculations, especially for intermediate and full power operating conditions, may predict maximum ejected rod worth below $1 reactivity ($\Delta\rho/\beta < 1.0$) indicating a non-prompt power excursion.

The above discussion relates to the potential pulse width effects on experimental data. The RIA empirical database used to derive the PCMI cladding failure thresholds consists of prompt critical, narrow-pulse power excursion experiments. Cladding failures reported in the broad pulse IGR facility were due to high temperature failure mechanisms. Therefore, these PCMI cladding failure thresholds may not be directly applicable to 1) non-prompt RIA scenarios (e.g., ejection of partially inserted control rod or low-worth control rod), 2) non-prompt accident overpower scenarios (e.g., PWR main steam line break), or 3) non-prompt anticipated operational occurrence overpower scenarios (e.g., PWR control rod bank withdrawal, BWR turbine trip). Relative to a prompt-critical, narrow-pulse power excursion, the broader power excursion exhibited in these scenarios allows additional time for the cladding temperature (and ductility) to increase such that brittle PCMI failure is less likely.

As shown in Figure 3.1-2, no experimental data exists between 76 ms and approximately 700 ms pulse width. Hence, it is difficult to determine a threshold for PCMI brittle failure susceptibility. As such, the NRC staff recommends applying the PCMI cladding failure thresholds (in addition to high temperature thresholds) to all PWR CRE and BWR CRDA scenarios. For the purpose of calculating fuel enthalpy for assessing PCMI failures, the fuel enthalpy rise is defined as the radial average fuel enthalpy rise at the time corresponding to one pulse width after the peak of the initial pulse.

With the exception of FK-10 (80 °C) and FK-12 (85 °C), the database supporting the BWR cladding failure criteria were all conducted from an initial temperature of 20 °C - consistent with cold startup BWR conditions. Due to temperature and hydrogen solubility effects, application of the BWR cladding failure criteria to higher operating temperatures is conservative. Future evaluation of hydrogen solubility and temperature effects may be pursued in order to refine the BWR PCMI failure criteria for application to higher operating temperatures. Another potential conservatism in the proposed criteria is the short NSRR pulse width relative to the broader pulse width of operating BWRs.

Based upon the effect of hydride distribution and orientation, separate PCMI failure curves were developed for SRA and RXA cladding materials. Each applicant must provide evidence of the hydride distribution and orientation in the irradiated condition to demonstrate applicability of the PCMI failure curves to their cladding alloy. As described in Reference 12 and the NEA report, hydride reorientation from the circumferential direction to the radial direction is possible when the fuel rod is heated and subsequently cooled under an applied tensile load (e.g., high rod internal pressure). Each applicant must address the possibility of hydride reorientation.

In summary, the range of applicability is limited to the following conditions:

- All PWR and BWR UO2 fuel rod designs with zirconium-based cladding, including

barrier designs and fuel rods with both annular and solid pellets.

- BWR cold startup conditions up through PWR hot full power operating conditions.

- An applicant must provide evidence of the hydride distribution and orientation in the irradiated condition to demonstrate applicability of the PCMI failure curves to their cladding alloy. As described in Reference 11 and the NEA report, hydride reorientation from the circumferential direction to the radial direction is possible when the fuel rod is heated and subsequently cooled under an applied tensile load (e.g., high rod internal pressure). Each applicant must address the possibility of hydride reorientation.

3.2.2.5 Analytical Considerations

For the application of these PCMI cladding failure thresholds, an approved alloy-specific cladding corrosion and hydrogen uptake model must be used to predict the initial, pre-transient cladding hydrogen content. The influence of (1) time-at-temperature (e.g., residence time, operating temperatures, steaming rate), (2) cladding fluence (e.g. dissolution of second phase precipitates), (3) enhanced hydrogen uptake mechanisms (e.g., shadow corrosion, proximity to dissimilar metal), and (4) crud deposition must be accounted for in these approved models. Hydrogen concentrations are expected to vary widely (1) across the population of fuel rods in the core and (2) axially, radially, and circumferentially along the cladding of a given fuel rod. The applicant may elect to subdivide fuel rod populations based on fuel enthalpy increase and hydrogen content in order to demonstrate compliance.

The empirically-derived PCMI cladding failure curves are based on a best fit of the reported fuel enthalpy change at failure and cladding hydrogen concentration. No built-in conservatism has been added to account for prediction or measurement uncertainties in time of failure, energy deposition, fuel enthalpy at failure, or cladding hydrogen content. For a majority of the data, cladding hydrogen content was calculated using best-estimate, alloy-specific corrosion and hydrogen uptake models based on measured oxide thickness and reported fuel burnup. An average value was utilized for instances where a range of oxide thickness was reported. Several recent NSRR and CABRI tests reported cladding hydrogen content. Similar to oxide thickness, an average hydrogen value was utilized where a range was reported.

Figures 3.18, 3.19, 4.5 and 4.6 of the PNNL report illustrate the LSQ fit along with error bars for the uncertainty in the data. Examination of these figures reveals that a failure threshold based on a lower bound curve accounting for all uncertainties would be 10 - 30 Δcal/g lower at any given cladding hydrogen level.

Biases and uncertainties in the empirical database, as well as those in the analytical methods being used to demonstrate compliance, need to be explicitly addressed in the approved application methodology. The quantification and application of biases and uncertainties is an important part in defining the level of confidence in the final compliance demonstration. The level of confidence is often associated with the probability of the event. The BWR CRDA and PWR CRE are classified as Condition IV events. For this classification of accident, the staff has determined that the use of a best-fit failure threshold, in combination with high-confidence core physics predictions and cladding hydrogen estimates, is acceptable. An approved core physics model which accounts for biases and uncertainties should be used to provide high-confidence predictions (e.g., control rod worth, local power peaking, Doppler feedback, fuel temperature).

Likewise, an approved alloy-specific corrosion and hydrogen uptake model should be used to provide high-confidence estimates of peak cladding hydrogen content.

When applying the hydrogen dependent PCMI cladding failure curves, the cladding average (e.g., mid wall) temperature at the start of the transient should be used to define the excess hydrogen in the cladding. Use of the Kearns solubility correlation (Reference 8) is acceptable. For the purpose of calculating peak fuel enthalpy rise for CZP conditions, zero fuel enthalpy is defined at 20 °C (68 °F).

In summary, the following analytical considerations accompany the cladding failure thresholds:

- An approved alloy-specific cladding corrosion and hydrogen uptake model must be used to predict the initial, pre-transient cladding hydrogen content. The influence of (1) time-at-temperature (e.g., residence time, operating temperatures, steaming rate), (2) cladding fluence (e.g. dissolution of second phase precipitates), (3) enhanced hydrogen uptake mechanisms (e.g., shadow corrosion, proximity to dissimilar metal), and (4) crud deposition must be accounted for in these approved models.

- High confidence cladding hydrogen predictions which account for axial, radial, and circumferential variability and uncertainties should be used when implementing the PCMI failure thresholds. Use of nominal or best-estimate cladding hydrogen predictions is not acceptable.

- High confidence core physics predictions which account for biases and uncertainties should be used when implementing the PCMI failure thresholds. Use of nominal or best-estimate core physics parameters is not acceptable.

- When applying the hydrogen dependent PCMI cladding failure curves, the cladding average (e.g., mid wall) temperature at the start of the transient should be used to define the excess hydrogen in the cladding. Use of the Kearns solubility correlation (Reference 8) is acceptable.
- CZP and HZP calculations should encompass both (1) BOC conditions and (2) re-start following recent full power operation.

- Intermediate power levels up to HFP conditions should be evaluated to confirm power-dependent core operating limits (e.g., control rod insertion limits, rod power peaking limits, axial and azimuthal power distribution limits).

- For the purpose of calculating peak fuel enthalpy for CZP, zero fuel enthalpy is defined at 20 °C (68 °F).

- Cladding hydrogen levels and predicted fuel enthalpy change are expected to vary widely (1) across the population of fuel rods in the core and (2) axially along a given fuel rod. Fuel loading patterns and operating history (e.g., time-in-cycle, rodded operation) will also impact these predictions. The applicant may elect to subdivide fuel rod populations based on fuel enthalpy change and fuel rod burnup in order to demonstrate compliance.

- Given that the PCMI failure threshold changes with cladding hydrogen content, the limiting scenario with respect to maximum number of failed rods may not be the highest worth control rod. Applicants may need to survey a larger population of BWR blade drops and PWR ejected rods core locations and exposure points to identify the limiting scenario.

3.2.2.6 Revised Criteria and Guidance

Figure 3.2.2-16 provides a comparison of the various PCMI failure thresholds (fuel enthalpy increase versus excess cladding hydrogen) for SRA cladding at PWR hot operating conditions along with the EPRI scaled NSRR data. Note that the EPRI scaled data does not reflect the revised NSRR data. Figure 3.2.2-17 provides the same failure curves along with the latest empirical database (data scaled using PNNL approach). Based on the discussions above, the staff decided to adopt the new fit based on the revised NSRR data.

Figure 3.2.2-18 shows the PCMI failure thresholds (fuel enthalpy increase versus excess cladding hydrogen) for RXA cladding at PWR hot operating conditions along with the latest empirical database (data scaled using PNNL approach). Neither the SRP interim guidance nor EPRI report proposed RXA-specific failure curves at PWR hot operating conditions. The PNNL threshold employs a logarithmic function to fit the failure data, similar to the SRA plot in Figure 3.2.2-15. However, the RXA failure data is limited in both quantity and range of hydrogen. Extrapolation of the logarithmic function to lower hydrogen levels is not justified, especially since non-failed test results appear above the proposed failure threshold. Based on the discussions above, the staff decided to adopt the revised curve depicted in Figure 3.2.2-18.

Figure 3.2.2-19 shows the PCMI failure thresholds (fuel enthalpy increase versus excess cladding hydrogen) for SRA cladding at BWR cold startup conditions along with the latest empirical database (data scaled using PNNL approach). Neither the SRP interim guidance nor EPRI report proposed SRA-specific failure curves at BWR cold startup conditions. Based on the discussions above, the staff decided to adopt the revised curve depicted in Figure 3.2.2-19. Figure 3.2.2-20 provides a comparison of the various PCMI failure thresholds (fuel enthalpy increase versus excess cladding hydrogen) for RXA cladding at BWR cold startup conditions along with the latest empirical database (data scaled using PNNL approach). The PNNL threshold employs a logarithmic function to fit the failure data, similar to the SRA plot in Figure 3.2.2-19. However, the RXA failure data is limited in both quantity and range of hydrogen. Extrapolation of the logarithmic function to lower hydrogen levels is not justified, especially since non-failed test results appear above the proposed failure threshold. Based on the discussions above, the staff decided to adopt the revised curve depicted in Figure 3.2.2-20.

PWR Hot Operating Conditions

Fully Recrystallized Cladding (RXA)
See Figure 3.2.2-21

Stress Relief Annealed Cladding (SRA)
See Figure 3.2.2-22

BWR Cold Start-Up Conditions

Fully Recrystallized Cladding (RXA)
See Figure 3.2.2-23

Stress Relief Annealed Cladding (SRA)
See Figure 3.2.2-24

Table 3.2.2-1: Pulse Width Variability

Scenario / Test Facility	Pulse Width (ms)	
	Minimum	Maximum
PWR HZP CRE	25	65
PWR HFP CRE	400	4500
BWR CZP CRDA	45	75
BWR HZP CRDA	45	140
SPERT-CDC	13	31
PBF	11	16
IGR	750	950
BIGR	2.5	3.1
NSRR	4.3	9.0
CABRI	8.8	75

Notes:

(1) Estimated PWR and BWR pulse widths based on realistic and moderately conservative computer analyses. Data from Section 2.2 of Reference 2.

(2) Ranges of pulse widths from RIA test facilities listed in Appendix A of Reference 2.

Figure 3.2.2-1

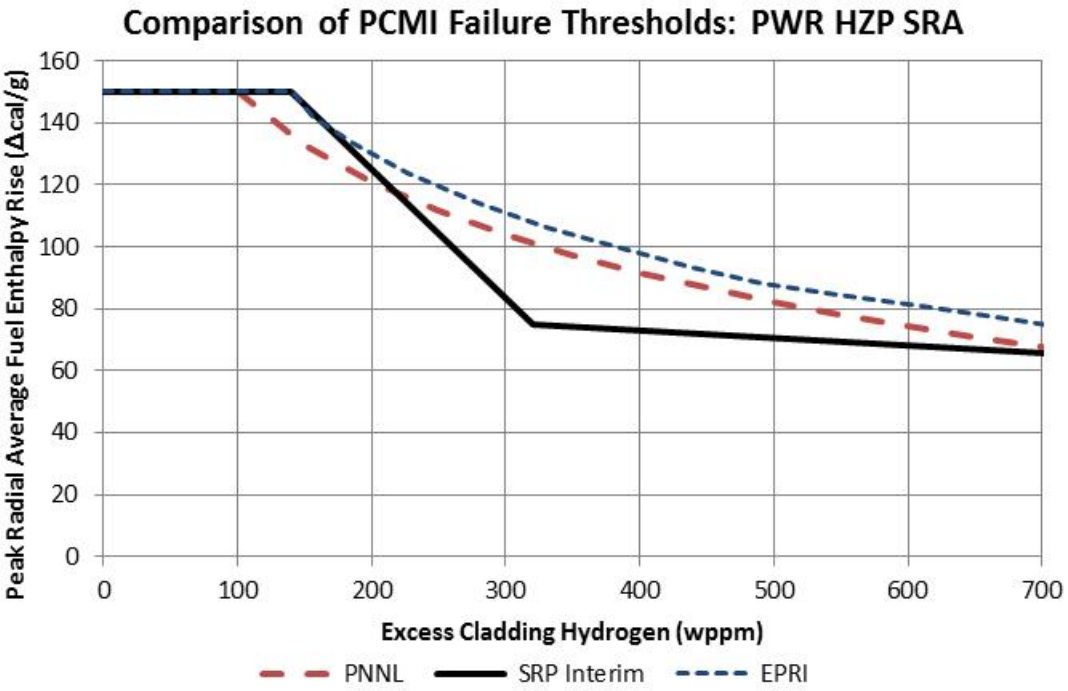

Figure 3.2.2-2

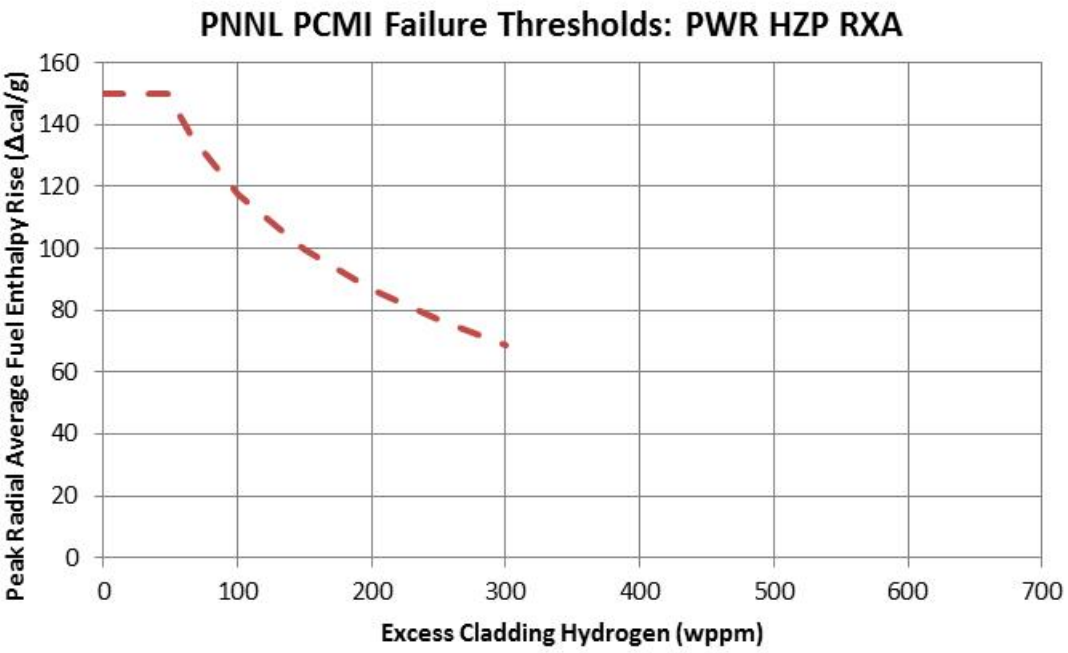

Figure 3.2.2-3

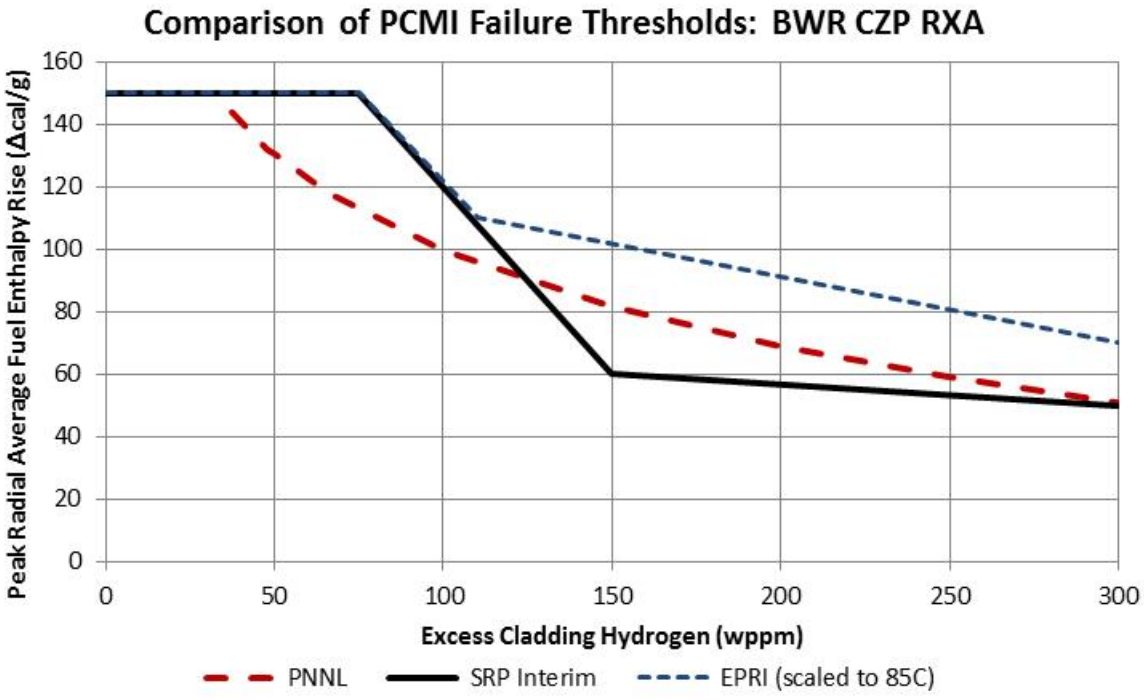

Figure 3.2.2-4

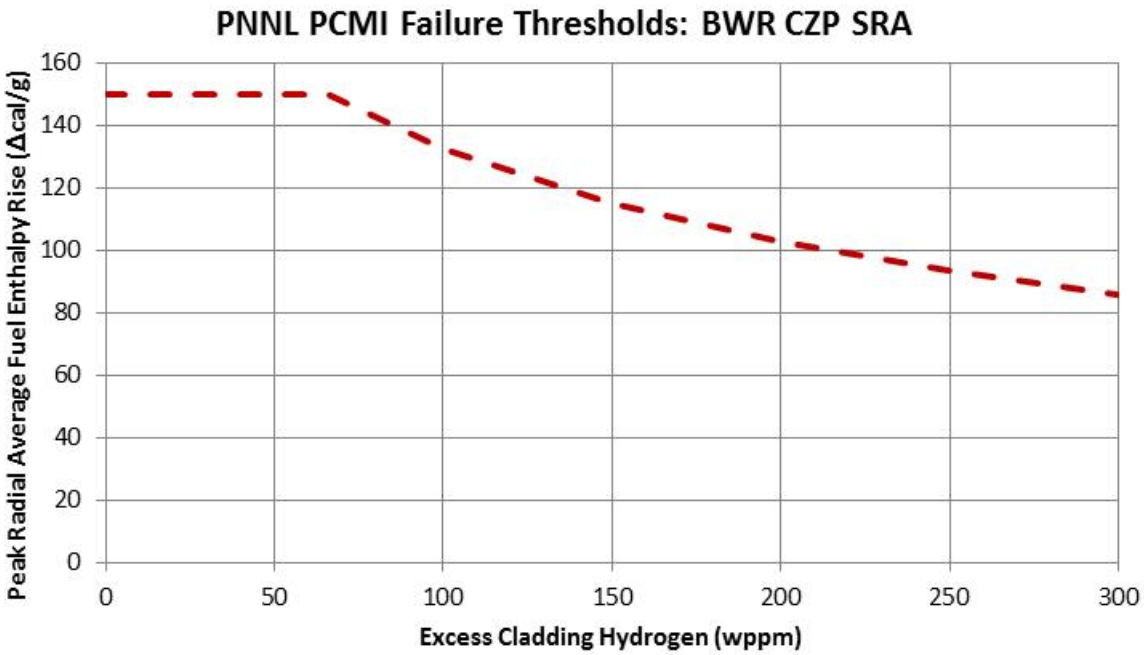

Figure 3.2.2-5

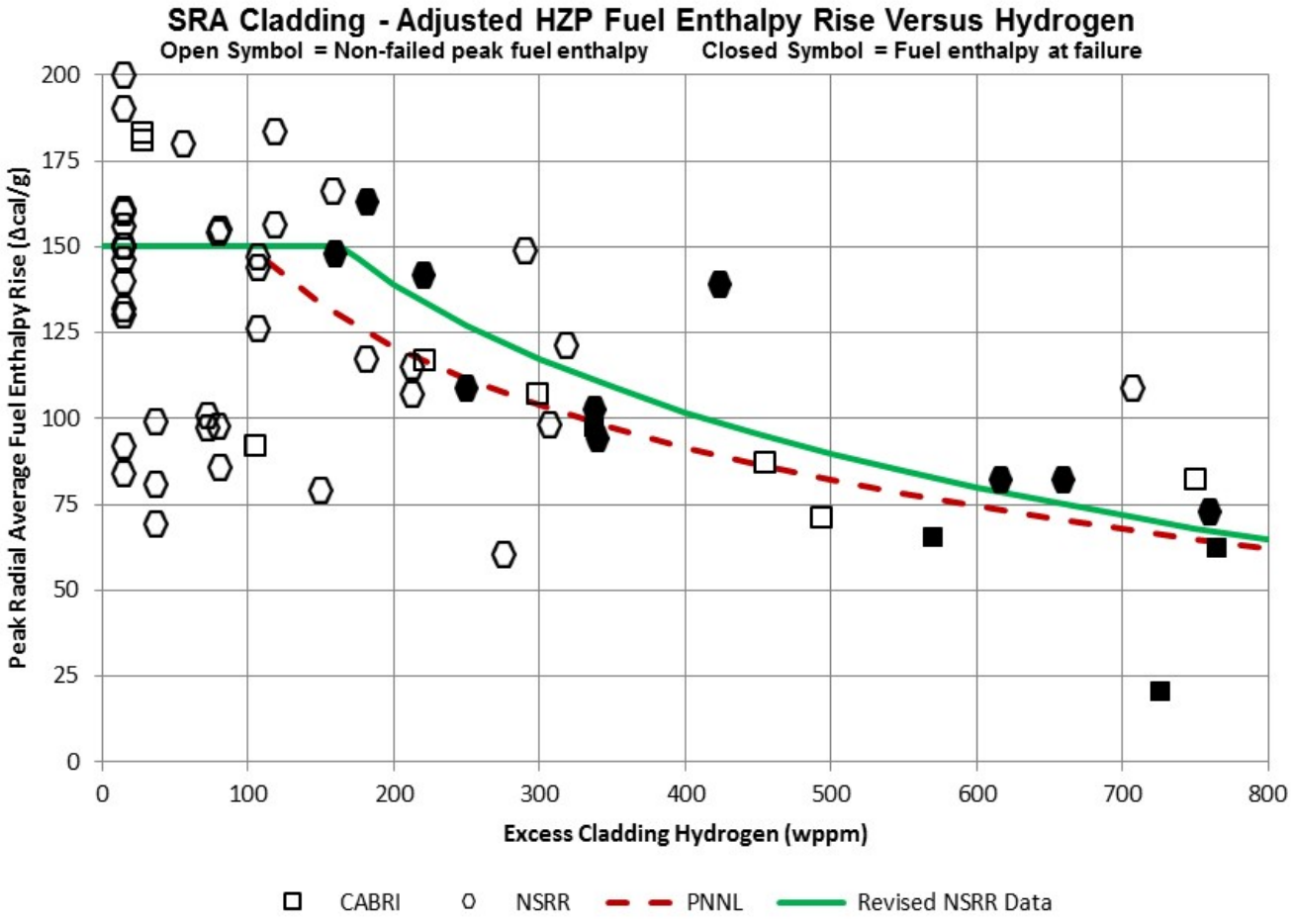
SRA Cladding - Adjusted HZP Fuel Enthalpy Rise Versus Hydrogen
Open Symbol = Non-failed peak fuel enthalpy
Closed Symbol = Fuel enthalpy at failure
Peak Radial Average Fuel Enthalpy Rise (Δcal/g)
200
175
150
125
100
75
50
25
0
0
100
200
300
400
500
600
700
800
Excess Cladding Hydrogen (wppm)
CABRI
NSRR
PNNL
Revised NSRR Data

Figure 3.2.2-6

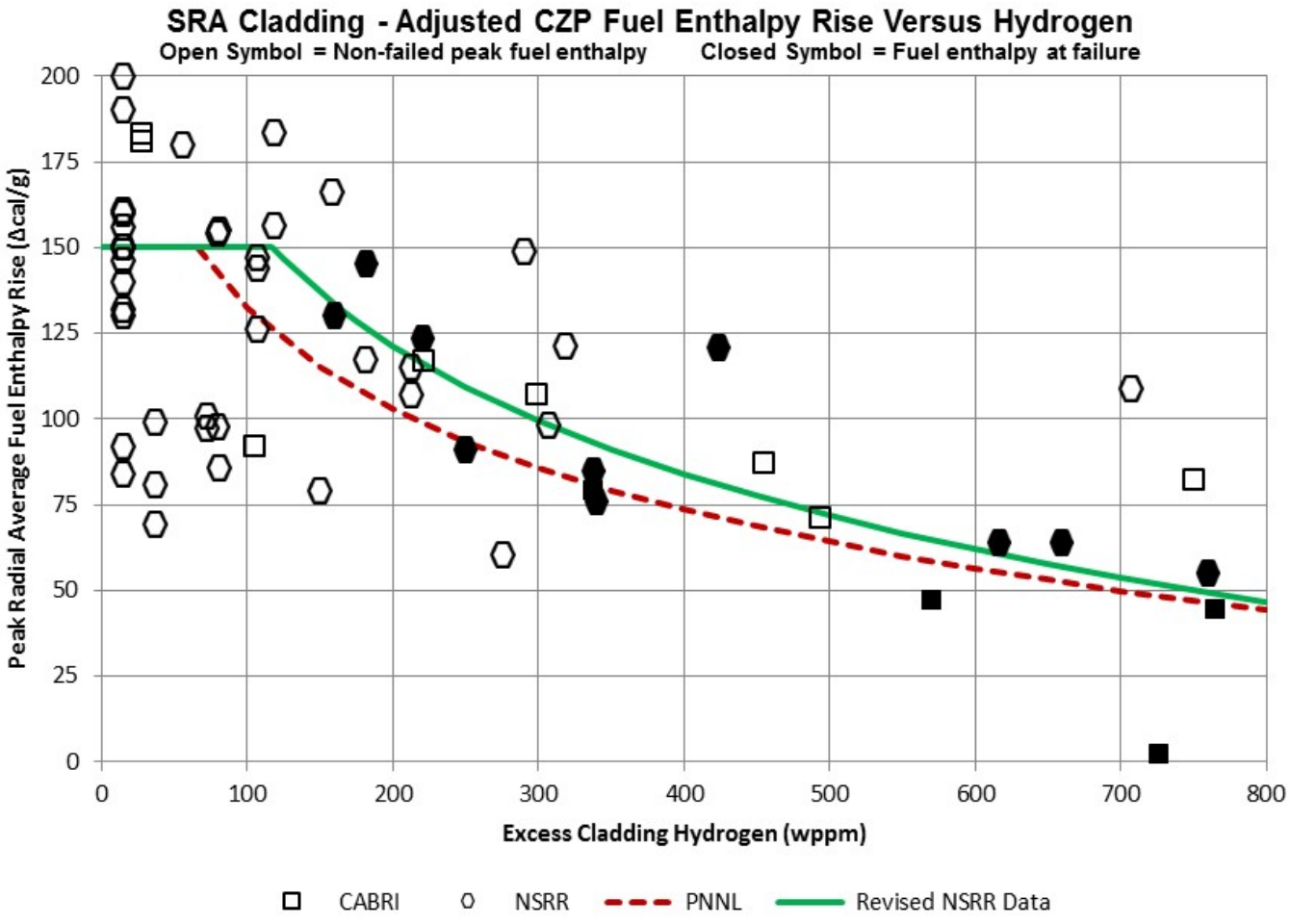
SRA Cladding - Adjusted CZP Fuel Enthalpy Rise Versus Hydrogen
Open Symbol = Non-failed peak fuel enthalpy
Closed Symbol = Fuel enthalpy at failure
Peak Radial Average Fuel Enthalpy Rise (Δcal/g)
200
175
150
125
100
75
50
25
0
0
100
200
300
400
500
600
700
800
Excess Cladding Hydrogen (wppm)
CABRI
NSRR
PNNL
Revised NSRR Data

Figure 3.2.2-7

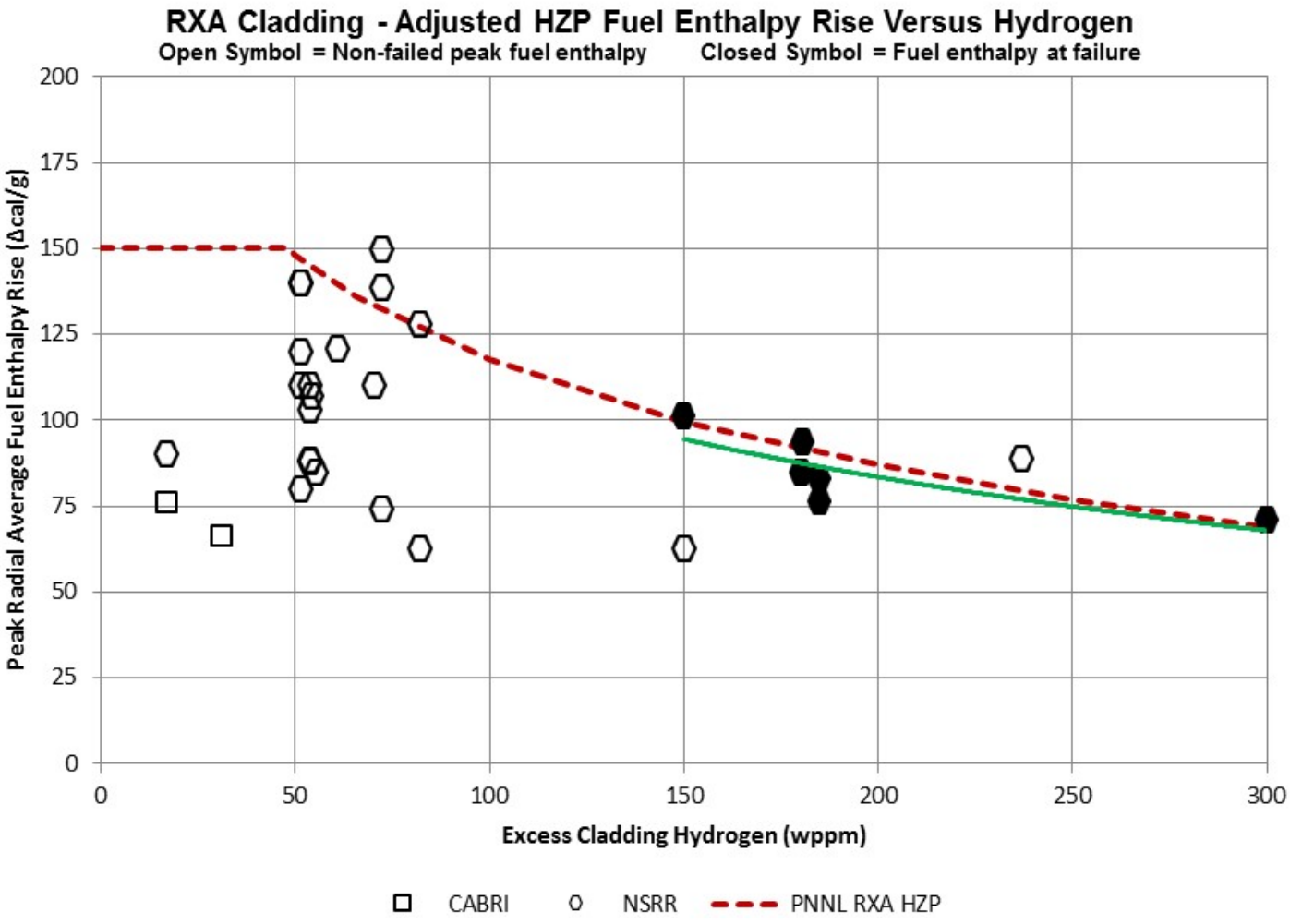
RXA Cladding - Adjusted HZP Fuel Enthalpy Rise Versus Hydrogen
Open Symbol = Non-failed peak fuel enthalpy
Closed Symbol = Fuel enthalpy at failure
Peak Radial Average Fuel Enthalpy Rise (Δcal/g)
200
175
150
125
100
75
50
25
0
0
50
100
150
200
250
300
Excess Cladding Hydrogen (wppm)
CABRI
NSRR
PNNL RXA HZP

Figure 3.2.2-8

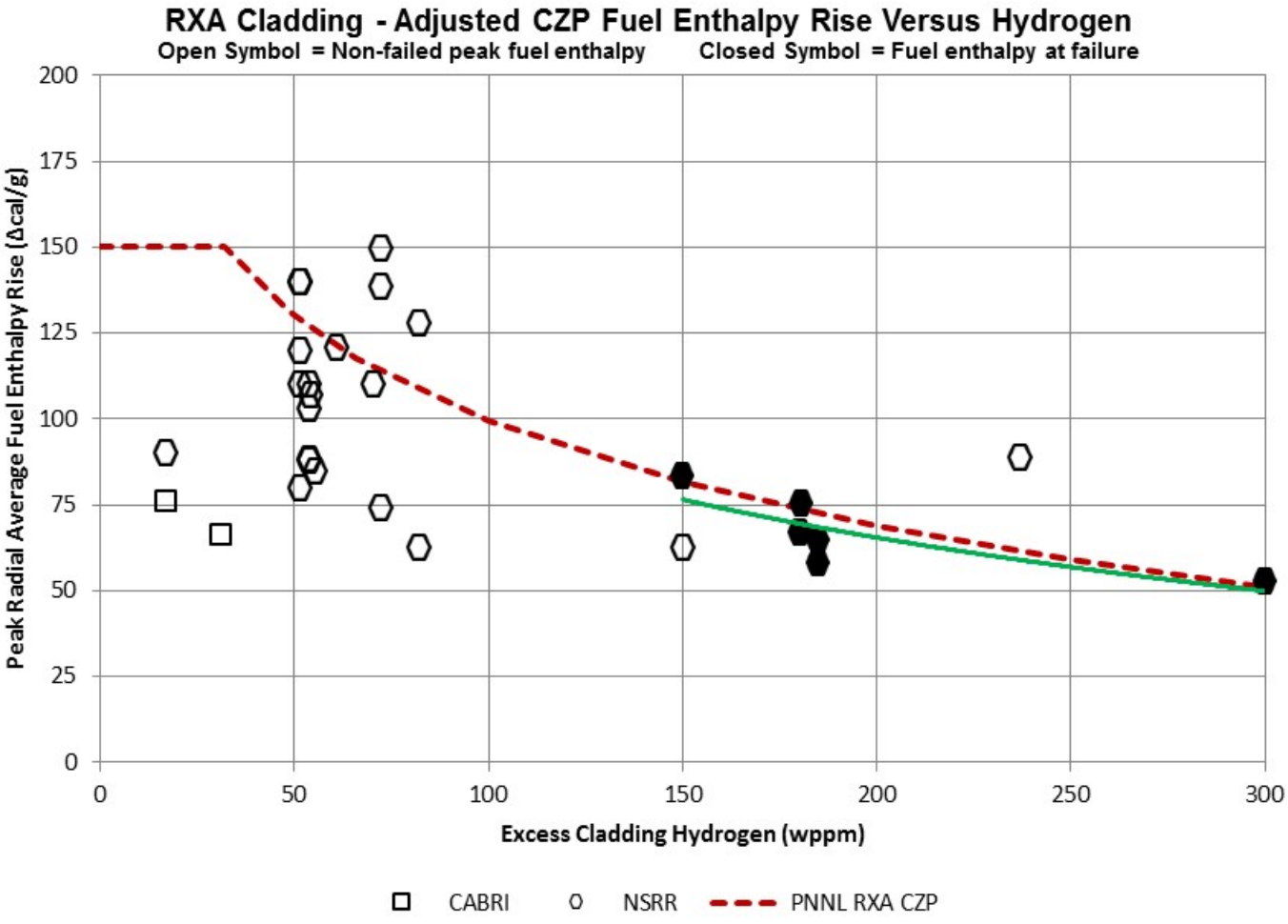
RXA Cladding - Adjusted CZP Fuel Enthalpy Rise Versus Hydrogen
Open Symbol = Non-failed peak fuel enthalpy
Closed Symbol = Fuel enthalpy at failure
Peak Radial Average Fuel Enthalpy Rise (Δcal/g)
200
175
150
125
100
75
50
25
0
0
50
100
150
200
250
300
Excess Cladding Hydrogen (wppm)
CABRI
NSRR
PNNL RXA CZP

Figure 3.2.2-9

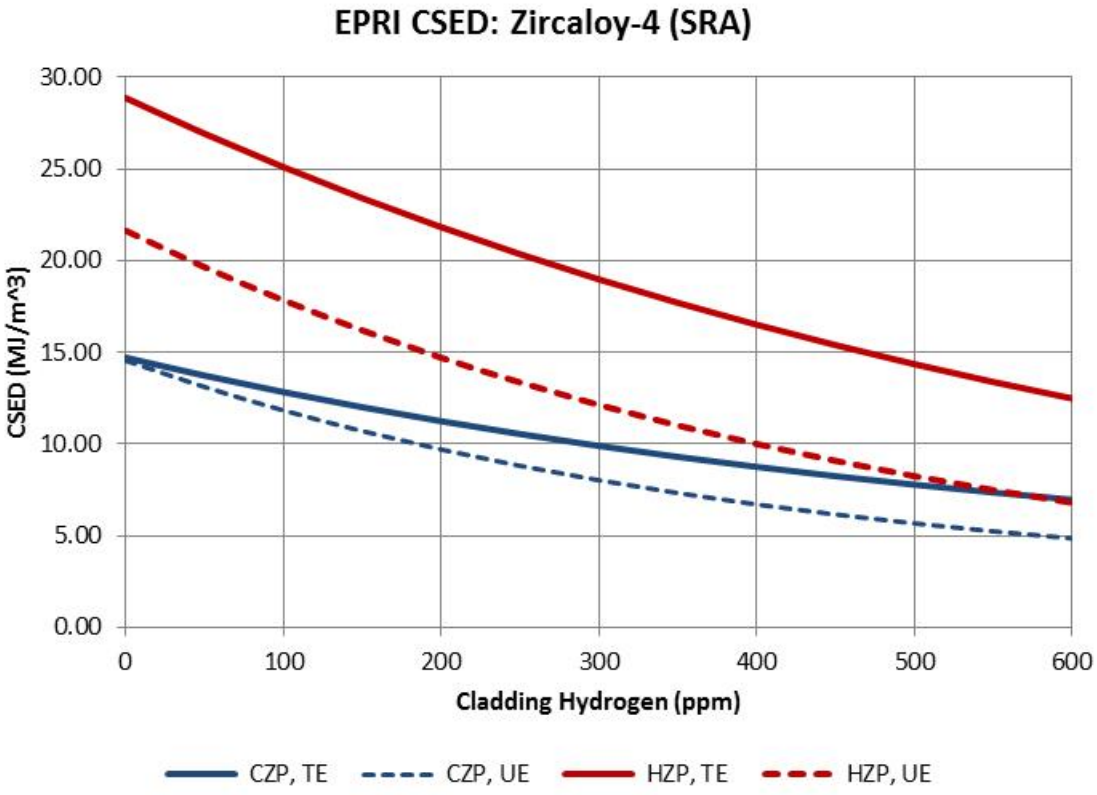
EPRI CSED: Zircaloy-4 (SRA)
CSED (MJ/m^3)
30.00
25.00
20.00
15.00
10.00
5.00
0.00
0
100
200
300
400
500
600
Cladding Hydrogen (ppm)
CZP, TE
CZP, UE
HZP, TE
HZP, UE

Figure 3.2.2-10

(Reproduction of Figure 4-14 of Reference 3, converted to excess hydrogen)

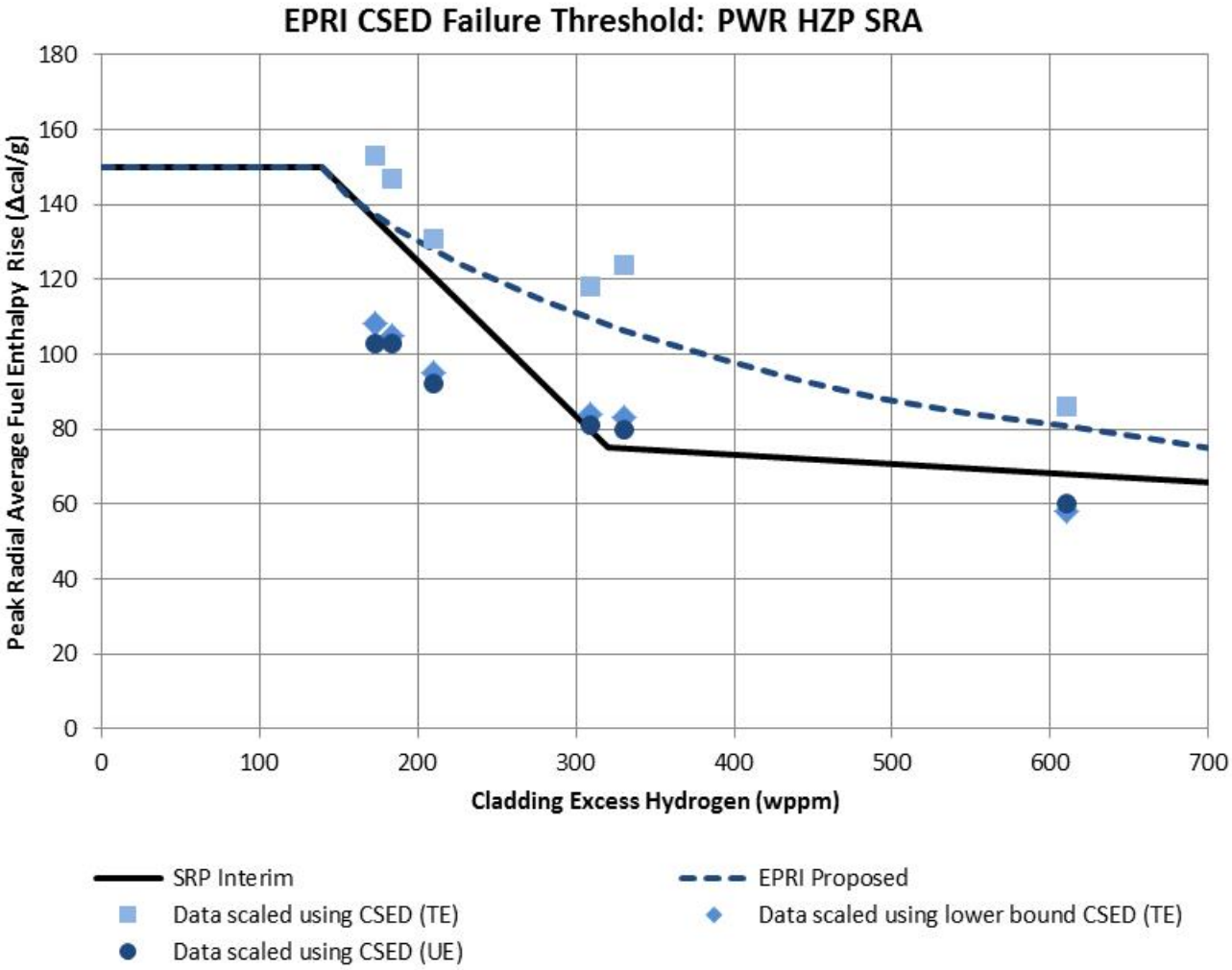

Figure 3.2.2-11

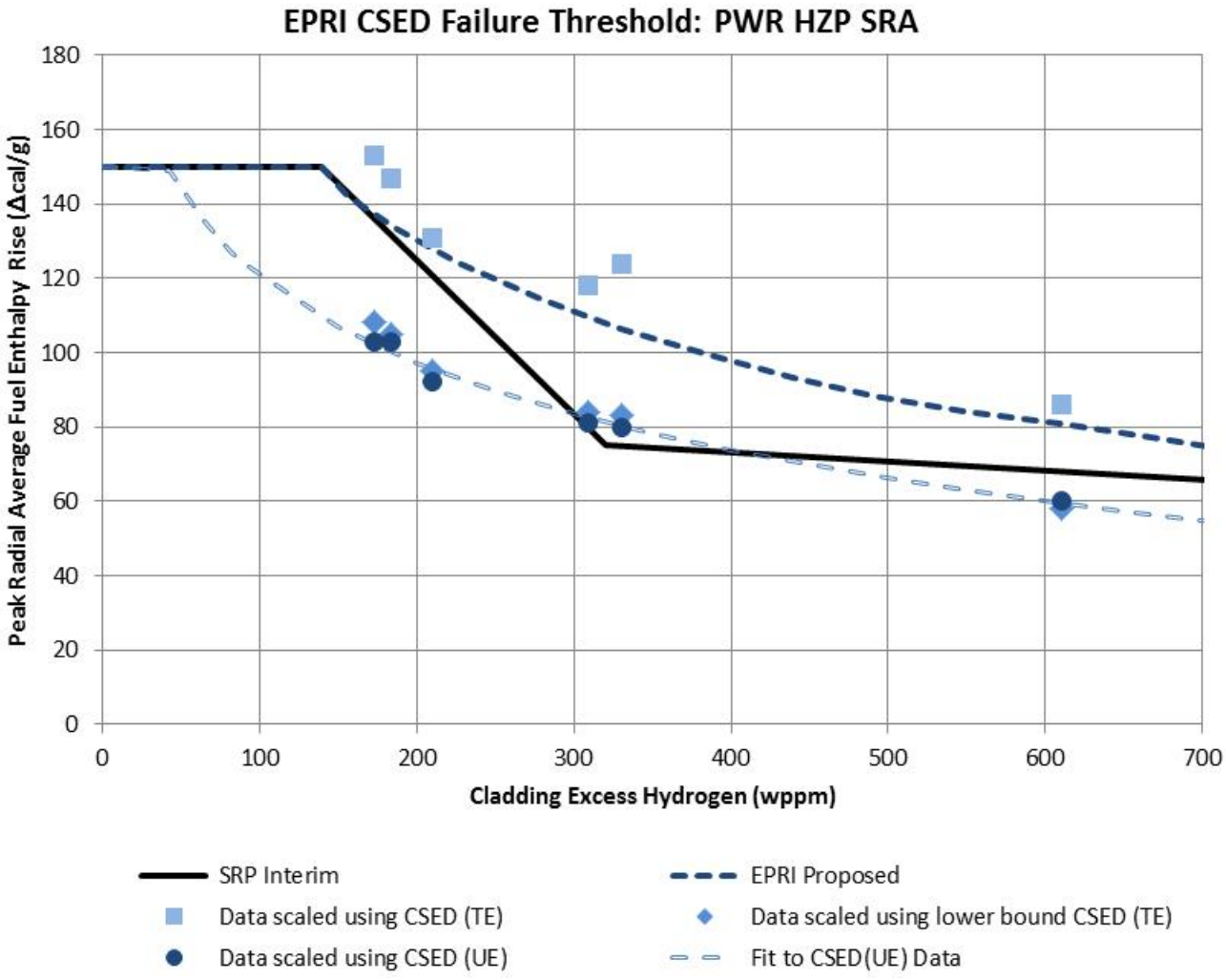

Figure 3.2.2-12

(a) High Burnup RXA Cladding

Zry-2 (50 GWd/t)
(Source: Reference 9)

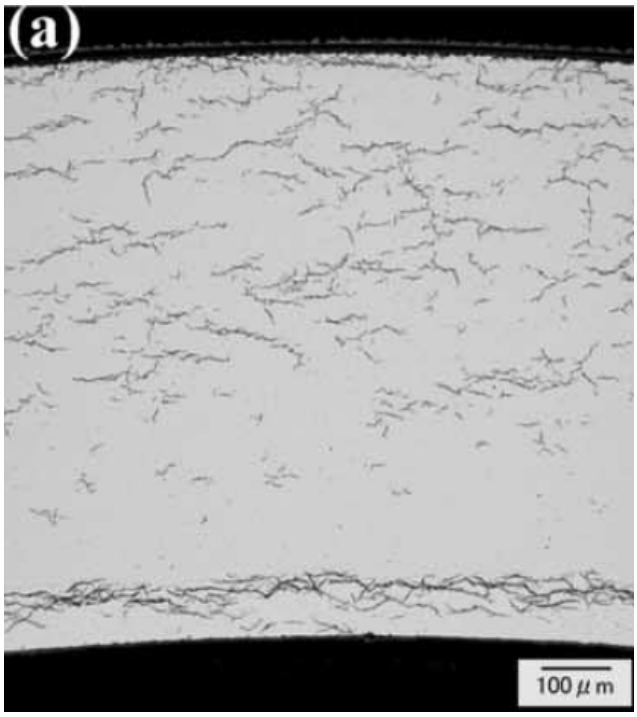

M5 (69 GWd/MTU)
(Source: Reference 10)

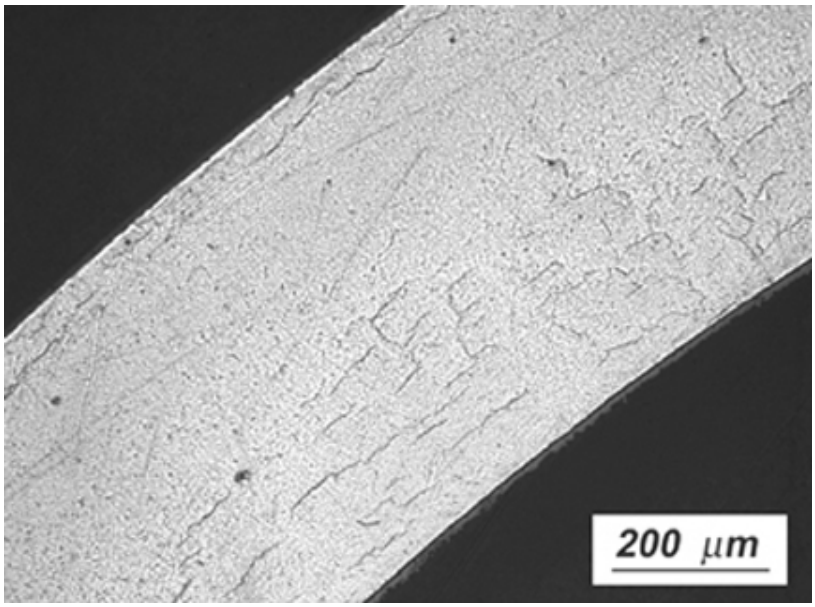

(b) High Burnup Zry-4 SRA Cladding

Zry-4 (67 GWd/MTU)
(Source: Reference 10)

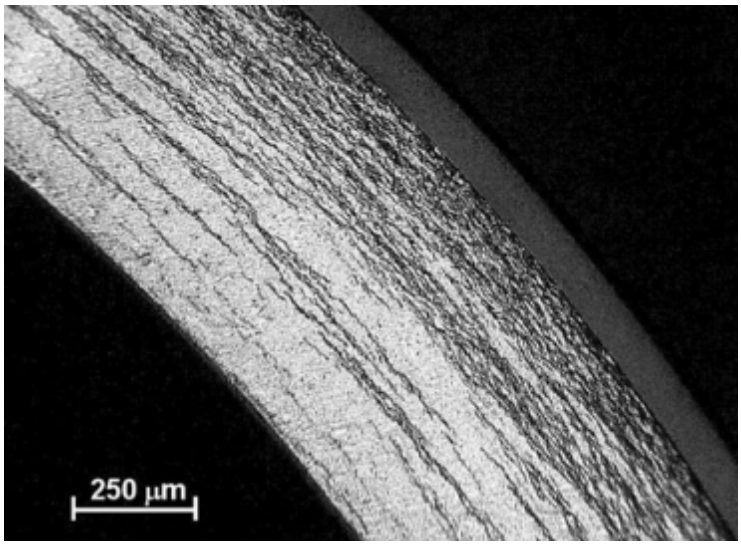

ZIRLO (70 GWd/MTU)
(Source: Reference 10)

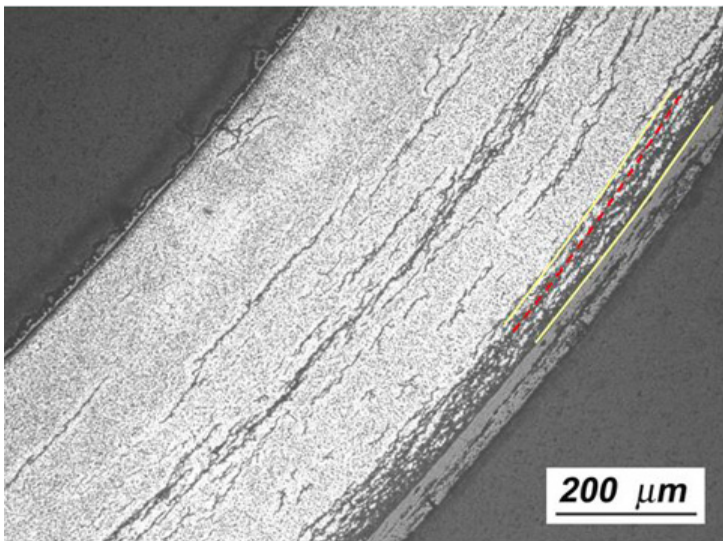

Figure 3.2.2-13

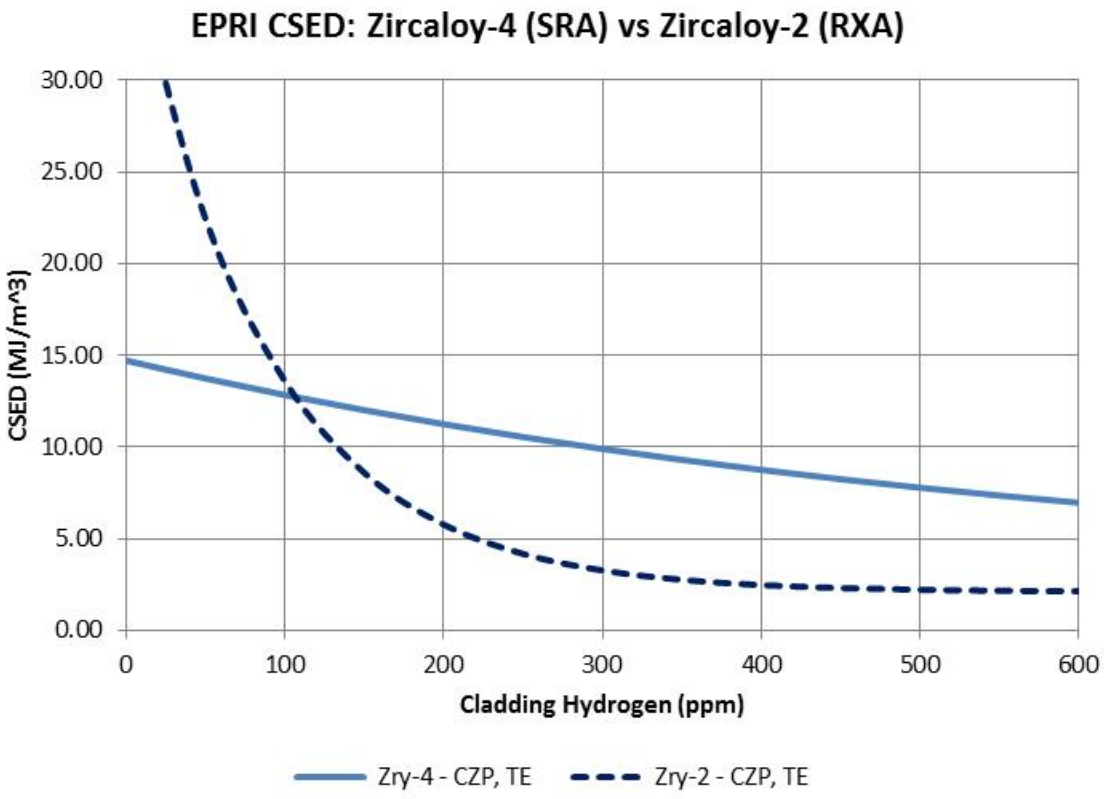

Figure 3.2.2-14

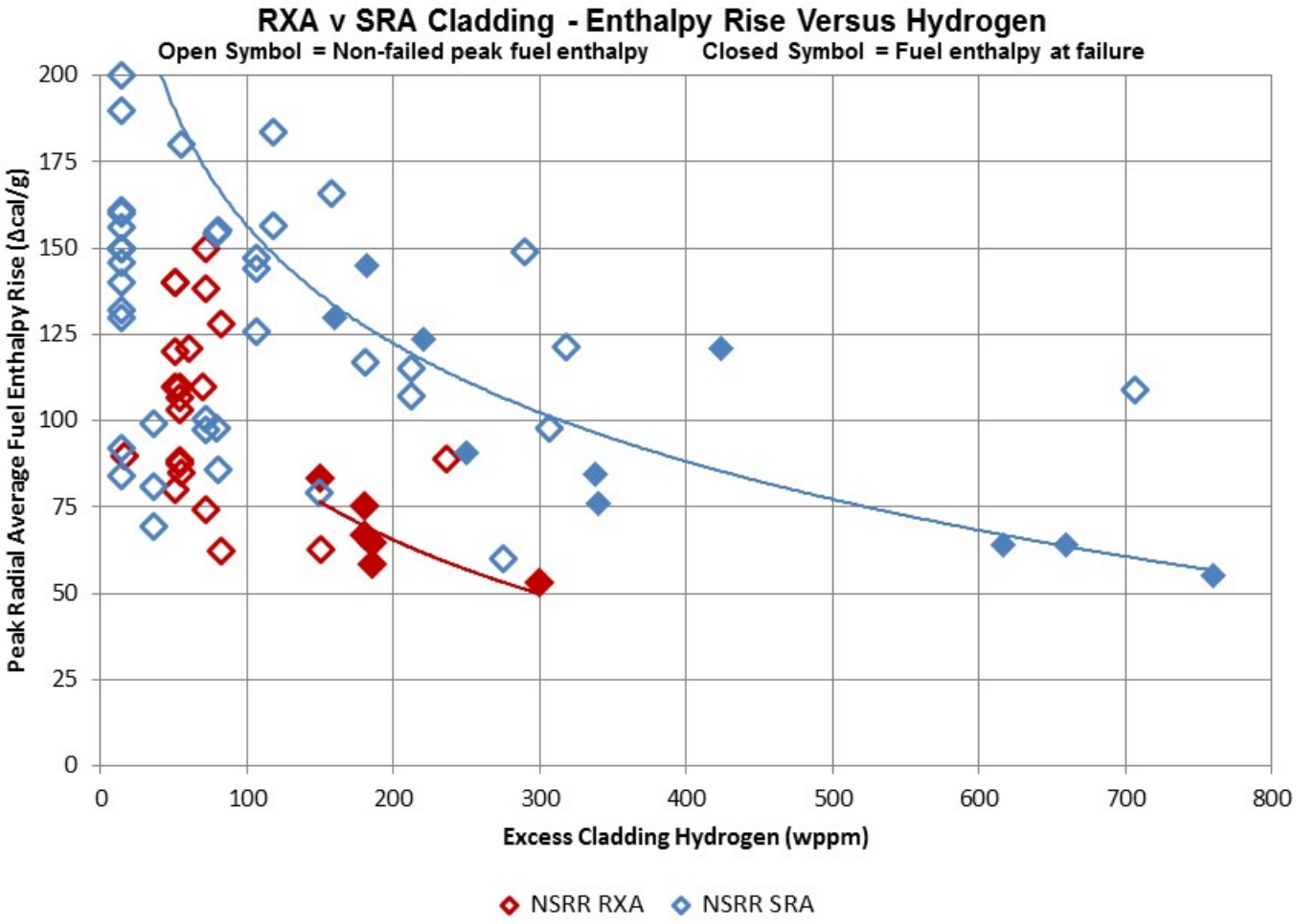

Figure 3.2.2-15

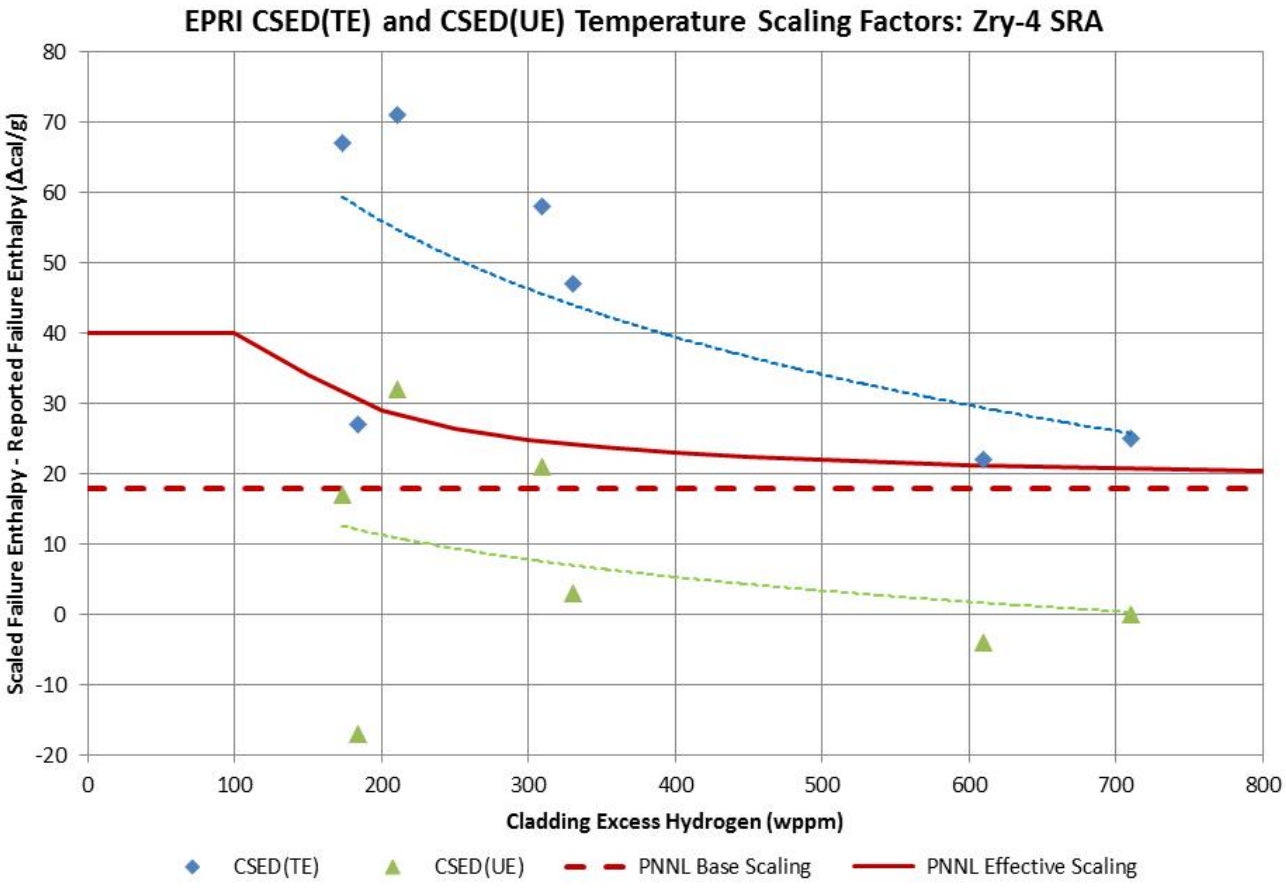

Figure 3.2.2-16

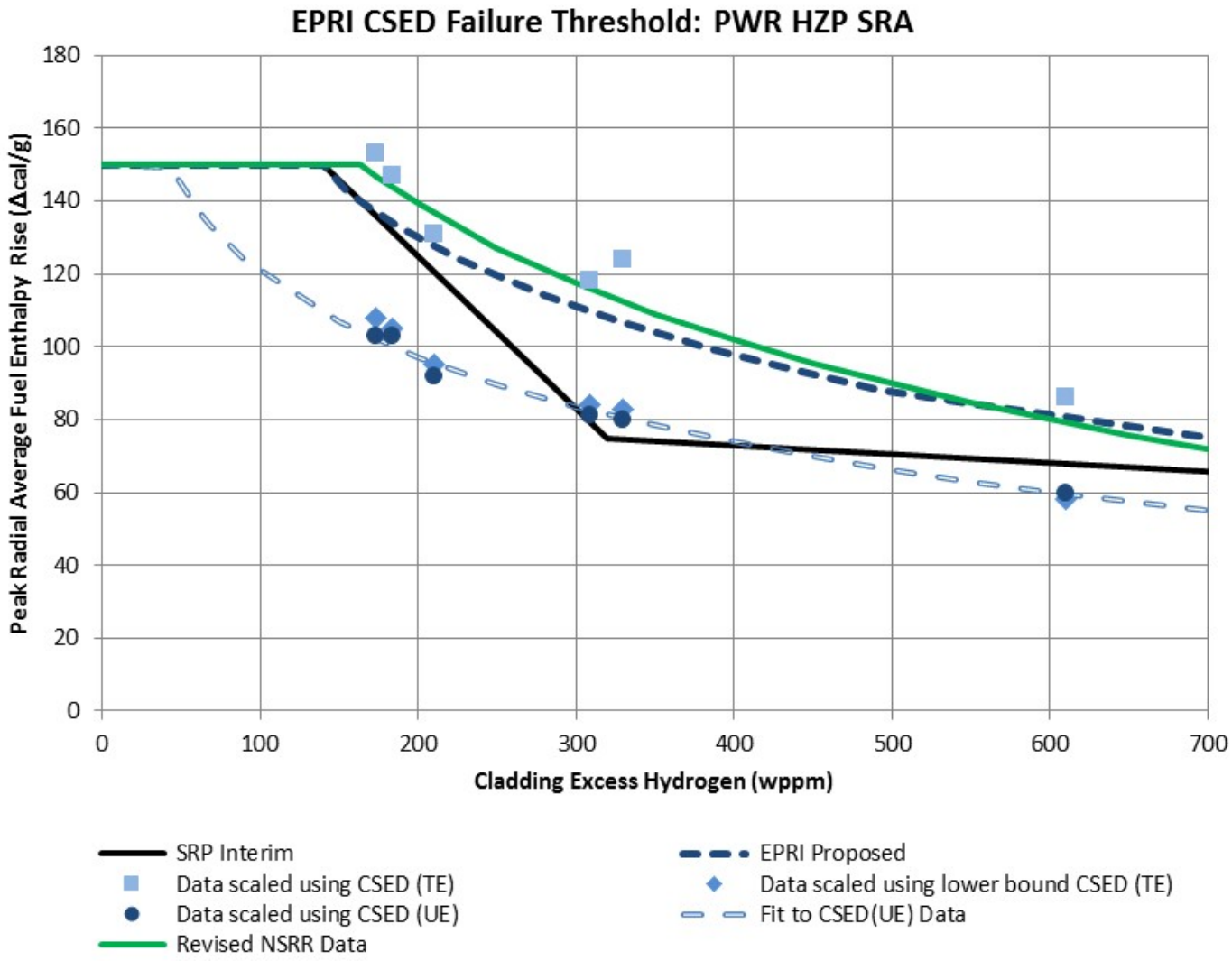

Figure 3.2.2-17

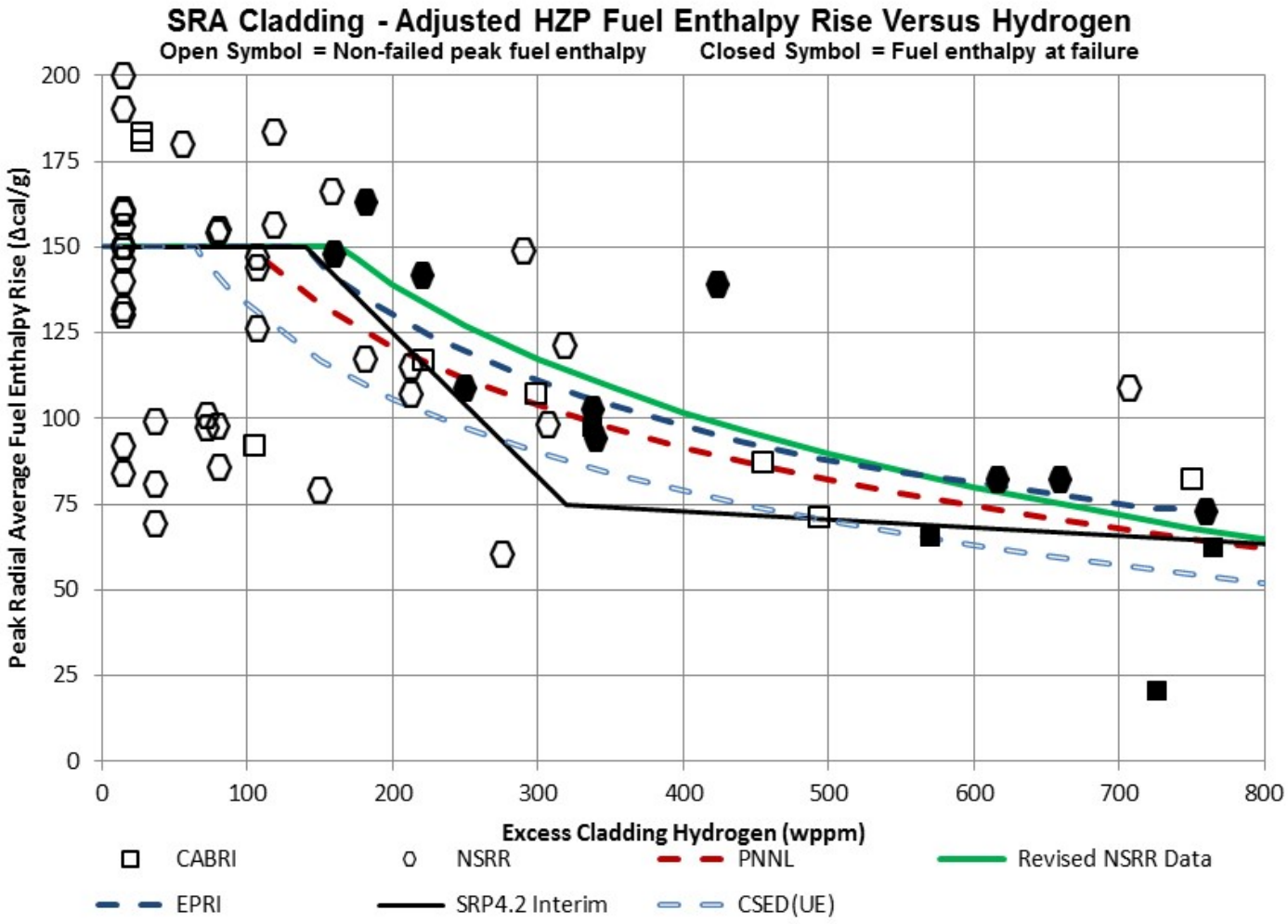

Figure 3.2.2-18

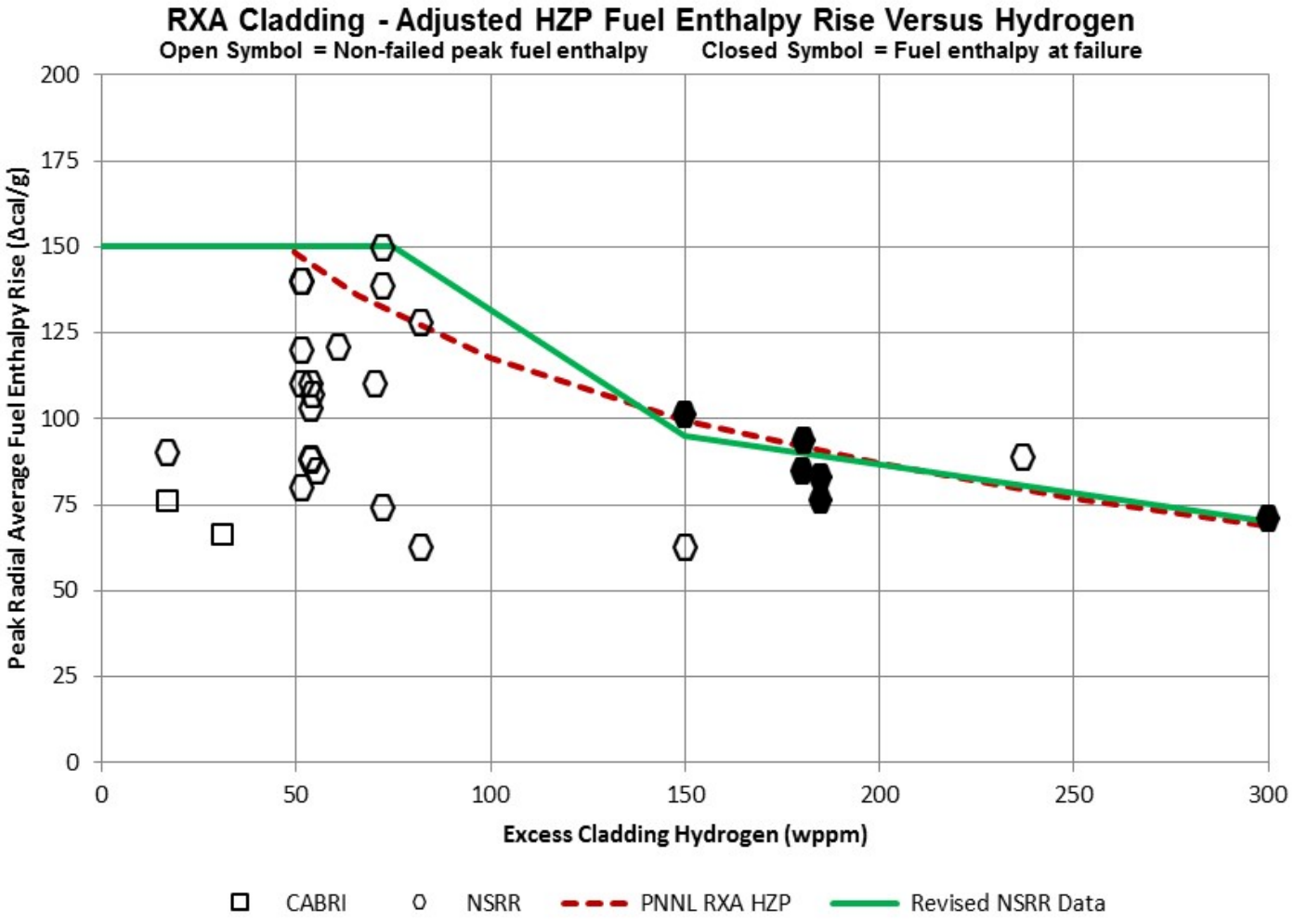

Figure 3.2.2-19

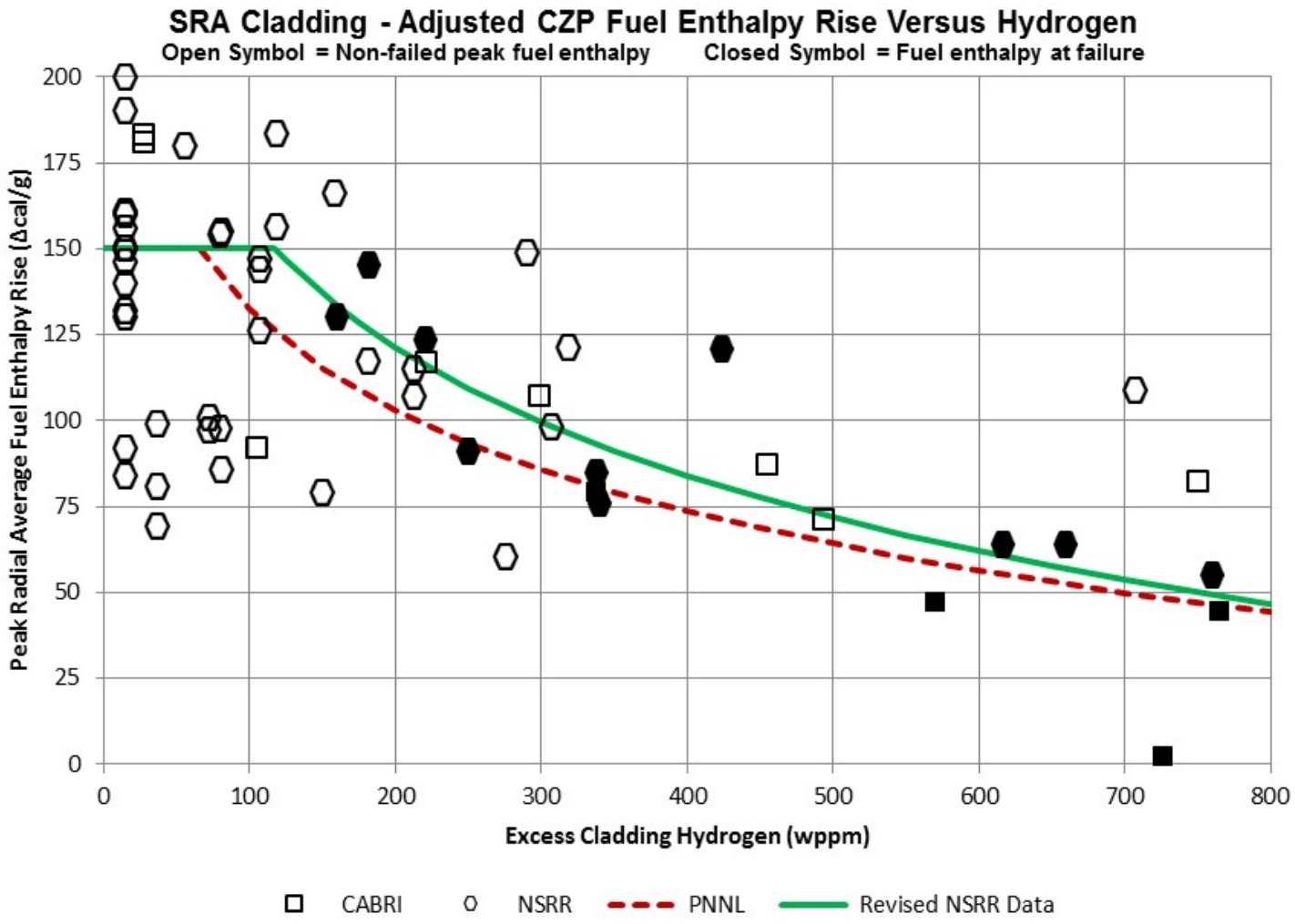

Figure 3.2.2-20

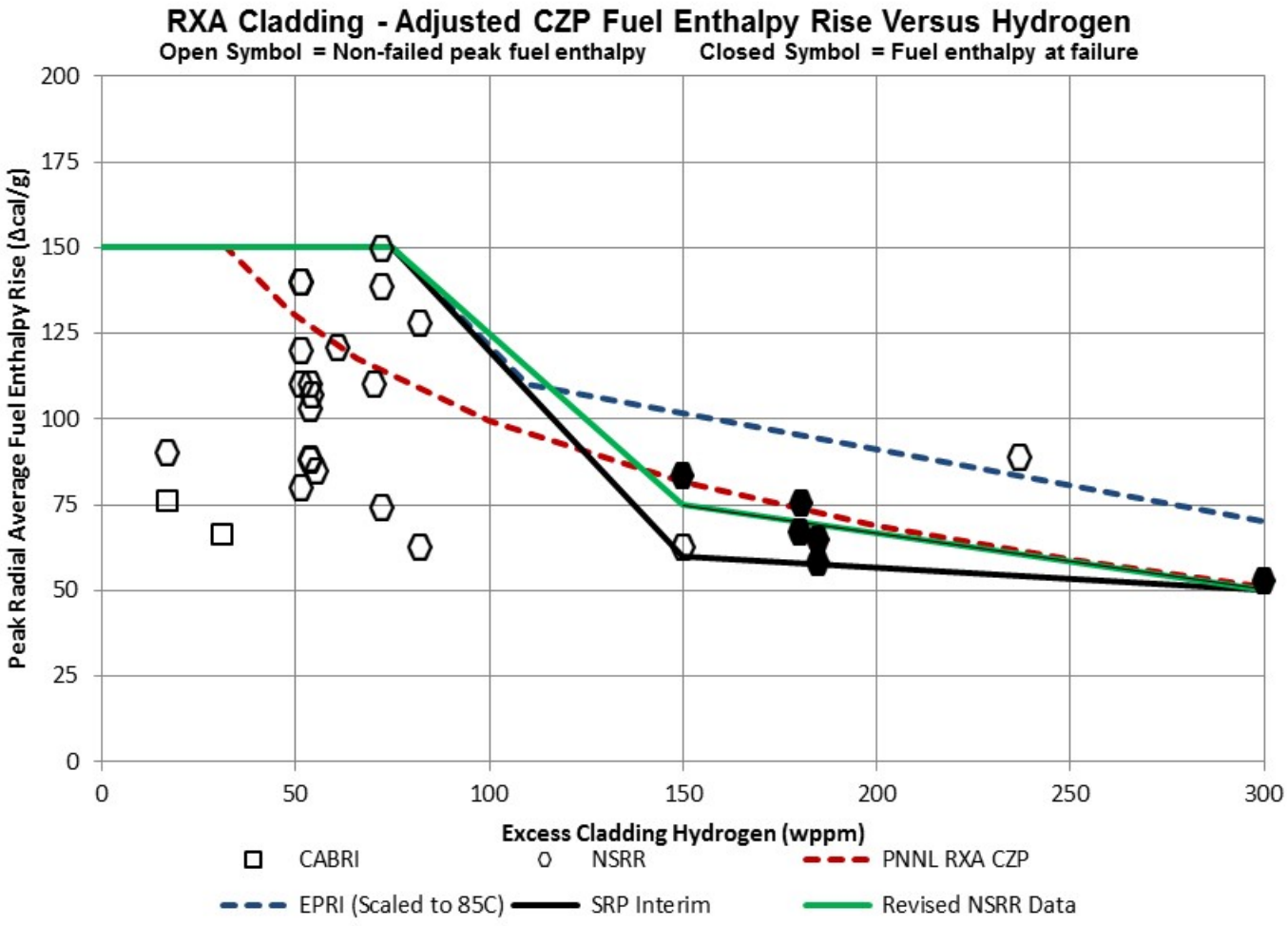

Figure 3.2.2-21

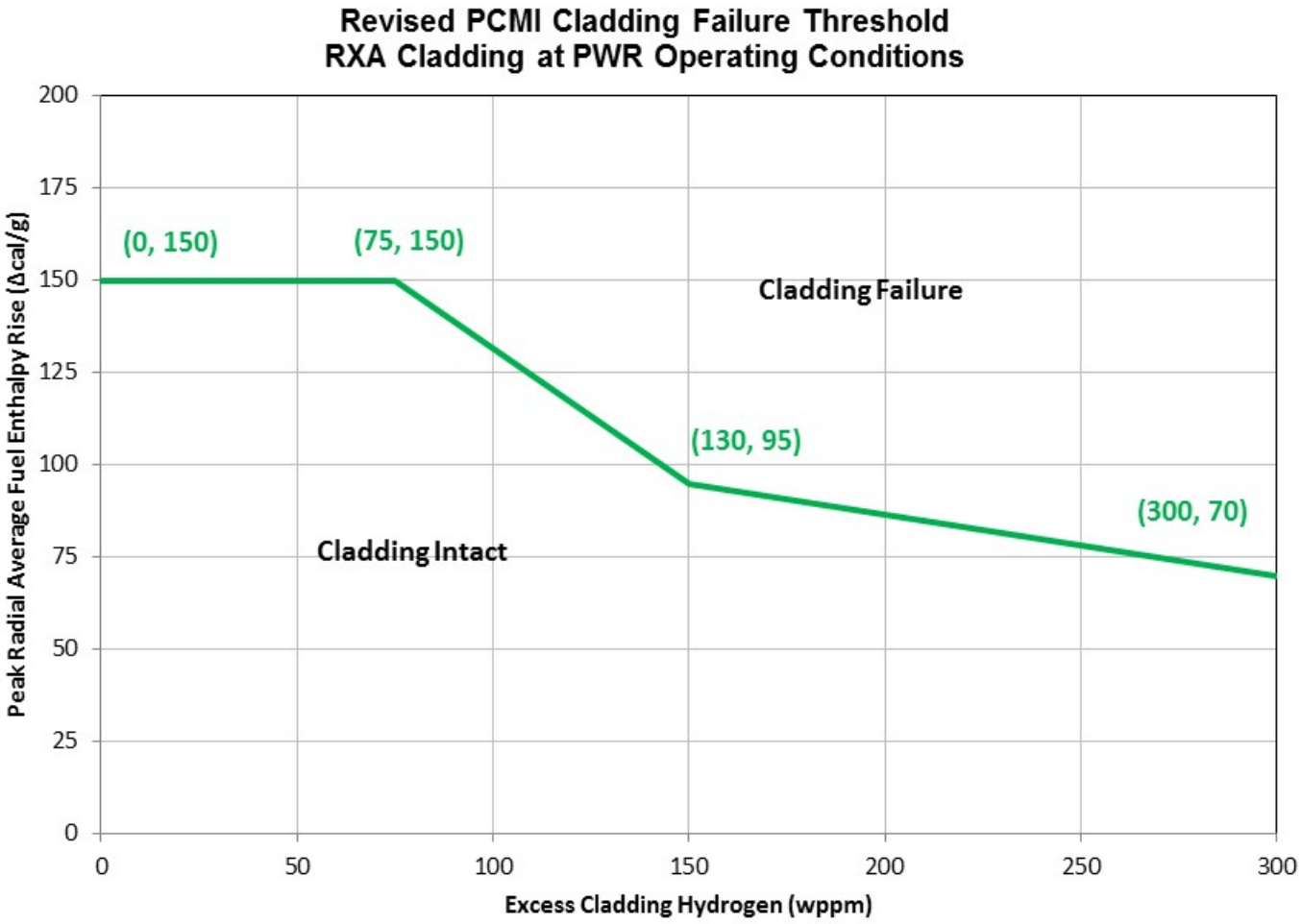

Figure 3.2.2-22

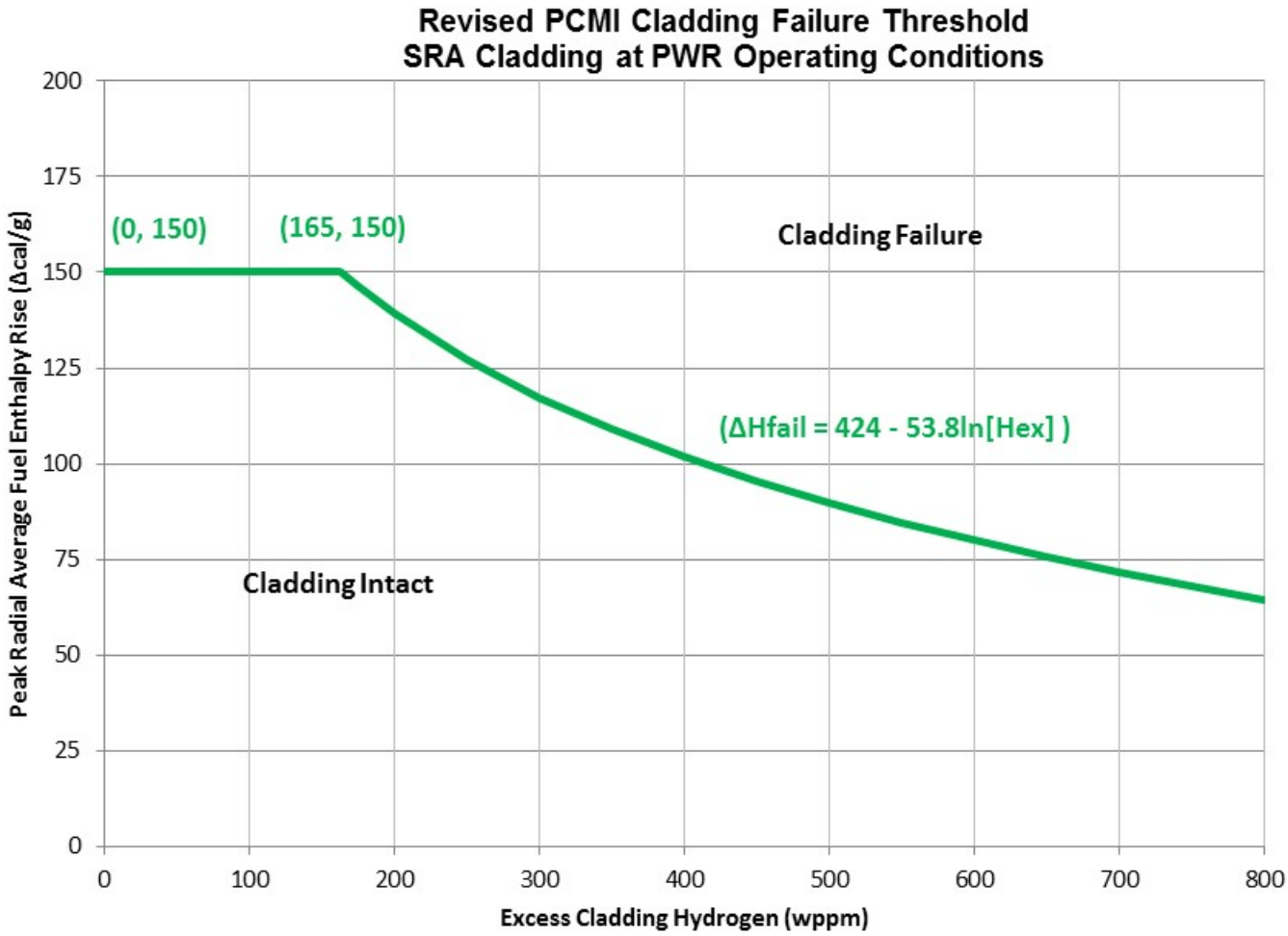

Figure 3.2.2-23

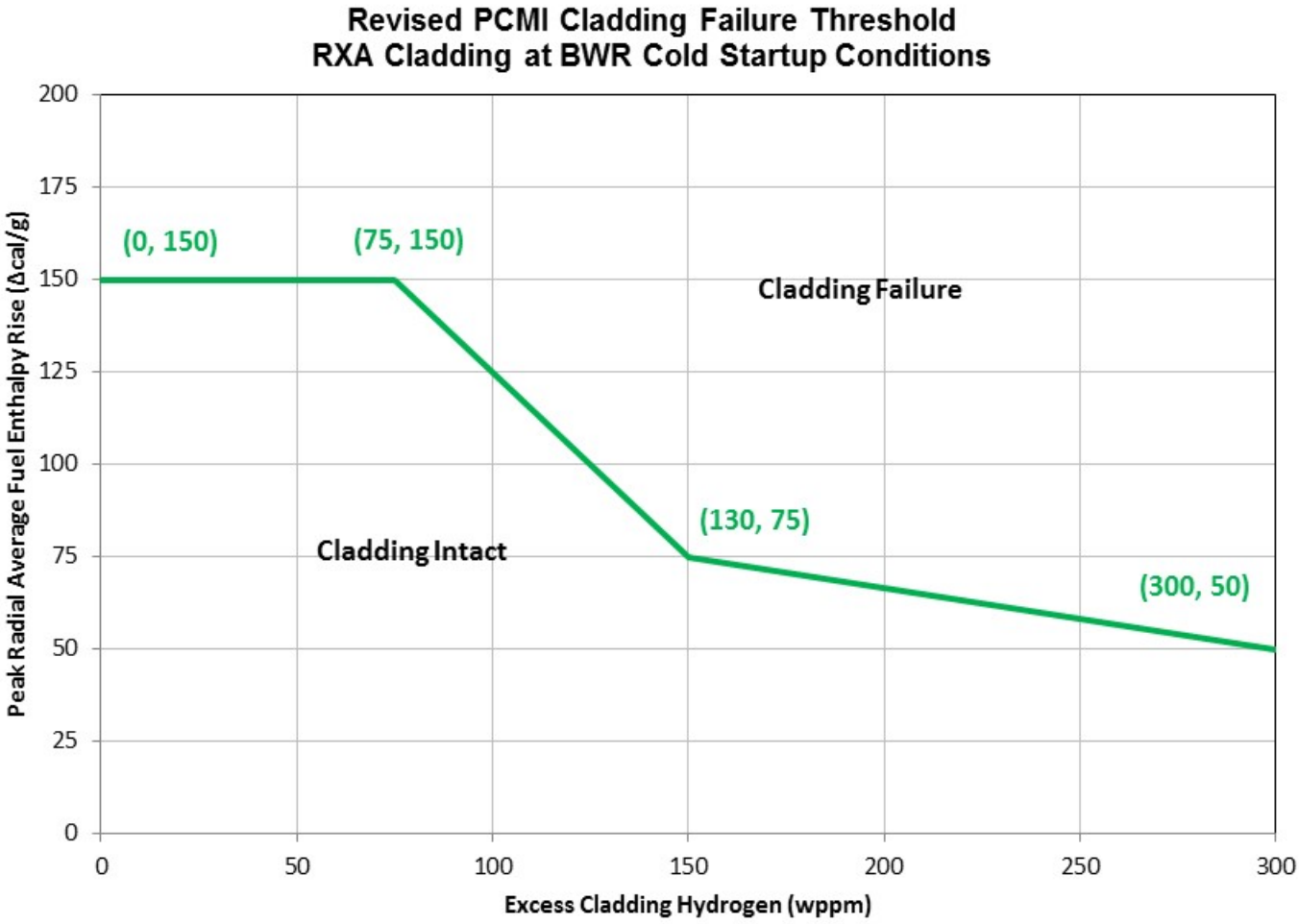

Figure 3.2.2-24

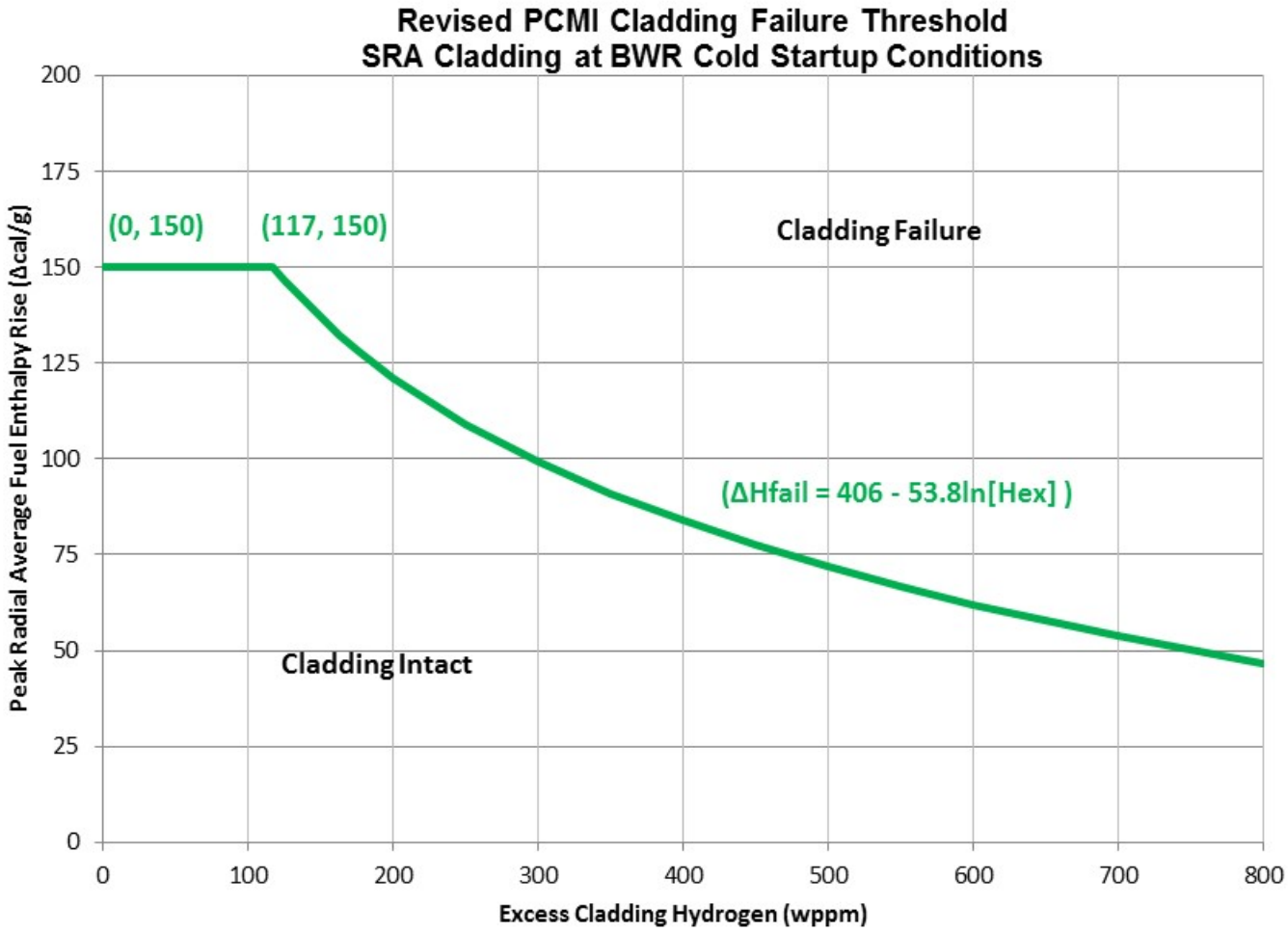

3.3 Molten Fuel Technical Basis

To address molten fuel-induced swelling PCMI cladding failure (item #4 above) and molten FCI, the interim RIA acceptance criteria and guidance (SRP 4.2 Appendix B) preclude fuel temperatures above incipient melting conditions. SRP 4.2 Appendix B lists the following coolability criteria:

- Peak radial average fuel enthalpy must remain below 230 cal/g.

- Peak fuel temperature must remain below incipient fuel melting conditions. Fuel temperature predictions must be based upon design-specific information accounting for manufacturing tolerances and modeling uncertainties using NRC approved methods including burnup-enhanced effects on pellet power distribution, fuel thermal conductivity, and fuel melting temperature.

As shown in Figure 21 of the NEA report, the maximum allowable peak fuel enthalpy to preclude fuel melting decreases with exposure and will likely become more limiting that the 230 cal/g coolability limit at approximately 30 GWd/MTU pellet burnup.

The intent of the above criteria was to maintain the fuel rod array and avoid the energetic reaction associated with molten FCI. The no melt criterion also precludes cladding failure due to molten fuel swelling PCMI.

The impact of new information (items #1 through #6, Section 1) on the interim fuel melting coolability criterion is described below.

1. OECD Nuclear Energy Agency State-of-the-art Report, “Nuclear Fuel Behaviour under RIA Conditions,” 2010 (Reference 2).

    - Section 6.1.1 of the NEA report details the effects of fuel burnup and pellet radial power distribution on fuel melting. With the exception of information presented on MOX fuel, the NEA report is consistent with the basis of the interim criterion. Note that the interim criteria and guidance is not applicable to MOX fuel.

2. EPRI Report 1021036, “Fuel Reliability Program: Proposed RIA Acceptance Criteria,” December 2010 (Reference 3).

    - No new information related to fuel melting.

3. Revised RIA transient fission gas release fractions (Reference 4).

    - No new information related to fuel melting.

4. PNNL Report 22549, “Pellet-Cladding Mechanical Interaction Failure Threshold for Reactivity Initiated Accidents for Pressurized Water Reactors and Boiling Water Reactors,” June 2013 (Reference 5).

    - No new information related to fuel melting.

5. Published results from NSRR Hot Capsule RIA Test VA3, VA4, RH2, BZ3, and LS2 (See Appendix A Reference 5).

    - No new information related to fuel melting.

6. JAEA published revised fuel enthalpy predictions for 43 previous NSRR test specimens (Reference 12).

    - No new information related to fuel melting.

Over the years, many PWRs have adopted refined acceptance criteria relative to those described in RG 1.77. The following text was extracted from a typical Westinghouse plant's Updated Final Safety Analysis Report (UFSAR).

- Average fuel pellet enthalpy at the hot spot below 225 cal/g for unirradiated fuel and 200 cal/g for irradiated fuel.

- Fuel melting will be limited to less than the innermost 10% of the fuel volume at the hot spot even if the average fuel pellet enthalpy is below the limits of criterion above.

The allowable hot spot fuel enthalpy for fresh fuel and decrease due to irradiation effects are similar to the interim guidance. However, unlike the interim guidance which avoids fuel melting, the Westinghouse criteria allow a limited volume of molten fuel.

As shown below, regulatory guidance documents provide an acceptable method for addressing fuel melting during the postulated BWR CRDA and PWR CRE accident. However, this guidance pertains only to radiological source term and does not address the thermal-mechanical reaction of molten FCI (e.g., pressure surge).

- BWR CRDA, RG 1.183 Appendix C: The release attributed to fuel melting is based on the fraction of the fuel that reaches or exceeds the initiation temperature for fuel melting and on the assumption that 100% of the noble gases and 50% of the iodines contained in that fraction are released to the reactor coolant.

- PWR CRE, RG 1.183 Appendix H: The release attributed to fuel melting is based on the fraction of the fuel that reaches or exceeds the initiation temperature for fuel melting and the assumption that 100% of the noble gases and 25% of the iodines contained in that fraction are available for release from containment. For the secondary system release pathway, 100% of the noble gases and 50% of the iodines in that fraction are released to the reactor coolant.

Employing the above radiological guidance, several licensees have presumed a small fraction of molten fuel within their onsite and offsite dose calculations. A survey of current UFSARs reveals that 33 of 35 BWRs and 32 of 65 PWRs include a small fraction of molten fuel in their dose calculations. For example, several licensees assume 0.25% of the core inventory is molten fuel (based on 10% pellet volume within 50% of axial height of 5% of the fuel rods). Fuel rods with fuel temperature above incipient melting conditions are assumed to experience cladding failure. The licensee combines this melt source term with the non-melt source term from fuel rods predicted (or assumed) to experience DNB to achieve the total RCS activity level.

A limited amount of fuel melting would be acceptable provided the applicant demonstrates that molten PCMI is precluded or specifically accounts for its effects. Recognizing past precedence, a revision to the interim criteria and guidance are proposed. As described above, the no fuel melting criterion was intended to avoid molten FCI. A limited amount of fuel melting is permissible provided the applicant demonstrate that this intent is satisfied. Limiting fuel melting to (1) fuel centerline region and (2) a small fraction of the pellet volume (i.e., 10%) has been judged acceptable in past applications.

3.3.1 Applicability

Due to effects of edge peaked power and lower solidus temperature, medium to high burnup fuel rods are more likely to experience fuel melting in the pellet periphery. Hence, the limited fuel centerline melt criterion may not apply. For these rods, fuel melting outside the centerline region must be precluded and this no melt criterion will likely be more limiting than the 230 cal/g upper limit on peak fuel enthalpy.

Due to chemical and heterogeneous effects on fuel thermal conductivity, pellet power profile, and local melting temperature, the above coolability criterion, as well as the 230 cal/g limit on radial average fuel enthalpy, is not applicable to MOX fuel rods.

3.3.2 Analytical Considerations

As described in Section 6.1.1 of Reference 2, the radial power and temperature profile during a prompt power excursion changes with fuel burnup. Specifically, the pellet radial power distribution becomes more edge peaked at higher burnup due to self-shielding. Hence, any fuel temperature prediction must account for this burnup-enhanced effect on pellet radial power distribution, as well as burnup-enhanced effects on fuel thermal conductivity and fuel melting temperature. This is consistent with the interim guidance and criteria.

Fuel temperature predictions are expected to vary widely (1) across the population of fuel rods in the core and (2) axially along the fuel stack of a given fuel rod. The applicant may elect to subdivide fuel rod populations based on peak fuel enthalpy and fuel rod burnup in order to demonstrate compliance.

3.3.3 Revised Criteria and Guidance

Based upon the above discussion, the following revision to the RIA acceptance criteria and guidance is proposed:

New Cladding Failure Threshold:

- If fuel temperature anywhere in the pellet exceeds incipient fuel melting conditions, then fuel cladding failure is presumed. Fuel temperature predictions must be based upon design-specific information accounting for manufacturing tolerances and modeling uncertainties using NRC approved methods including burnup-enhanced effects on pellet radial power distribution, fuel thermal conductivity, and fuel melting temperature. Increases in radiological source term due to predicted fuel melting must be accounted

for in dose calculations (See applicable guidance).

Revised Coolability Criterion:

- A limited amount of fuel melting is acceptable provided it is restricted to (1) fuel centerline region and (2) less than 10% of any pellet volume. For the outer 90% of the pellet volume, peak fuel temperature must remain below incipient fuel melting conditions. Fuel temperature predictions must be based upon design-specific information accounting for manufacturing tolerances and modeling uncertainties using NRC approved methods including burnup-enhanced effects on pellet radial power distribution, fuel thermal conductivity, and fuel melting temperature.

3.4 Coolable Core Geometry Criteria

Guidance and criteria for demonstrating that the coolable rod bundle array is maintained during the postulated accident are shown below. Note that the interim guidance and criteria has been revised based upon the new fuel melting guidance described in Section 3.3.

Coolability Criteria:

Fuel rod thermal-mechanical calculations must be based upon design-specific information accounting for manufacturing tolerances and modeling uncertainties using NRC approved methods including burnup-enhanced effects on pellet power distribution, fuel thermal conductivity, and fuel melting temperature.

1. Peak radial average fuel enthalpy must remain below 230 cal/g.

2. A limited amount of fuel melting is acceptable provided it is restricted to (1) fuel centerline region and (2) less than 10% of pellet volume. For the outer 90% of the pellet volume, peak fuel temperature must remain below incipient fuel melting conditions.

3. Mechanical energy generated as a result of (1) non-molten fuel-to-coolant interaction and (2) fuel rod burst must be addressed with respect to reactor pressure boundary, reactor internals, and fuel assembly structural integrity.

4. No loss of coolable geometry due to (1) fuel pellet and cladding fragmentation and dispersal and (2) fuel rod ballooning.

The impact of new information (items #1 through #6, Section 1) on the interim coolability criteria is described below.

1. OECD Nuclear Energy Agency State-of-the-art Report, “Nuclear Fuel Behaviour under RIA Conditions,” 2010 (Reference 2).

    - Section 7.2.2 of the NEA report describes the empirical database associated with fuel dispersal and FCI in RIA simulation tests.

2. EPRI Report 1021036, “Fuel Reliability Program: Proposed RIA Acceptance Criteria,” December 2010 (Reference 3).

    - No new information related to coolability.

3. Revised RIA transient fission gas release fractions (Reference 4).

    - No new information related to coolability.

4. PNNL Report 22549, “Pellet-Cladding Mechanical Interaction Failure Threshold for Reactivity Initiated Accidents for Pressurized Water Reactors and Boiling Water Reactors,” June 2013 (Reference 5).

    - No new information related to coolability.

5. Published results from NSRR Hot Capsule RIA Test VA3, VA4, RH2, BZ3, and LS2 (See Appendix A Reference 5).

    - No new information related to coolability.

6. JAEA published revised fuel enthalpy predictions for 43 previous NSRR test specimens (Reference 12).

    - The revised fuel enthalpy values shifts the relationship between peak fuel enthalpy, burnup, and fuel dispersal.

Based upon a review of the above references, criterion #1 (230 cal/g peak fuel enthalpy) remains unchanged. Changes to criterion #2 are described in Section 3.3 of this report.

Historically, limiting peak radial average fuel enthalpy and avoiding molten FCI were acceptable metrics to demonstrate coolable core geometry. Past applications did not specifically address items #3 and #4 above. An acceptable method for predicting the population of burst rods, amount of fuel fragmentation and dispersal, and converting the thermal-to-mechanical energy does not exist in regulatory guidance.

Section 7.2.2 of the NEA report (Reference 2) describes the empirical database associated with fuel dispersal and FCI in RIA simulation tests. The NEA report concludes that fuel dispersal occurs in connection with PCMI-type cladding failure and that balloon/burst failure does not lead to significant fuel dispersal. In contrast, recent Loss-Of-Coolant Accident simulation tests have exhibited fuel fragmentation and dispersal under balloon/burst conditions.

During PWR at-power scenarios with relatively low ejected rod worth, rod failure predictions will be more dominated by DNB than PCMI. In these scenarios, fuel rods operating with elevated rod internal pressure may balloon and burst. Since RIAs may experience multiple failure modes and each failure mode may have its own sensitivities with respect to fuel fragmentation and dispersal, more work is needed to develop guidance for addressing these complex phenomena.

Figure 3.4-1 illustrates reported fuel dispersal as a function of local burnup and peak fuel enthalpy during prompt power excursion tests performed at PBF, BIGR, IGR, CABRI, and NSRR. The solid blue diamonds represent specimens which exhibited an unacceptable level of fuel dispersal (i.e., >10%). The data suggests that higher burnup fuel rods are more susceptible to fuel dispersal. However, until regulatory guidance exists to address items #3 and #4 above, applicants need only demonstrate compliance to coolability criteria #1 and #2.

Figure 3.4-1: Reported Fuel Dispersal During Prompt Power Excursions

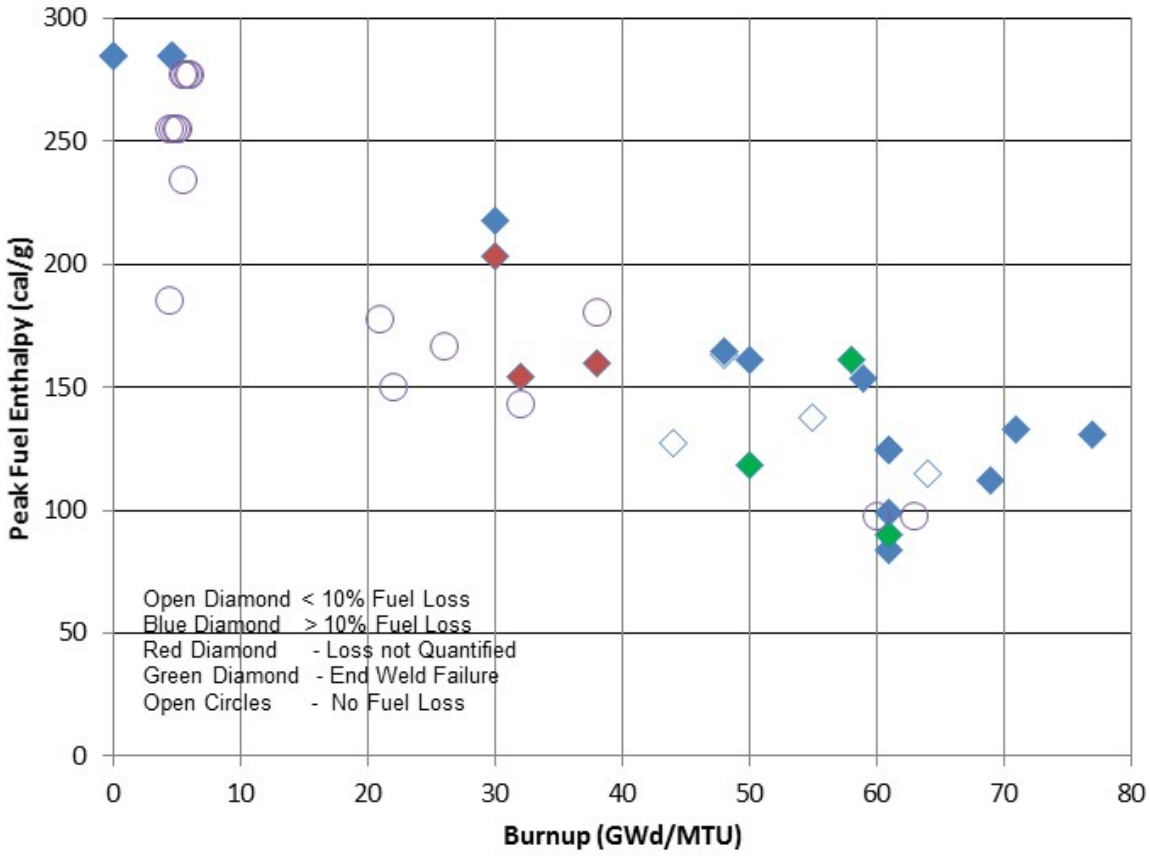

3.5 Radiological Fission Product Inventory Guidance

The impact of new information (items #1 through #6, Section 1) on the interim radiological fission product inventory guidance is described below.

1. OECD Nuclear Energy Agency State-of-the-art Report, "Nuclear Fuel Behaviour under RIA Conditions," 2010 (Reference 2).

    - Section 6.1.3 of the NEA report describes transient FGR and the supporting empirical database. No new data is presented.

2. EPRI Report 1021036, "Fuel Reliability Program: Proposed RIA Acceptance Criteria," December 2010 (Reference 3).

    - No new information related to transient FGR.

3. Revised RIA transient fission gas release fractions (Reference 4).

    - Basis for revised fission product inventories in pending RG 1.183 revision.

4. PNNL Report 22549, "Pellet-Cladding Mechanical Interaction Failure Threshold for Reactivity Initiated Accidents for Pressurized Water Reactors and Boiling Water Reactors," June 2013 (Reference 5).

    - No new information related to transient FGR.

5. Published results from NSRR Hot Capsule RIA Test VA3, VA4, RH2, BZ3, and LS2 (See Appendix A Reference 5).

    - No new information related to transient FGR.

6. JAEA published revised fuel enthalpy predictions for 43 previous NSRR test specimens (Reference 12).

    - No new information related to transient FGR. However, the reported changes directly impact the relationship between measured FGR and peak fuel enthalpy.

Revised fission product inventories (i.e., gap fractions), including contributions from transient FGR, are documented in Reference 4. This information was used to justify changes to the alternative source term gap fraction documented in DG-1199 (proposed revision to RG 1.183). However, the correlation between transient FGR and peak fuel enthalpy increase was derived before JAEA published revised test results.

Figure 3.5-1 illustrates the original transient FGR data along with the correlations proposed as part of the SRP-4.2 Appendix B interim criteria (0.2286ΔH – 7.1419) and DG-1199 (0.228ΔH). Figure 3.5-2 illustrates the revised transient FGR database including the latest reported JAEA data. A comparison of these figures reveals a more prominent distinction between high burnup (> 50 GWd/MTU) and lower burnup data. Note that additional data obtained from the NEA report was incorporated into the database.

A few observations regarding the revised database in Figure 3.5-2.

- Large spread in the data. However, this is not uncommon, even for steady-state FGR data.

- High burnup rods exhibit higher transient fission gas release (%). A combination of porous rim region with high concentration of fission gas bubbles and edge peaked power excursion would tend to maximize fission gas release in high burnup fuel.

- No discernable difference between medium burnup (30 – 50 GWd/MTU) and low burnup fuel rods (< 30 GWd/MTU).

- No prominent difference in fission gas release between MOX and UO2 fuel rods.

- No discernable difference in fission gas release between specimens with cladding failure (solid symbols) and those which reported no failure (open symbols).

Figure 3.5-3 shows the proposed, burnup-dependent transient FGR correlations along with the revised database. Due to the lack of data, it is difficult and likely overly conservative to attempt a 95/95 upper tolerance correlation. Instead, the staff elected to capture the leading edge of the two burnup intervals ($\geq$50, < 50 GWd/MTU). While a few data points exceed the correlations, the staff felt that, given the spread in the data, the proposed, burnup-dependent correlations provided a reasonable level of conservatism.

The revised transient FGR correlations are listed below. The total fission product inventory is equal to the steady state gap inventory plus the transient FGR derived with these correlations.

Peak Pellet BU < 50 GWd/MTU: Transient FGR (%) = [(0.26 * ΔH) - 13]

Peak Pellet BU $\geq$ 50 GWd/MTU: Transient FGR (%) = [(0.26 * ΔH) - 5]

Where:

FGR = Fission gas release, % (must be $\geq$ 0)

ΔH = Fuel enthalpy increase (Δcal/g)

These transient FGR correlations supersede the correlation derived in Reference 4 and presented in DG-1199.

Figure 3.5-1: Original Database of Transient FGR Versus Peak Enthalpy Increase

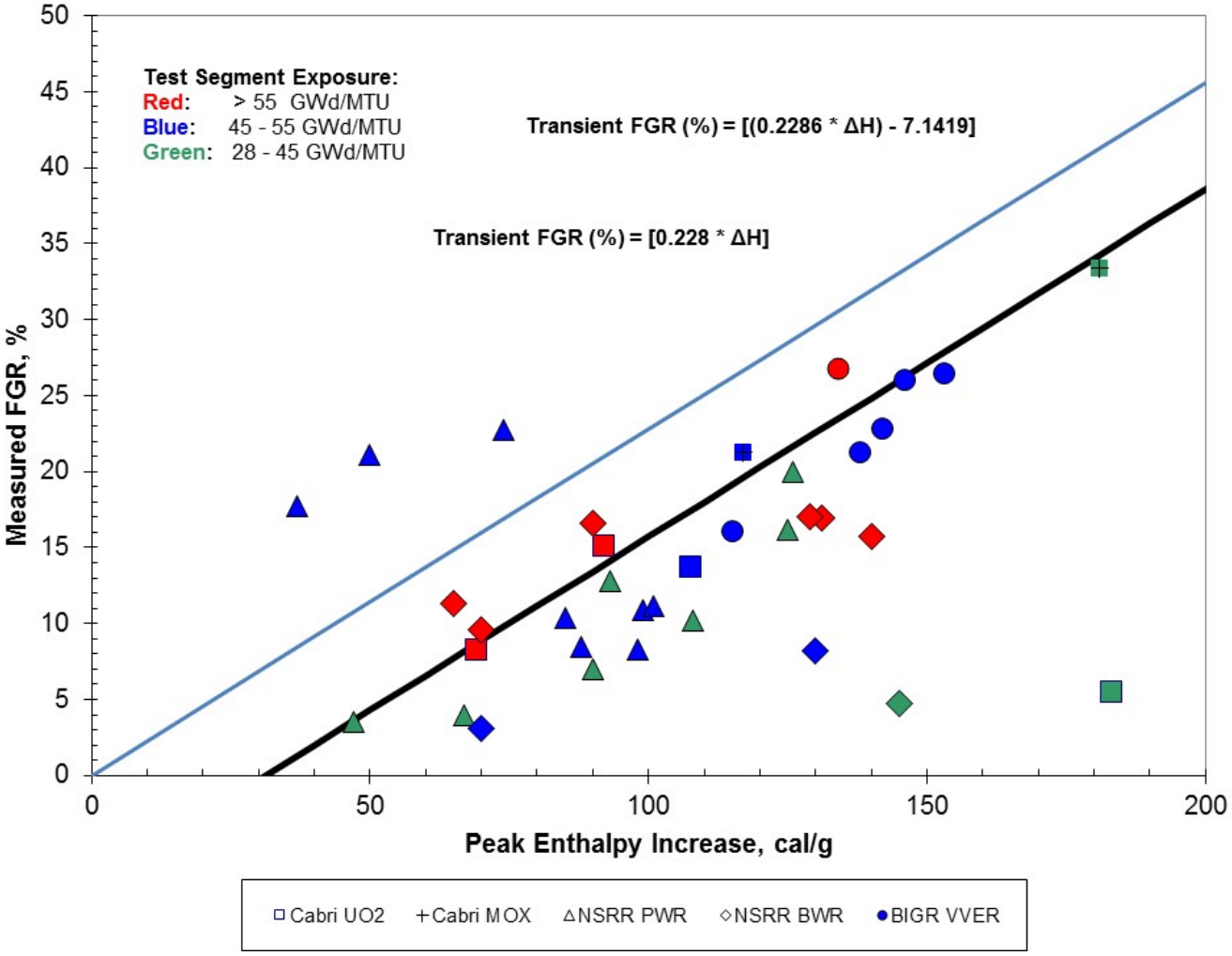

Figure 3.5-2: Revised Database of Transient FGR Versus Peak Enthalpy Increase

(Open symbols indicate non-failed, solid symbols indicate cladding failure)

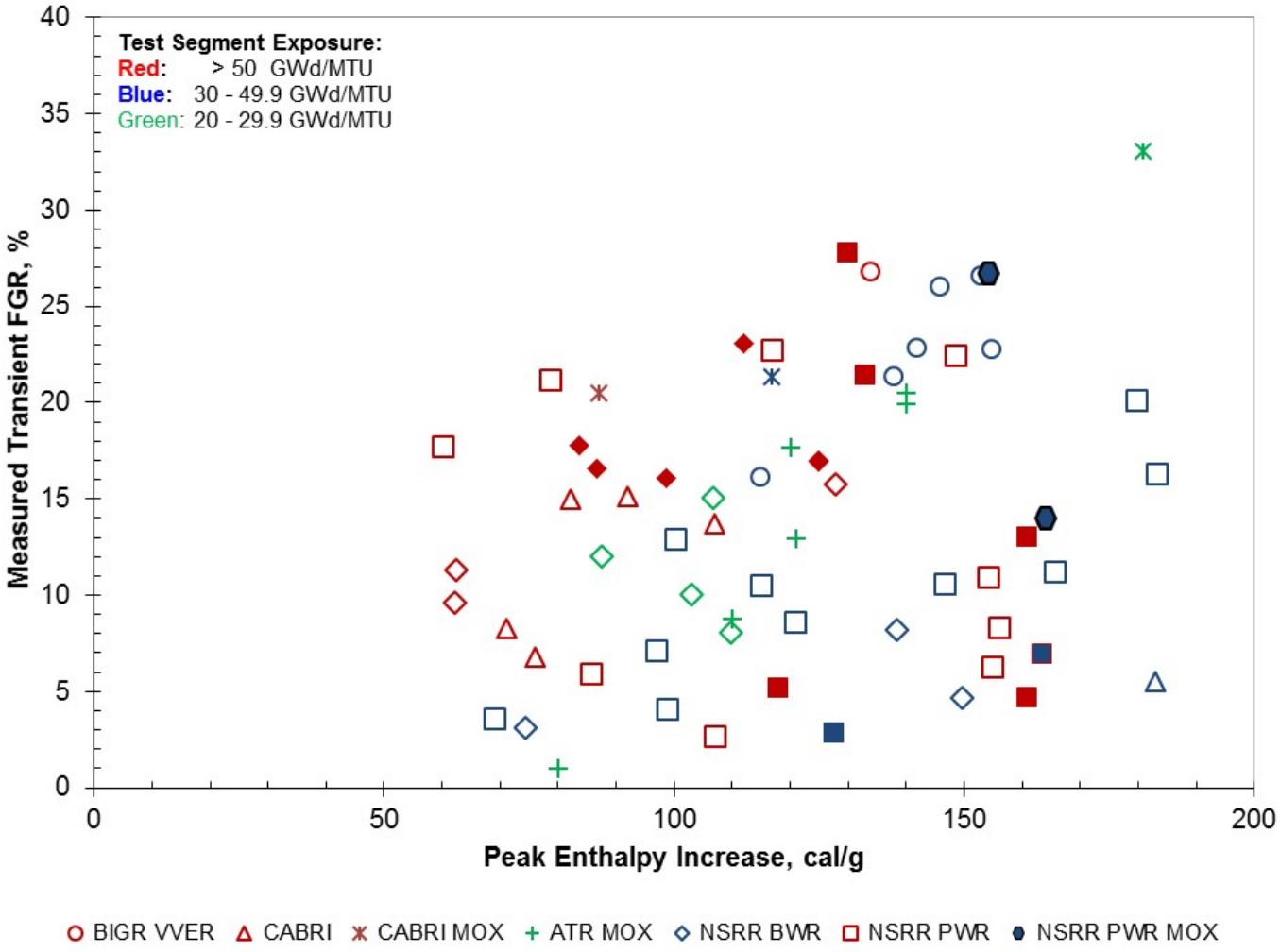

Figure 3.5-3: Burnup-Dependent Transient FGR Correlations

(Open symbols indicate non-failed, solid symbols indicate cladding failure)

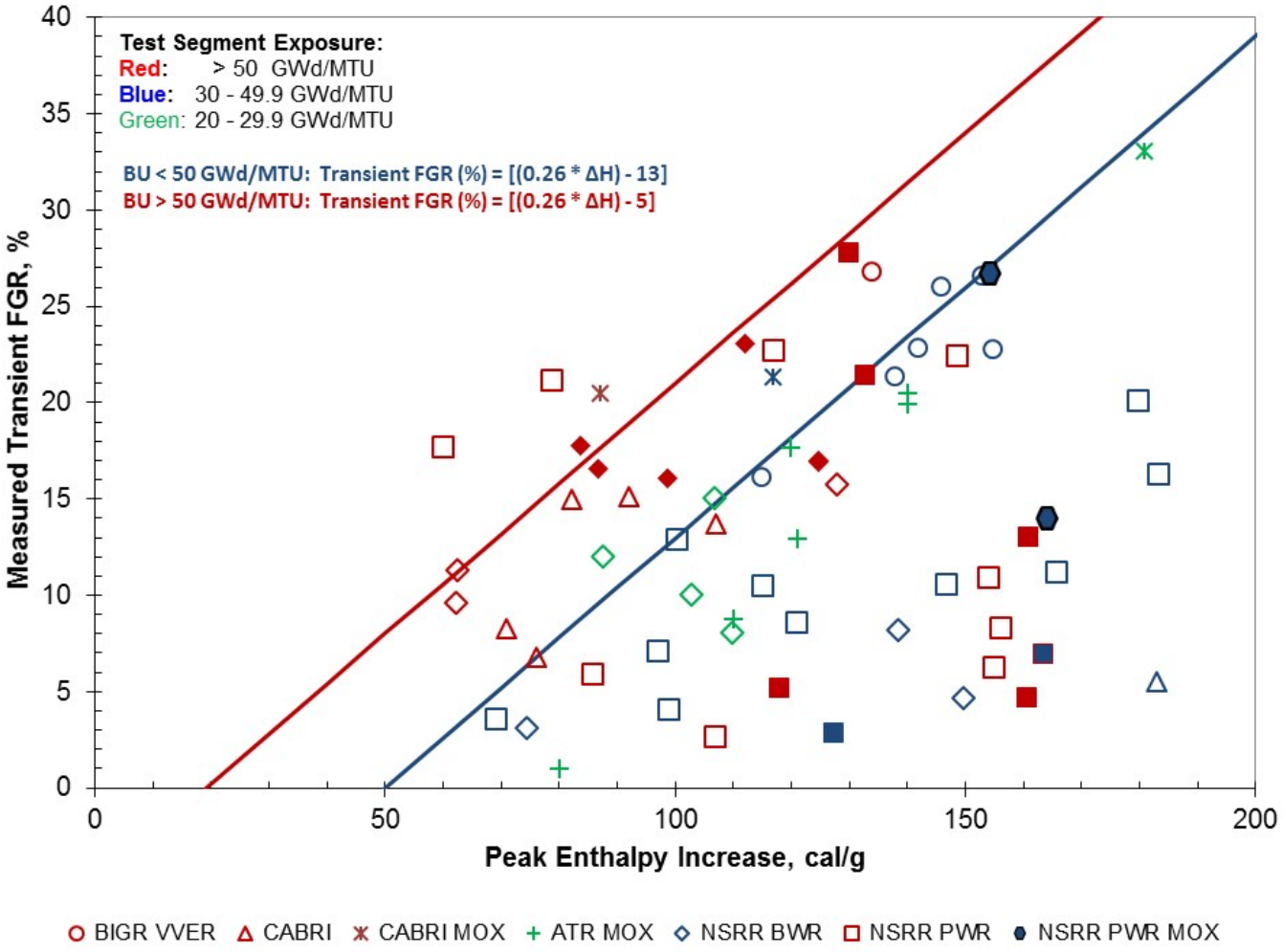

4.0 CONCLUSION

The purpose of this report is to document the technical and regulatory bases for the acceptance criteria and guidance for the RIA. RIAs consist of postulated accidents which involve a sudden and rapid insertion of positive reactivity. These accident scenarios include a CRE for PWRs and a CRDA for BWRs.

In 2007, the staff published the interim acceptance criteria and guidance based upon an assessment of the available empirical data from in-pile RIA test programs. The technical and regulatory basis of the interim criteria is documented in a memorandum dated January 19, 2007 (Reference 1). Since 2007, the following information has become available which has prompted the staff to update portions of the interim criteria and guidance:

1. OECD Nuclear Energy Agency State-of-the-art Report, "Nuclear Fuel Behaviour under RIA Conditions," 2010 (Reference 2).

2. EPRI Report 1021036, "Fuel Reliability Program: Proposed RIA Acceptance Criteria," December 2010 (Reference 3).

3. Revised RIA transient fission gas release fractions (Reference 4).

4. PNNL Report 22549, "Pellet-Cladding Mechanical Interaction Failure Threshold for Reactivity Initiated Accidents for Pressurized Water Reactors and Boiling Water Reactors," June 2013 (Reference 5).

5. Published results from NSRR Hot Capsule RIA Test VA3, VA4, RH2, BZ3, and LS2 (See Appendix A Reference 5).

6. JAEA published revised fuel enthalpy predictions for 43 previous NSRR test specimens (Reference 12).

Based upon new research data, revised research data, new analysis, and international perspectives, the NRC staff has revised portions of the interim criteria and guidance. Section 3 of this report documents the updated technical basis for the RIA acceptance criteria and guidance.

5.0 REFERENCES

1. NRC memorandum, “Technical and Regulatory Basis for the Reactivity-Initiated Accident Interim Acceptance Criteria and Guidance,” January 19, 2007 (ADAMS ML ML070220400).

2. OECD Nuclear Energy Agency State-of-the-Art Report, “Nuclear Fuel Behaviour under Reactivity-initiated Accident Conditions,” ISBN 978-92-99113-2, 2010 (ADAMS ML101460362).

3. EPRI Report 1021036, “Fuel Reliability Program: Proposed RIA Acceptance Criteria,” December 2010 (ADAMS ML13094A232).

4. NRC memorandum, “Technical Basis for Revised Regulatory Guide 1.183 (DG-1199) Fission Product Fuel-to-Cladding Gap Inventory,” July 26, 2011 (ADAMS ML112070117).

5. PNNL Report 22549, “Pellet-Cladding Mechanical Interaction Failure Threshold for Reactivity Initiated Accidents for Pressurized Water Reactors and Boiling Water Reactors,” June 2013 (ADAMS ML13277A368).

6. P. E. MacDonald, S. L. Seiffert, Z. R. Martinson, R. K. McCardell, D. E. Owen, and S. K. Fukuda, “Assessment of Light-Water-Reactor Fuel Damage During a Reactivity-Initiated Accident,” *Nuclear Safety*, Volume 21, 582, 1980.

7. NRC memorandum, “Research Information Letter No. 0401, An Assessment of Postulated Reactivity-Initiated Accidents for Operating Reactors in the U.S.,” March 31, 2004 (ADAMS ML040920189).

8. J. J. Kearns, “Thermal Soubility and Partinioning of Hydrides in the Alpha Phase of Zirconium, Zircaloy-2 and Zircaloy-4,” *Journal of Nuclear Materials*, 22:292-303, 1967.

9. M. Aomi, T. Baba, T. Miyashita, K. Kamimura, T. Yasuda, Y. Shinohara, and T. Takeda, “Evaluation of Hydride Reorientation Behavior and Mechanical Properties for High-Burnup Fuel-Cladding Tubes in Interim Dry Storage,” *Journal of ASTM International*, Vol. 5, No. 9, 2011.

10. NUREG/CR-6967, “Cladding Embrittlement During Postulated Loss-of-Coolant Accidents, July 2008 (ADAMS ML082130389).

11. M. Billone, T. Burtseva, and Y. Liu, “Baseline Properties and DBTT of High Burnup PWR Cladding Alloys,” Proceedings of the 17th International Symposium on PATRAM, 2013.

12. Y. Udagawa, T. Sugiyama, M. Amaya (JAEA), "Reevaluation of Fuel Enthalpy in NSRR Test for High Burnup Fuels," WRFPM 2014, Paper No. 100066, Sendai, Japan, September 14-17, 2014.